TOWARD INFRASTRUCTURE MOBILITY FOR NEXT-GENERATION WIRELESS NETWORKS

A Thesis
Presented to
The Academic Faculty

By

Yubing Jian

In Partial Fulfillment
of the Requirements for the Degree
Doctor of Philosophy in the
School of Electrical and Computer Engineering

Georgia Institute of Technology

August 2020

TOWARD INFRASTRUCTURE MOBILITY FOR NEXT-GENERATION WIRELESS NETWORKS

Approved by:

Dr. Raghupathy Sivakumar, Advisor
School of Electrical and Computer Engineering
Georgia Institute of Technology

Dr. Douglas M Blough
School of Electrical and Computer Engineering
Georgia Institute of Technology

Dr. John R. Barry
School of Electrical and Computer Engineering
Georgia Institute of Technology

Dr. Gee-Kung Chang
School of Electrical and Computer Engineering
Georgia Institute of Technology

Dr. Karthik Ramachandran
Scheller College of Business
Georgia Institute of Technology

Date Approved: July 23, 2020

Appreciate everyone I met through my journey.

ACKNOWLEDGEMENTS

First and foremost, I would like to thank my family. Their encouragement, love, sacrifice and support have helped me go through this journey possible. This dissertation is dedicated to my beloved parents and girlfriend - thanks for all the support and encouragement.

I would like to express my deepest gratitude to my advisor, Prof. Raghupathy Sivakumar, for his continuous support, guidance, and encouragement during my Ph.D. study. Without his help, I would not become a professional and confident research specialist in the domain of telecommunications. With the wise broad vision, innovative ideals, strong enthusiasm and dedication, and effective communication and collaboration, he has served not only as a research advisor but also a ideal model for me to learn from.

Second, I would like to thank Prof. Douglas M. Blough, Prof. John R. Barry, Prof. Geekung Chang, and Prof. Karthik Ramachandran for serving on my proposal and dissertation committee and providing many insightful comments and feedback that greatly improved the quality of this work.

My gratitude extends to the members of the GNAN research group. I thank Chaofang Shih, Bhuvana Krishnaswamy, Uma Parthavi Moravapalle, Mohit Agarwal, Shyam Krishnan Venkateswaran, and Ekansh Gupta for their valuable support and encouragement, feedback, and assistance during my Ph.D. study.

I would also like to thank every inspiration and motivation provided by everyone I met. Without all these support and encouragement, I would never gain such a wonderful experience during my journey of Ph.D. study.

TABLE OF CONTENTS

LIST OF TABLES

LIST OF FIGURES

SUMMARY

Global IP wireless data usage is expected to increase from 59 exabytes per month in 2017 to 281 exabytes per month in 2022 [1]. This impending explosion is driving research in the rapid development of next generation wireless technologies. Harsh wireless channel conditions are a fundamental limitation of network performance. At a high level, harsh channels result in poor wireless signal quality on the receiver side. A better-quality signal results in smaller packet transmission times, which in turn improves overall network performance. In this dissertation, we consider the problem of enhancing the robustness of wireless communications using *infrastructure mobility*; given more freedom of mobility, wireless infrastructures (e.g., access points [APs]) can alter locations to provide better wireless channel conditions to the overall network. To further study infrastructure intelligence, we also investigate *infrastructure interference mitigation*; given a centralized controller, the central controller can mitigate interference from various wireless technologies to improve wireless channel conditions.

The position of a wireless device in a network has considerable influence on the performance of the network, as wireless signal quality at the receiver side heavily depends on physical environmental features. Conventional telecommunication technologies have no ability to improve physical environmental conditions, if necessary. The design of algorithms and protocols for wireless networks is been based on the assumption that the clients are mobile; and the AP, or base station is static. In addition, the client mobility is driven by user needs and behavior, which can potentially degrade network performance. With the recent and significant advancements in wireless communications, robotics, and embedded systems, robotic-based wireless networks can be meaningfully and practically devised to combat the non-robust wireless channel conditions. The concept of robotic wireless networks can be applied in extensive scenarios (e.g., industrial internet of things [IIoT])). Robotic networks have the advantage of mobility, so the wireless channel conditions can

be significantly improved from the perspective of infrastructure. In this dissertation, we first consider the application of infrastructure mobility in ultra high frequency (UHF) and super high frequency (SHF), e.g., 2.4GHuz unlicensed band. We observe that movements as small as a few centimeters can result in significant network performance improvements primarily due to the impact of multipath effect and interference. Designing and developing a solution to leverage the possible benefits of infrastructure mobility is a non-trivial problem. First, we must deduce the optimal location of the AP or base station within the physical space that maximizes performance for the network as a whole. Next, we must solve the physical mobility problem of reaching the AP or base station to the deduced location. Further, there is also the condition of whether the theoretically optimal location is reachable in the first place, and; what needs to be done if the answer is no. Thus, we first explore the UHF and SHF infrastructure mobility in this dissertation.

Extremely high frequency (EHF) typically referred as mmWave is an essential enabling technology for next-generation wireless networks. Using a large bandwidth, it can deliver multi-gigabit performance. For example, IEEE 802.11ad operating in the 60GHz unlicensed mmWave band can deliver $\sim$7Gbps performance using a 2160MHz bandwidth. While the performance is quite promising; when compared to UHF and SHF, mmWave is vulnerable to non-line-of-sight (NLOS) conditions. There is an *extremely high signal attenuation* in mmWave communications. The communication performance drops significantly when the wireless link has an obstacle such as a wall or cabinet in its way. For example, if a human blocking the line-of-sight (LOS), there could be an $\sim$30dBm additional path loss for 60GHz mmWave band. Thus, mmWave is especially sensitive to physical channel conditions. In this context, infrastructure mobility provides an attractive degree of freedom for mmWave communication, due to the creation of LOS conditions that can have a profound impact on network performance. In this dissertation, given the significant difference in signal propagation characteristics between EHF and UHF/SHF, we also explore the potential of using infrastructure mobility to improve the LOS conditions for clients within an indoor

mmWave network.

Interference is another significant phenomenon that can impact the wireless channel conditions. If multiple wireless links transmit at the same time, there may be an unsuccessful transmission for all wireless links. The unlicensed offloading technique (e.g., unlicensed LTE) has become an essential research direction for cellular networks. The offloading technique aims to assist cellular operators with offloading cellular data from licensed to unlicensed bands. In this context, the unlicensed bands can potentially become even more crowded, leading to more interference. Even worse, centralized medium control protocol (MAC) and distributed MAC are utilized for cellular and WiFi networks. The distributed nature of WiFi MAC makes the traffic patterns of individual client random and unpredictable. The incompatible MAC protocols of cellular and WiFi make it hard for them to coexist without communication guidelines at the system level that ensure fair access to the spectrum for both technologies while maintaining high efficiency of the channel. If unlicensed LTE and WiFi networks operate in the same spectrum as-is, the throughput of the WiFi network is significantly reduced, because the unlicensed LTE controller, in a centralized manner, attempts to maximize the channel efficiency of the unlicensed LTE network, and allows the unlicensed LTE devices to transmit. The channel is kept busy, and thus, the WiFi devices, due to their distributed nature, can only transmit when the channel is idle. Finally, we also explore an infrastructure interference mitigation algorithm between unlicensed cellular and WiFi technologies to improve channel efficiency.

CHAPTER 1

INTRODUCTION

WiFi is a ubiquitous and impactful wireless technology used everyday and everywhere. According to the Cisco Visual Networking Index report [1], there is an expected 3.5 times overall internet traffic increase from 2017 to 2022 as shown in Fig. 1.1. WiFi is and will remain a dominant wireless technology for nearly half of the Internet traffic during this time frame. WiFi Internet traffic generated by the mobile platforms is the fastest growing type, and, the amount of WiFi traffic generated by the mobile WiFi platform is expected to increased approximately 10 times between 2017 and 2022 [1]. Fig. 1.2 shows that the number of WiFi devices will grow from 10 billion in 2017 to 27 billion in 2022 [2]. The Internet of Things (IoT) WiFi devices will become the most rapid increase device type, accounting for nearly half of WiFi devices in 2022. Globally, the number of WiFi capable device per person are expected to increase 2.5 time from 2017 to 2022 [2, 3]. This translates to more than three WiFi capable devices per person in 2022.

Given the above analytic prediction on internet traffic and the expected number of WiFi results devices, it is clear 1) *WiFi has had and will have the dominant impact on internet traffic* and *WiFi is and will be ubiquitous*. However, there is a significant gap between the

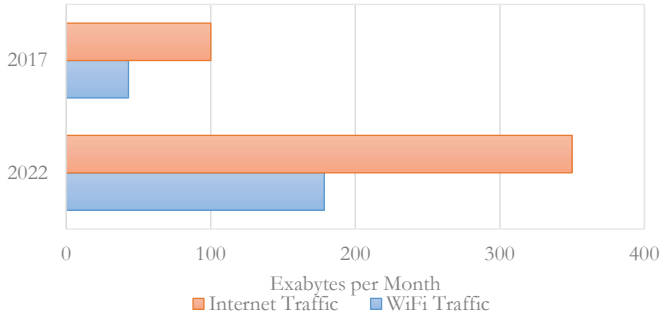

Figure 1.1: Internet Traffic

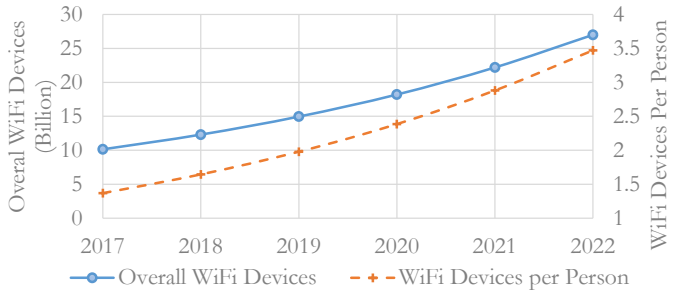

Figure 1.2: WiFi Devices

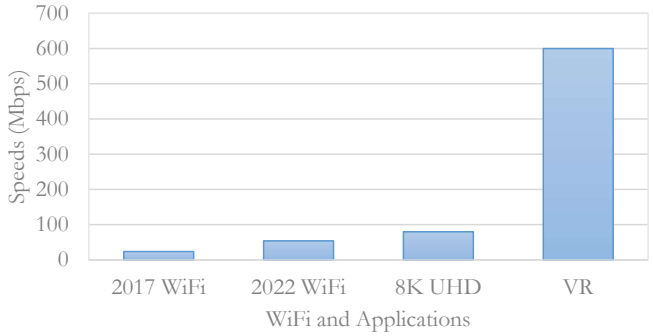

Figure 1.3: Performance Gap

average performance of WiFi and the performance requirements of state-of-the-art applications [1, 4, 5]. The WiFi average performance is predicted to increase from 24Mbs to 54Mbps from 2017 to 2022. While the more than doubling of WiFi performance improvement is significant, the demand for WiFi is still much higher than the WiFi average rate even in 2022. Fig. 1.3 shows the performance of average WiFi speeds and the performance requirements of novel applications. Specifically, 8K UHD video requires at least 80Mbps application throughput; for virtual reality with high quality video, the application for a single user requires 600Mbps, more than 10 times the expected average WiFi speeds in 2022. Clearly, there is a pressing need to boost WiFi performance for supporting desirable services from novel applications.

1.1 WiFi Research Landscape

Due to the dominance and ubiquity of WiFi networks, WiFi performance optimization is an area of active research. Fig. 1.4 shows a high-level research landscape of enhancement in protocols and algorithms for WiFi networks within the last 20 years. In this landscape, the X axis represents the WiFi research scope, including MAC, PHY, system, and environment. The Y axis represents the the time duration of landmark research or landmark implementation. We categorize the optimization methods as standardized and non-standardized, since WiFi standard only defines the PHY and MAC layer-related optimization methods. In environment-wise non-standardized optimization, given a specific environment configurations, AP planning investigates how to identify optimal location for the AP. The size of the circle represents the amount of research in a specific area. The bullet point bellow the circle represents the landmark research or implementation for a specific research area. From the system perspective, there is also research starting to investigate the degree of freedom of mobility to improve WiFi performance. From perspective of the PHY layer, research outcomes related to MCS, beamforming, and MIMO can significantly improve WiFi performance. Because distributed coordinate function (DCF) is utilized in WiFi MAC, contention-based interference is an important research problem, especially in large WiFi networks. Thus, use of an optimization method to mitigate interference can significantly improve WiFi network performance. To replace the traditional distributed MAC, it is possible to optimize Quality of Service (QoS) for WiFi networks or utilized high efficiency centralized MAC for WiFi. In this thesis, the research contribution is primarily within the scope of *mobility optimization* and *interference mitigation*, which are further illustrated in the following section.

1.2 Research Contributions

The research methodology of this work is to perform motivation analysis, design, implement and evaluate proposed algorithms using theoretical, simulation and experimental

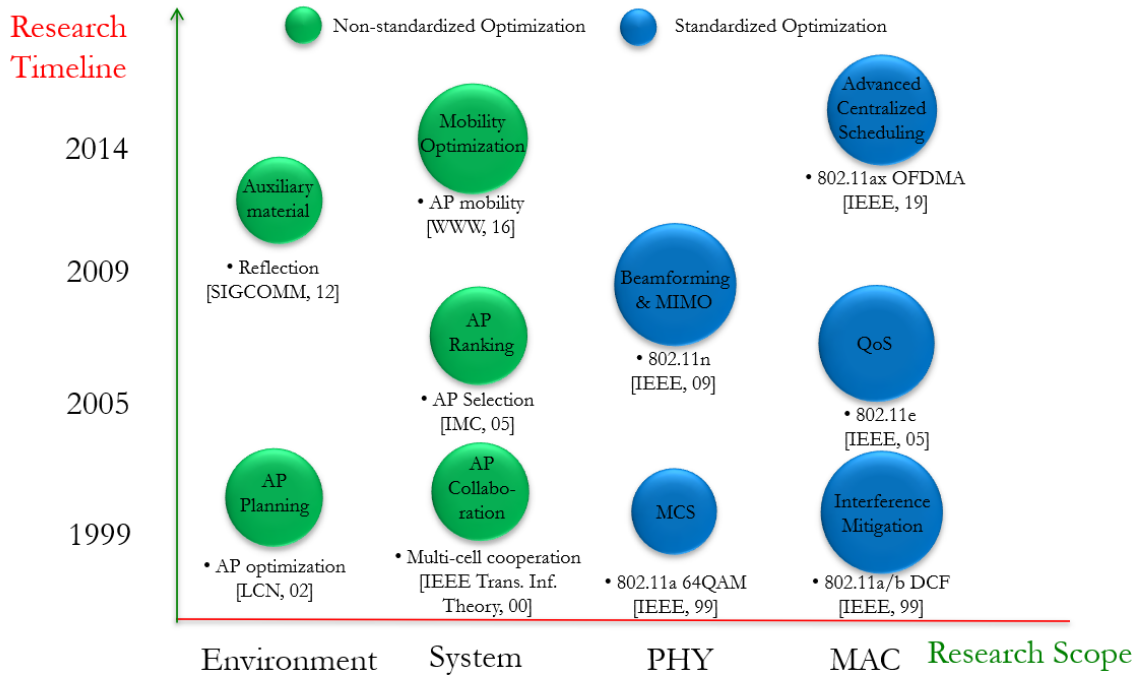

Figure 1.4: WiFi Research Landscape

evaluations. For the research portion of infrastructure mobility, we identified the solution to alter wireless access point's location to provide better wireless channel conditions to optimize the overall network performance for both 2.4/5GHz and 60GHz WiFi. For the second research portion of infrastructure interference mitigation, we designed a central controller which mitigates interference between LTE-U and WiFi to improve the overall wireless spectral efficiency. The detailed research summary is discussed in the following paragraphs.

Harsh wireless channel conditions are a fundamental limitation of network performance. At a high level, harsh channels result in poor wireless signal quality on the receiver side. A better-quality signal results in smaller packet transmission times, which in turn improves overall network performance. In this thesis, we consider the problem of enhancing the robustness of wireless communications using infrastructure mobility; given more freedom of mobility, wireless infrastructures (e.g., access points [APs]) can alter locations to provide better wireless channel conditions to the overall network. To further study in-

frastructure intelligence, we also investigate infrastructure interference mitigation; given a centralized controller, the central controller can mitigate interference from various wireless technologies to improve wireless channel conditions.

The position of a wireless device in a network has considerable influence on the performance of the network, as wireless signal quality at the receiver side heavily depends on physical environmental features. Conventional telecommunication technologies have no ability to improve physical environmental conditions, if necessary. The design of algorithms and protocols for wireless networks is been based on the assumption that the clients are mobile; and the AP, or base station is static. In addition, the client mobility is driven by user needs and behavior, which can potentially degrade network performance. With the recent and significant advancements in wireless communications, robotics, and embedded systems, robotic-based wireless networks can be meaningfully and practically devised to combat the non-robust wireless channel conditions. The concept of robotic wireless networks can be applied in extensive scenarios (e.g., industrial internet of things [IIoT])). Robotic networks have the advantage of mobility, so the wireless channel conditions can be significantly improved from the perspective of infrastructure. In this dissertation, we first consider the application of infrastructure mobility in ultra high frequency (UHF) and super high frequency (SHF), e.g., 2.4GHuz unlicensed band. We observe that movements as small as a few centimeters can result in significant network performance improvements primarily due to the impact of multipath effect and interference. Designing and developing a solution to leverage the possible benefits of infrastructure mobility is a non-trivial problem. First, we must deduce the optimal location of the AP or base station within the physical space that maximizes performance for the network as a whole. Next, we must solve the physical mobility problem of reaching the AP or base station to the deduced location. Further, there is also the condition of whether the theoretically optimal location is reachable in the first place, and; what needs to be done if the answer is no. Thus, we first explore the UHF and SHF infrastructure mobility in this dissertation.

Extremely high frequency (EHF) typically referred as mmWave is an essential enabling technology for next-generation wireless networks. Using a large bandwidth, it can deliver multi-gigabit performance. For example, IEEE 802.11ad operating in the 60GHz unlicensed mmWave band can deliver $\sim$7Gbps performance using a 2160MHz bandwidth. While the performance is quite promising; when compared to UHF and SHF, mmWave is vulnerable to non-line-of-sight (NLOS) conditions. There is an *extremely high signal attenuation* in mmWave communications. The communication performance drops significantly when the wireless link has an obstacle such as a wall or cabinet in its way. For example, if a human blocking the line-of-sight (LOS), there could be an $\sim$30dBm additional path loss for 60GHz mmWave band. Thus, mmWave is especially sensitive to physical channel conditions. In this context, infrastructure mobility provides an attractive degree of freedom for mmWave communication, due to the creation of LOS conditions that can have a profound impact on network performance. In this dissertation, given the significant difference in signal propagation characteristics between EHF and UHF/SHF, we also explore the potential of using infrastructure mobility to improve the LOS conditions for clients within an indoor mmWave network.

Interference is another significant phenomenon that can impact the wireless channel conditions. If multiple wireless links transmit at the same time, there may be an unsuccessful transmission for all wireless links. The unlicensed offloading technique (e.g., unlicensed LTE) has become an essential research direction for cellular networks. The offloading technique aims to assist cellular operators with offloading cellular data from licensed to unlicensed bands. In this context, the unlicensed bands can potentially become even more crowded, leading to more interference. Even worse, centralized medium control protocol (MAC) and distributed MAC are utilized for cellular and WiFi networks. The distributed nature of WiFi MAC makes the traffic patterns of individual client random and unpredictable. The incompatible MAC protocols of cellular and WiFi make it hard for them to coexist without communication guidelines at the system level that ensure fair access to

the spectrum for both technologies while maintaining high efficiency of the channel. If unlicensed LTE and WiFi networks operate in the same spectrum as-is, the throughput of the WiFi network is significantly reduced, because the unlicensed LTE controller, in a centralized manner, attempts to maximize the channel efficiency of the unlicensed LTE network, and allows the unlicensed LTE devices to transmit. The channel is kept busy, and thus, the WiFi devices, due to their distributed nature, can only transmit when the channel is idle. Finally, we also explore an infrastructure interference mitigation algorithm between unlicensed cellular and WiFi technologies to improve channel efficiency.

1.3 Thesis Statement

The already ubiquitous WiFi technology is facing unprecedented pressures on its performance by emerging applications in-spite of newer standards providing for larger bandwidths and spectral efficiencies. Infrastructure mobility is a hitherto unexplored dimension of optimization that can be effectively harnessed to provide significant performance benefits to WiFi networks.

1.4 Thesis Organization

This dissertation is organized as follows. In Chapter 2, we review the related literature review in the domain of wireless performance optimization. In Chapters 3 and 4, we present our contributions to *ultra high frequency (UHF) and super high frequency (SHF) infrastructure mobility* and *extremely high frequency (EHF) infrastructure mobility*, where practical systems and algorithm are designed to optimize the location of WiFi APs. In Chapter 5, we introduce our contributions to *infrastructure interference mitigation*, where a adaptive centralized coexistence algorithm is proposed to solve the coexistence issue between LTE-U and WiFi. In Chapter 6, we discuss some of the existing challenges for the proposed work and present additional research directions.

CHAPTER 2
LITERATURE SURVEY

In this chapter, we will discuss research works related to infrastructure intelligence in the perspective of ultra high frequency (UHF) and super high frequency (SHF) infrastructure mobility, extremely high frequency (EHF) infrastructure mobility, and infrastructure interference mitigation that we consider in this thesis. Specifically, the performance of WiFi in UHF, SHF, and EHF are significantly different from each other. The evolution of WiFi in these bands can be observed from 2.1.

2.1 Infrastructure Mobility in Ultra High and Super High Frequency

For wireless communications, the wireless link performance heavily depends on the physical environment, due to its large impact on both propagation loss and multipath effect (especially for indoor scenarios). Specifically, propagation loss in a wireless network is the attenuation of a transmitted signal as it propagates through a medium to the receiver side. While it happens because of a variety of factors such as penetration loss, absorption, etc., it is strongly inversely proportional to the distance between the transmitter and receiver. There are extensive studies of propagation loss model for various environments, where a particular path loss models can only be applied in limited scenarios. Propagation loss is a dominant component for the link performance of a wireless system. Clearly, given the impact of propagation loss on a wireless system, the shorter the distance between the transmitter and receiver, the better the link performance can be achieved. On top of the propagation loss, multipath has always been identified as an important contributor to the unreliability of wireless links, due to the richness of the multipath effect [6]. For wireless communications, there can exist multiple propagation links between the transmitter and receiver. The reason is that the transmitted wireless signals may be reflected or scattered with respect to various interfaces on its propagation path. The multipath effect is a minor

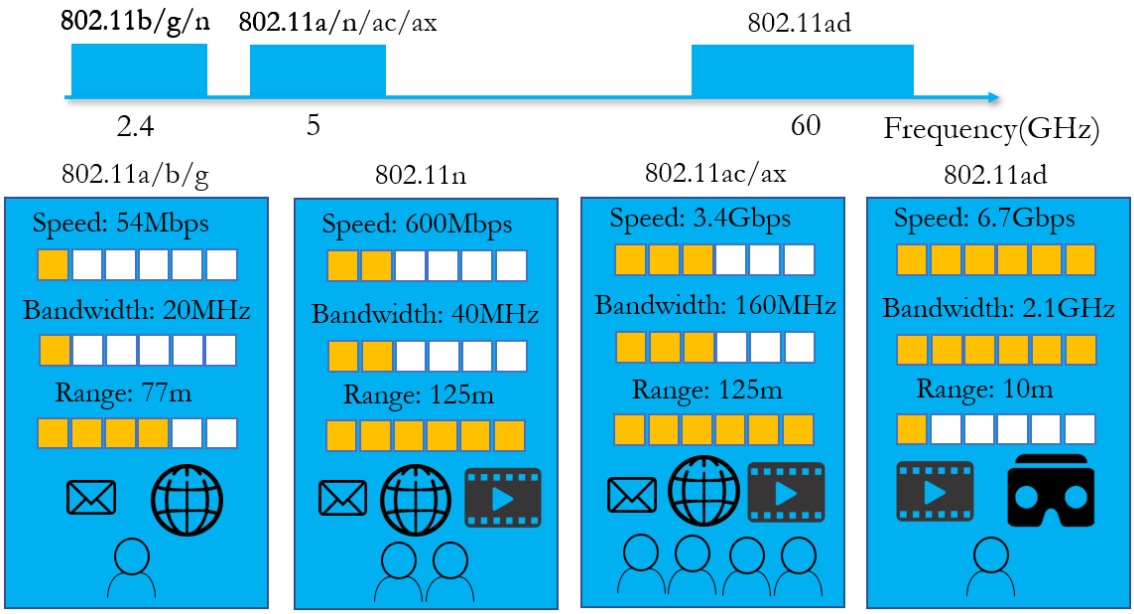

Figure 2.1: **WiFi Evolution**

component for the wireless link performance compared to propagation loss. Explicitly, [7] states that when the distance between two locations is greater than 1/4 wavelength, the phase difference between the responses on the two locations changes by $\pi/2$, which causes a significant change in the overall received signal strength. For a 5GHz signal, the movement of wireless devices between 1/4 to 1/2 of the wavelength translates to movement between 1.5cm to 3cm. More specifically, the movement of a transmitter or a receiver of even several centimeters can appreciably increase the received signal quality [8, 9]. Antenna diversity at both transmitter and receiver sides discussed in [10] is an effective solution to deal with the multipath effect. For indoor UHF and SHF wireless communications, considering the impact of both propagation loss and multipath effect, recent works suggest that the overall path loss prediction can provide decent m. level accuracy.

Due to the recent and significant advances in the domains of robotics, wireless communications, and embedded systems, infrastructure mobility become an attractive solution to combat both multipath and propagation loss issue in both micro and macro level. For example, an affordable and well-performed iRobot Create 2 provides the possibility to control

its floor-based movement through serial communications, where decent movement accuracy could be achieved. Most recently, in [8], the authors present a simple, but effective solution wherein the AP moves within a 4ft.^{2} region and uses an optimal stopping theory (OST) strategy to find the location within that region that would maximize the aggregate throughput performance of the network. They show that the solution can deliver average performance improvements of 70%. In [11], the authors study an approach that improves throughput performance by up to 80% by merely adapting the AP's antenna and base orientations. The method in [11] has a reduced movement complexity while it is possible to achieve meaningful performance improvement. However, this work doesn't suggest an intelligent algorithm other than a brute force search. Other somewhat related works include [12] where robotic APs make adjustments to their positions to converge to an optimum position where client-specific bandwidth requirements can be satisfied, and [13] where positions of antenna elements in a multi-element array are adapted to improve link capacity (with network performance improvements of 98%). [14] present promising results for mobility based mechanisms which can achieve significant network performance improvement by combating multipath effect in a mobile mesh network. Inspired by the previously mentioned works, in this thesis, we design a system, *Hermes*, which first considers both utilizing macro-positioning achieving a communication centroid (CC) to minimize average path loss and maximize average link quality between the AP and clients, and afterward using micro-mobility to combat multipath effect based on the brute force searching. It is also interesting to notice that a similar problem exists for identify a optimized location for facilities. One of the representative problem is named as Weber problem. It requires finding a point in the plane that minimizes the sum of the transportation costs from this point to n destination points, where different destination points are associated with different costs per unit distance. A variety of solutions are proposed to optimize the location of facility in order to achieve customized requirement [15, 16].

2.2 Infrastructure Mobility in Extremely High Frequency

Among the latest advances in wireless communications, mmWave is emerging as an essential enabling technology for the next-generation wireless networks. The key advantage of the mmWave band as compared to UHF and SHF WiFi is the availability of a massive amount of spectrum. However, achieving multi-gigabit performance in a mmWave network is not a trivial problem, since the mmWave signal propagation characteristics significantly differ from that of the UHF and SHF. The major difference is that mmWave communication has *extremely high signal attenuation* [17] generally caused by: 1) high propagation loss: there is an additional signal attenuation of 22dB at 60GHz compared to that of 5GHz based on the free space propagation loss model, and the properties of the propagation media can also significantly increase the signal attenuation (e.g., oxygen absorption at 60GHz); 2) high penetration loss: the attenuation impact is amplified when there is shadow fading or NLOS between the transmitter and receiver pair; and 3) sparse multipath diversity: multipath components propagating through objects tend to have low signal power due to longer propagation paths and additional reflection loss. Note that a consequent advantage of mmWave communication compared with the UHF and SHF is that the high signal attenuation naturally lowers the probability of interference.

As LOS connectivity becomes an essential bottleneck for mmWave communication, there are many research works that can be employed to compensate for the challenging issue. We categorize related works that have addressed the challenges related to LOS connectivity into three types: 1) multi-band, 2) improving channel quality, and 3) establishing indirect LOS connectivity.

For multi-band approaches, the methodology is that mmWave is only utilized for good (e.g, LOS) connections, and the UHF and SHF band is utilized when the mmWave connections experiencing poor propagation (e.g., NLOS) conditions. [18] utilizes localization of tracking angle change to steer the beam to a new location for mobile STAs, and re-direct ongoing user traffic to the robust interface (e.g., from 60GHz to 5GHz). [19] presents a

dual connectivity protocol that enables mobile user equipment devices to maintain physical layer connections to 4G and 5G cells simultaneously. [20] studies the performance of MPTCP over 4G and 5G links and identifies the throughput-optimal combinations of secondary paths and congestion control algorithms in various conditions.

To provide good signal reception between AP and STAs, some possible approaches are: 1) infrastructure mobility [21, 22, 23], 2) multiple APs [24], and 3) relays. Of these, only infrastructure mobility can improve physical channel conditions. For UHF and SHF WiFi, some work has studied mobility based wireless systems to boost WiFi network performance [8, 25]. Other somewhat related works include [12] where robotic APs make adjustments to their positions to converge to an optimum position. Another approach is to deploy more than one AP in a single scenario to increase the probability of LOS between AP and STAs. For the multi-AP based approach, [26] presents an infrastructure side predictive AP switching solution which can identify a proper AP for a specific STA to connect. The third approach is to utilize relays to improve signal quality at the receiver end. [27, 28] presents an optimal and efficient algorithm for choosing the relay-assisted path with maximum throughput. Also, [29] utilizes relays to improve signal quality at the receiver end. Of these, only infrastructure mobility can improve physical channel conditions dynamically.

The third approach is to utilize the indirect LOS connectivity between AP and STA, which typically has a higher requirement in terms of the propagation environment [30, 31]. For example, [30] presents a solution where 60GHz signals can bounce off data center ceilings, thus establishing indirect LOS between any two racks. [32] shows that a wide beam width, low gain antenna at the mobile receiver can capture more energy in scattered NLOS environments and thus, can provide more gain than a narrow beam (high gain antenna) for mobile communication.

2.3 Infrastructure interference mitigation

Innovations in communication technology and densely deployed networks have brought about ubiquitous high-speed broadband access. Such broadband access makes our daily lives increasingly dependent on the Internet for a wide variety of content and services. Internet users constitute over 78% of the population in North America [33], and the mobile service revenue is estimated to become $270 billion in 2016 [34]. The global mobile data usage has grown nearly 70% annually in recent years, and it is expected to increase nearly tenfold between 2014 and 2019 [35]. In order to sustain the possible growth in mobile services, LAA-LTE [35] or LTE-U [36, 37] is emerging as a candidate technology for telecommunication companies to utilize unlicensed spectrum for wireless data traffic offloading. Based on carrier aggregation between licensed and unlicensed bands, LAA-LTE delivers cellular services to mobile users in the 5GHz unlicensed bands. Due to maximum power limitation in unlicensed bands, small cell is an ideal application to operate LAA-LTE. Small cell technology is a promising solution to offload cellular traffic, which can improve the local channel capacity in hot spots compared with macro cell [38]. Thus, combining LAA-LTE with small cell can further relieve the burden of overloaded cellular networks.

As bandwidth has become a precious resource for wireless communications, MAC utilization has always been an important optimization criteria for various wireless communications research problems [39, 40, 41, 42, 43, 44, 45, 46]. Cellular operators intend to offload portions of cellular traffic from the licensed band to the unlicensed band. Among the cellular offloading technologies, unlicensed LTE becomes a practical and fruitful research direction. There are three types of unlicensed LTE has been designed by industrial: 1) LTE-U: without adhering the listen before talk (LBT) policy, it can aggregate both licensed and unlicensed bandwidth in a cellular network; 2) LAA: standardized by the 3GPP in Rel-13, LAA adheres to the LBT requirements to aggregate both licensed and unlicensed bandwidth, which follows the same principle of WiFi distributed MAC protocol;

and 3) MulteFire: operate LTE solely in the unlicensed spectrum without link aggregation with the licensed band, which also adheres to the LBT requirements. Among these technologies, LTE-U does not follow LBT protocols to operate in a distributed fashion. A centralized MAC protocol can be designed for LTE-U, which has the potential to reach the highest channel efficiency among these unlicensed LTE technologies.

As unlicensed band becomes even more crowded, interference mitigation becomes an important research direction for unlicensed band. We will discuss the related research of interference mitigation or coexistence approaches between unlicensed LTE and WiFi herein. Through experimental analysis, [39] shows that LTE operating in the unlicensed band indeed has a significant impact on WiFi performance in various scenarios. [47] introduce coexistence algorithm by implementing a contention based algorithm in LAA, e.g., Listen-Before-Talk (LBT). LBT introduces extra delay due to the contention time overhead, which can lead to inefficient channel usage. [48] proposes a channel selection mechanisms in LTE-U to avoid channel sharing of LTE-U and WiFi. However, if a clean channel is absent, LTE-U has to hold until the channel becomes idle. Qualcomm proposes CSAT, which is based on the ON/OFF duty cycle coexistence mechanism, but no fairness model is considered, and different load condition and hidden terminal problems are out of the scope of CSAT. Other than offloading cellular traffic to unlicensed LTE, offloading cellular data to WiFi networks is another method to relieve the burden of cellular networks. Systems to offload mobile traffic to WiFi network have been introduced in [49]. However, offloading cellular data to WiFi networks can generate extra overhead for system level communications due to the different core networks and backhauls between unlicensed LTE and WiFi.

CHAPTER 3

INFRASTRUCTURE MOBILITY IN ULTRA HIGH AND SUPER HIGH FREQUENCY

The position of an access point (AP) in a WiFi network has considerable influence on the performance of the network. In this chapter, we consider the problem of a WiFi AP self-positioning itself adaptively based on the network conditions to deliver improved network performance. Through extensive experimental evaluation, we show that there are indeed significant performance benefits to be attained by allowing the AP to move intelligently. We also rely on theoretical analysis, simulations, and experimental studies to show that the AP optimal location search problem can be split into two parts: a macro-search problem to minimize average path loss between AP and clients, and a micro-search problem to tackle real-time multipath fading effects. We then present *Hermes*, a self-positioning WiFi AP system that relies on a suite of algorithms to compute and then move to an optimal location within the network. Using a prototype implementation, we show that *Hermes* can perform up to 117% better than WiFi with no AP mobility, and up to 73% better than related work that allows for AP mobility.

Historically, the design of algorithms and protocols for wireless networks has been based on the assumption that the clients are mobile and the AP is static. The client mobility, furthermore, is driven by user needs and behavior as opposed to optimizing the network performance. In this work, we consider the problem of an AP positioning itself dynamically based on the network conditions to deliver improved network performance. Recent and significant advances in domains such as wireless communications and robotics have made it possible to meaningfully and practically devise a solution for a self-positioning AP system. An obvious question to ask before developing such a solution is the following: *are the benefits of AP self-positioning significant enough to warrant the potential overheads and complexities?* Through a detailed experimental analysis, we identify that even move-

ments as small as a few centimeters can result in network performance improvements up to 116%. However, designing and developing a solution to leverage the possible benefits is a non-trivial problem. First, the optimal location of the AP within the physical space that maximizes performance for the network as a whole has to be first deduced. Second, the physical mobility problem of reaching the AP to the deduced location has to be solved. Further, there is also the condition of whether the theoretically optimal location is reachable in the first place, and what needs to be done if the answer is no.

This is not the first paper to identify or leverage the benefits of AP mobility. Most recently, in [8], the authors present a simple, but effective solution wherein the AP moves within a 4ft.^{2} region, and uses an optimal stopping theory (OST) strategy to find the location within that region that would maximize the aggregate throughput performance of the network. They show that the solution can deliver average performance improvements of 70%. In [11], the authors study an approach that improves throughput performance by up to 80% by simply adapting the AP's antenna and base orientations. The approach in [11] has a reduced movement complexity while achieving meaningful performance improvement. Other somewhat related works include [12] where robotic APs make adjustments to their positions to converge to an optimum position where client-specific bandwidth requirements can be satisfied, and [13] where positions of antenna elements in a multi-element array are adapted to improve link capacity (with network performance improvements of 98%).

At a high level, the key contribution of this paper is the systematic study of the self-positioning problem when the AP has both large-scale and small-scale mobility. When the scope of AP mobility is expanded, there is a search space complexity problem that has to be handled. In other words, if a 2D search space is R square units, and the possible granularity of mobility is r units, the number of potential search locations is $(\frac{R^{0.5}}{r}+1)^2$. For a typical room of 16m^2 size, the number of search locations could vary from $50,000$ to $250,000$ depending for search granularities of 5cm and 1cm respectively. We address the search complexity problem by showing that it can be split into a macro-search problem

to optimize network performance based on the *path loss* phenomenon, and a micro-search problem to further optimize network performance based on the *multipath* phenomenon. This significantly reduces the complexity of search and makes AP self-positioning solvable.

The specific contributions we make are as follows:

- We first use an extensive set of experimental results to show the benefits of AP self-positioning under a variety of conditions spanning from different environmental characteristics to different network configurations. We use these results to show that AP self-positioning is an attractive strategy to achieve performance improvements within WiFi networks.

- We rely on systematic experimental analysis using WiFi APs, WiFi clients, an *anechoic chamber*, a *Tolomatic Programmable linear actuator*, and an *iRobot Create 2* and theoretical analysis to show that the AP location search problem can be split into two subproblems: a macro-search problem to tackle path loss and a micro-search problem to tackle multipath.

- We then present *Hermes*, a self-positioning WiFi AP system that relies on a suite of algorithms to compute and move to an optimal location of the network. Based on the location of clients, we introduce the notion of a **communication centroid (CC)** that is akin to the geometric median but adapted for the path loss exponent. *Hermes* relies on the CC to solve the macro-position problem[1]. It then relies on a brute-force search algorithm at the CC to perform fine-grained adaptation to solve the micro-search problem. Then, we utilize ns-3 and MATLAB simulations to further analyze the algorithm performance of *Hermes*.

- Using a prototype implementation, we show that, on average, the proposed suite of algorithms can perform up to 117% better than default WiFi with no AP mobility, and up to 73% better than related work that allows for AP mobility.

[1] Although [9] identifies the macro-search problem, it simply searches for the optimum position (maximum throughput) and does not specify how to systematically or theoretically derive the optimal macro position.

Figure 3.1: A self-positioning AP system

3.1 Motivation Analysis Methodology

In this section, we first provide experimental analysis results to illustrate the potential benefits of *AP position diversity*. We conduct **8** sets of experiments to investigate the benefits of self-positioning AP under various network conditions.

3.1.1 System Overview

Fig. 3.1 shows a self-positioning AP system, with an AP and a laptop mounted on a robotic platform. The main components of this system are as follows: 1) *Netgear AC 2350* AP, 2) *iRobot Create 2* robotic platform [50], and 3) *Lenovo Y410P* controller. *iRobot Create 2* carries both the AP and the controller, in order to enable the movement capability of the AP. A *MATLAB* toolbox provided by [50] is used by the controller to control the movement of the robot through serial communications. To monitor the AP's performance, the controller is connected to the AP via an Ethernet cable.

3.1.2 Methodology

The major goal of this section is to identify the gain of *AP position diversity* under the following **7** sets of experiments: 1) 2D Locations, 2) Spectrum, 3) 2D vs. 3D Locations, 4)

Traffic Direction, 5) Multiple Clients, 6) Wireless Backhaul, and 7) Anechoic Chamber.

Metrics: The main metric we focus on is the **aggregate throughput** between AP and clients. The traffic and corresponding throughput is controlled and measured by *Iperf3* [51]. The throughput is measured over a period of 20s, and an average result is obtained over three 20-second periods. We present the gain based on the following formula:

$$Average\,Gain = \frac{Max(throughput_i)}{\sum_{i=1}^{x} throughput_i/x} \tag{3.1}$$

where, i represents AP located at position i, and x is the total number of tested AP locations. More specifically, for every single set of experiment, the maximum throughput represents the achievable optimum throughput as a result of the advantages brought by *AP position diversity*.

Experimental Settings: We categorize the AP's location into the following two types: 1) *Standard location*: AP is located at the corners or the center of a room; 2) *Intelligent bad location*: If obstacles (with a minimum size of $0.2625m^3$ and a minimum penetration loss of ˜15dBm) prevent Line-of-sight (LoS) condition between AP and its clients, we define the corresponding AP location as an intelligent bad position.

To validate the benefits of *AP position diversity* in different indoor scenarios, three different environments are chosen; namely, a research lab (58.5 m^2), an apartment (62.5 m^2), and a classroom (119 m^2). Since these scenarios are presented in uncontrolled environments, the experiments are predominantly performed during the night and over the weekends so as to avoid dynamic channel conditions caused by dynamic environments or interference (e.g. unpredictable neighboring WiFi traffic and people moving around). For each set of experiment, we test the throughput performance at 5 *intelligent bad locations* and 5 *standard locations* (4 corners and 1 center of the room). For all the experiments, clients are placed within 10m away w.r.t. the AP. The default experimental parameters are listed in Table 3.1. If not otherwise mentioned, the experimental settings follow Table 3.1. In the interest of brevity, we present only a subset of all the experimental results and focus

Table 3.1: Default Experimental Settings

	Default Settings
AP	Netgear AC 2350
Client	Lenovo Y700
Client Number	1
Traffic Direction	Downlink
Transport Protocol	UDP
Experimental Scenario	Apartment
WiFi Spectrum	5GHz

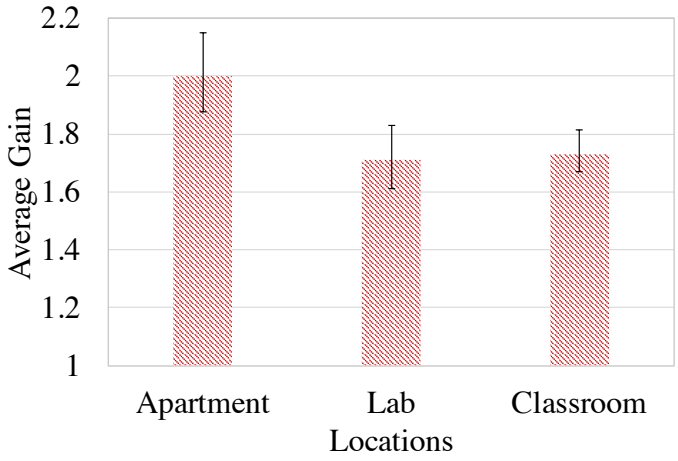

Figure 3.2: 2D Locations

on the most important conclusions.

3.1.3 Evaluation Results

2D Locations: Here, we vary the AP's location to identify its impact on the network performance. To vary the AP's location, we follow the AP location categories identified in Section 3.1.2. The AP is placed at 5 standard and 5 intelligent bad locations. The throughput between the AP and its client is measured at the 10 AP locations.

Fig. 3.2 illustrates the *Average Gain* as the AP is located at the aforementioned 10 locations. It can be observed that the ideal AP location provides *Average Gain* of almost 2x. More specifically, the average throughput is 159Mbps, and the optimal throughput is

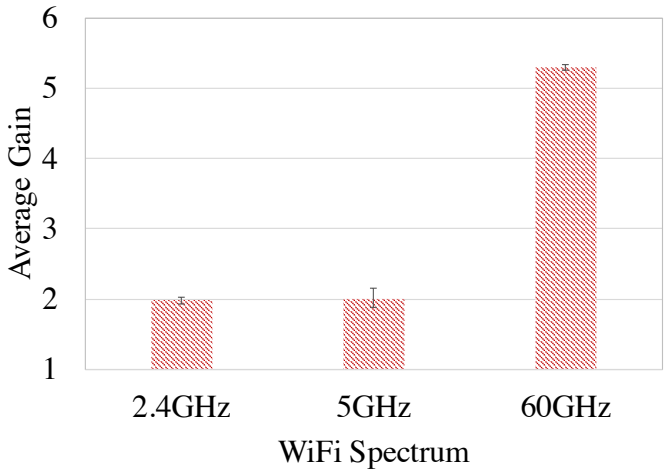

Figure 3.3: Spectrum

320Mbps. Also, 2D *AP position diversity* can achieve more than 1.7x *Average Gain* in all three environments, which validates the fact that the location of the AP does have a large impact on the network performance. Additionally, the gain without considering the intelligent bad location is 1.5x on an average as a result of *AP position diversity*. We can also identify that the throughput improvement brought by *AP position diversity* is very site-specific. *This experiment indicates AP position diversity promises significant benefits, as the AP moves in a 2D plane.*

Spectrum: Here, we investigate the performance benefits of *AP position diversity* when WiFi carrier frequency varies among 2.4GHz, 5GHz and 60GHz. The experimental methodology is the same as the 2D locations experiment methodology. For 2.4GHz and 5GHz bands, we follow the default devices configurations given in Table 3.1. For the 60GHz experiment, we utilize a *TP LINK AD7200* as AP, and an *Acer TravelMate P648-M-59KW* laptop as client.

Fig. 4.1 shows 2x, 2x, and 5.3x *Average Gain* as a result of *AP position diversity* for 2.4GHz, 5GHz, and 60GHz, respectively. There is no difference between the *Average Gain* of 2.4GHz and 5GHz. Since 2.4GHz and 5GHz spectrum are close to each other, there is no significant difference in signal propagation characteristics. However, *AP position diversity* is able to provide 5.3x performance improvement for 60GHz (mmWave spectrum). The

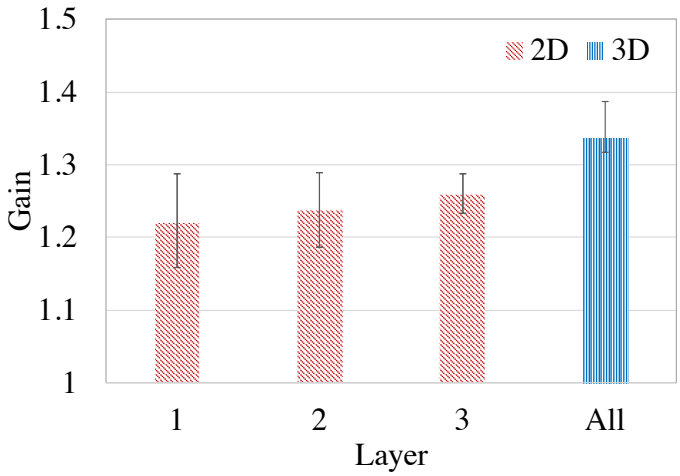

Figure 3.4: **2D/3D Locations**

major reason is that both propagation loss and penetration loss of mmWave signals are significantly higher than that of 2.4GHz and 5GHz [52]. Additionally, the gain without considering the intelligent bad location is 1.6x, 1.7x, and 2.7x as a result of *AP position diversity* for 2.4GHz, 5GHz, and 60GHz, respectively. It reveals the fact that location (especially, LoS condition) matters substantially for mmWave. *The key observation here is* AP position diversity *is a significantly promising application for mmWave.*

2D vs. 3D Locations: From the 2D locations experiments, it can be seen that *AP position diversity* can bring significant network performance improvement. Here, we additionally study the impact on network performance while moving the AP in a 3D space. We construct the experiment using a 3-layer platform with size $1 * 1.25 * 1.75 \text{m}^3$. The AP can be placed on any layer of this platform, where AP is in LoS or Non-LoS (NLoS) with its client on layer 3 or layer 1 and 2, respectively. The AP is placed at 9 different positions on each layer. The gain of 3D locations is defined as the maximum throughput identified from all 3 layers divided by the lowest average throughput among 3 layers. The similar concept is applied for the gain of 2D locations, where maximum and lowest throughput is constrained within a specific layer. Fig. 3.4 presents the comparison results as the AP location varies in a 2D plane or a 3D space; the performance improvement ranges from 1.22x to 1.33x. Even though moving the AP in a 3D space can provide LoS conditions

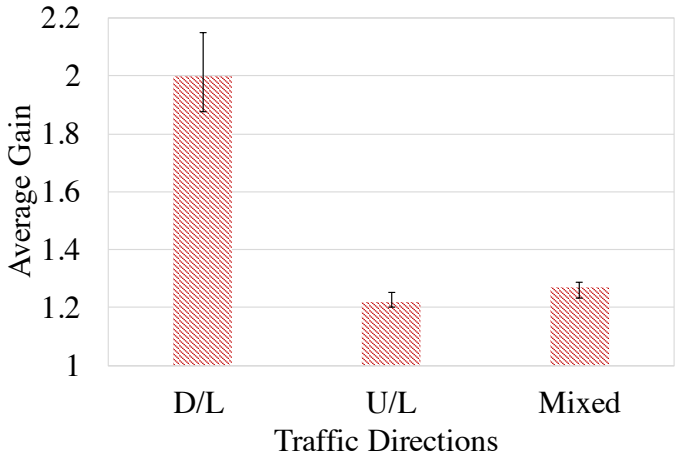

Figure 3.5: **Traffic Direction**

in this set of experiment, the 3D movement does not achieve significant improvement as compared with 2D movement. The first reason is that 3D movement (allowing an additional z-axis change for AP position) does not significantly change the distance between the AP and the client. Thus, the 3D movement does not have a notable impact on the path loss. Another reason is that multipath can be mitigated with either 2D or 3D movement of an AP. *This experiment indicates that the AP's 3D movement does not provide considerable benefits over AP's 2D movement regarding reducing path loss or mitigating the multipath effect.*

Traffic Direction: Here, we investigate the benefits of *AP position diversity*, when the traffic direction varies among uplink (UL), downlink (DL), and hybrid of UL and DL.

Fig. 3.5 presents the *Average Gain* for the various traffic directions. Intuitively, it would be expected that the *Average Gain* for DL and UL traffic condition is similar due to channel reciprocity. However, in the experimental results, the *Average Gain* for DL traffic is much higher than the *Average Gain* of UL. The reasons are: 1) different features of network interface controller (NIC) of AP and client (e.g., transmission power), 2) different multipath characteristics of UL and DL, and 3) different interference characteristics (e.g., hidden terminals). *This experiment implies that channel reciprocity cannot be assumed for WiFi networks.*

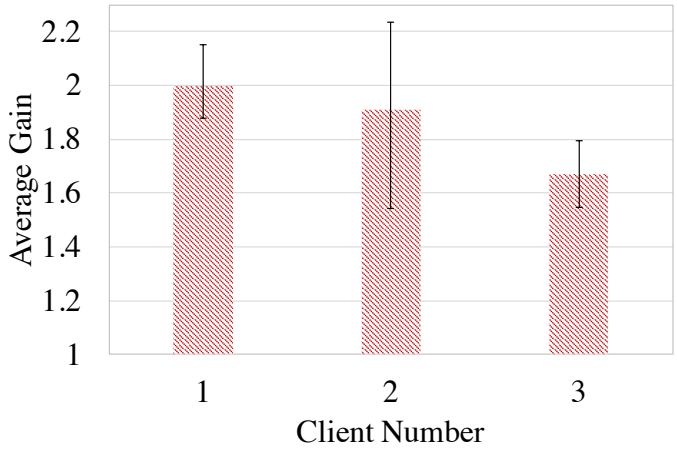

Figure 3.6: **Number of Clients**

This indicates that maximizing SNR from clients proposed in [8] at the AP side may lead to biased channel condition for uplink and downlink. Fig. 3.5 presents the experiment results as the experiment are conducted in the classroom environment. Clearly, *AP position diversity* can improve network performance with more than 1.7x *Average Gain*. Again, the difference between classroom experimental results and home experimental results indicate the *Average Gain* of *AP position diversity* is very site-specific. This further indicates the necessity for developing an intelligent AP self-positioning algorithm to identify the optimal position in different scenarios.

Multiple Clients: In this section, we will identify the *Average Gain* as the number of clients varies from 1 to 3 (clients selection priority: *Lenovo Y700* > *Dell E6520* > *MacBook Air*).

In Fig. 3.6, the *Average Gain* is more than 1.6x, as the client number varies from 1 to 3. We can also observe that the performance improvement decreases as the number of client increases. When the AP is located at a standard location, the overall network performance of multiple clients scenario is likely to perform better than the single client scenario. The major reason is that there is a higher probability that the AP will have good channel condition between itself and any of the clients, which in turn leads to slightly

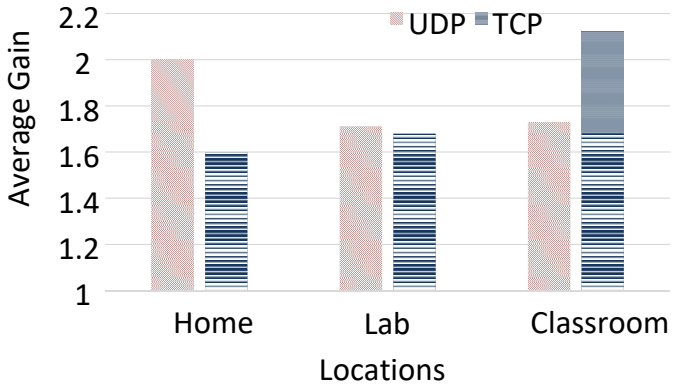

Figure 3.7: Transport Protocol

higher overall performance at standard locations for multiple clients scenario. Thus, the *Average Gain* of multiple client scenarios decreases compared with single client scenario. For multiple clients scenario, it is not trivial to identify the optimum position for AP. It indicates the necessity for developing an intelligent AP self-positioning algorithm. *This experiment indicates there can also be significant performance improvement of AP position diversity for multiple clients scenario.*

Transport Protocol: The performance benefits of *AP position diversity* is investigated when different transport protocols are utilized, viz. TCP and UDP. Here, we show the experimental results for scenario with 3 clients.

In Fig. 3.7, the results from the three scenarios show that the average aggregate throughput for TCP and UDP is 201Mbps and 169Mbps, respectively. The reason for TCP showing better throughput performance than UDP, is that the packet loss rate of TCP is lower than UDP. In TCP, the congestion window of the link with the best channel quality increases faster than other links. The link with best channel quality also has lower packet error rate and higher modulation rate. The more packets are transmitted through the link with the best channel quality (with higher and increasing congestion window), the higher the aggregate TCP throughput can be achieved. From the TCP experimental results, the average throughput of the link with the best channel quality is 107Mbps, which is 53% of the average aggregate throughput. It also indicates that unfairness is more likely to happen for

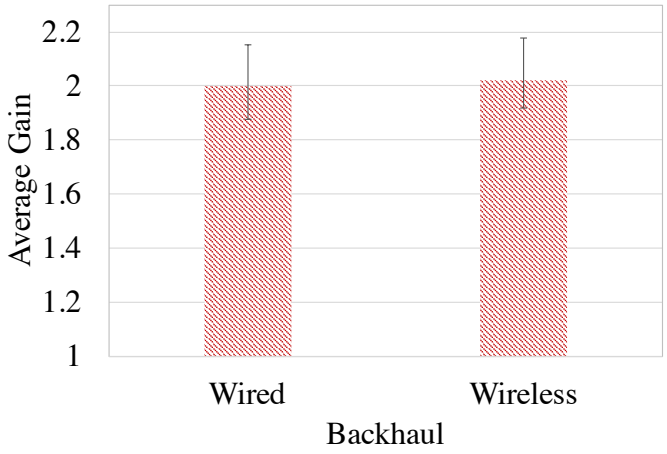

Figure 3.8: Wireless Backhaul

TCP. *This experiment implies the unfairness problem can be relieved by AP mobility (e.g., by moving the AP to a location where the channel condition between AP and each client is similar).*

Wireless Backhaul: The key advantages of wireless backhaul (from the AP to the backbone) are to eliminate the Ethernet cable physical constraints of a self-positioning AP, and to extend the boundaries of the AP's transmission and movement range. A specific application case is embedding the self-positioning functionality in household robots to improve corresponding network performance. Also, we consider such a scenario due to its promising application by providing LoS condition in ad hoc fashion mmWave networks.

To conduct this experiment, we utilize a *Dell E6250* to mimic wireless backhaul and a *Lenovo Y700* as a client. The minimum throughput of the link from wireless backhaul to AP and the link from AP to the client is defined as the performance metric for wireless backhaul. We utilize the performance of wired backhaul AP as the baseline. The position of AP is varied among the aforementioned 10 locations (with a fixed client and the wireless backhaul in this set of the experiment).

From Fig. 3.8, it can be observed that *AP position diversity* can provide around 2x throughput improvement for both wireless and wired backhaul. Here, *AP position diversity* can provide significant *Average Gain* improvement for both wireless and wired backhaul.

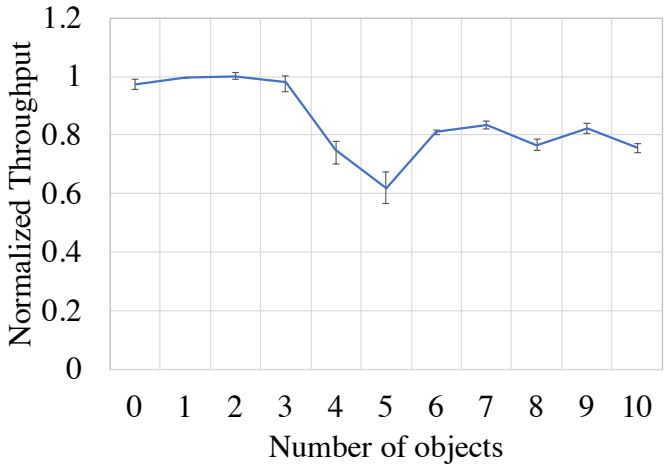

Figure 3.9: Multipath Effect

The *Average Gain* of wireless backhaul is slightly higher than that of wired backhaul. Theoretically, *AP position diversity* matters more in wireless backhaul scenario, since both links are impacted by the location of AP. Either of the links with bad channel condition can limit the performance of wireless backhaul. *The results from this experiment indicate that the benefits of AP position diversity can also be attained in wireless backhaul scenarios.*

Anechoic Chamber: In an effort to have a fully controlled environment, the following experiments were performed in a $4\ m^2$ anechoic chamber. The anechoic chamber is equipped with 90dBm attenuation walls which are used to eliminate any outside interference. Also, the inside of the anechoic chamber is fully covered with radio absorption materials to eliminate multipath. Thus, this chamber provides an ideal environment with no dynamic channel conditions or multipath effects.

Multipath effect investigation: The AP movement of even a few centimeters can appreciably increase the received signal quality due to multipath [6, 9]. More specifically, for WiFi networks, multipath can have a large impact when the signal quality change resulted by multipath leads to the change of modulation and coding rate due to signal quality achieving various minimum sensitivity requirements. Here, our methodology is to put various numbers of metallic objects (with a minimum size of $0.005m^3$) in the chamber to simulate scenarios with different multipath conditions. Fig. 3.9 illustrates how networks

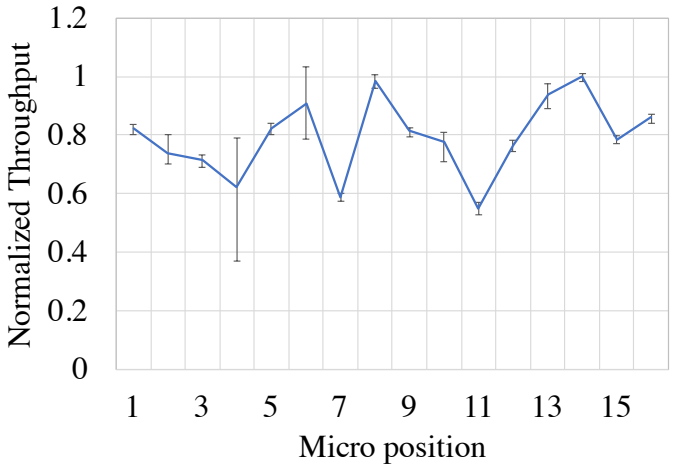

Figure 3.10: **Micro-Mobility**

are impacted by different multipath conditions. As can be seen from Fig. 3.9, when no object is in the chamber, the throughput is at its maximum. As the number of objects inside the chamber is increased, the throughput varies significantly. E.g., for five objects, throughput drops to 60% of the maximum throughput. *It can conclusively be seen that the multipath has a large impact on the network performance.*

Micro-mobility investigation: Here, the number of objects in the anechoic chamber is fixed as 4. The micro-positioning is achieved by changing the position of the AP with an interval granularity of 2cm. As can be seen from Fig. 3.10, micro-positioning can introduce significant performance impact for throughput performance in an ideal environment, which further indicates interference is not the major reason which leads to performance variance for all the experiments. *Here, we observe that micro mobility of AP has a large impact on the network performance.*

To further analyze the micro-mobility impact, We evaluate the network performance with 12 different base orientations that are obtained by rotating the AP with a 30step size belonging to the set: {0,30,...,330}. From Fig. 3.11, changing only the base orientation can improve the network performance up to 1.5x. Also, it is clear that the performance improvement varies across the different scenarios. This can be attributed to the fact that multipath is very site-specific. Thus, slight changes in the AP base orientation can result in

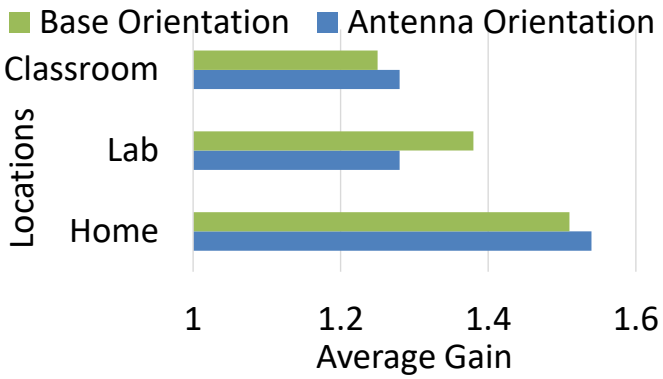

Figure 3.11: **Base vs. Antenna Orientation**

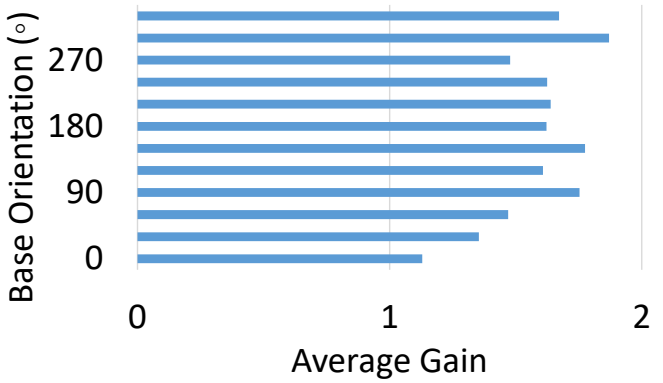

Figure 3.12: **Joint Orientation**

promising network performance improvement and different variances on the average gain for different scenarios.

There are 4 antennas, and each antenna has a 45or a 90antenna orientation configuration; there are therefore 16 different antenna orientation configurations for which the network performance is investigated. Similar to the results of changing base orientation, changing the antenna orientation is capable of improving the network performance up to 1.5x as shown in Fig. 3.11.

The impact of changing both the antenna and base orientation is also evaluated. We evaluate the network performance in the lab environment with 12 different base orientations, and at each base orientation, we evaluate 16 different antenna orientations; for a total of 192 different configurations. The average gain is calculated as the ratios of the maximum

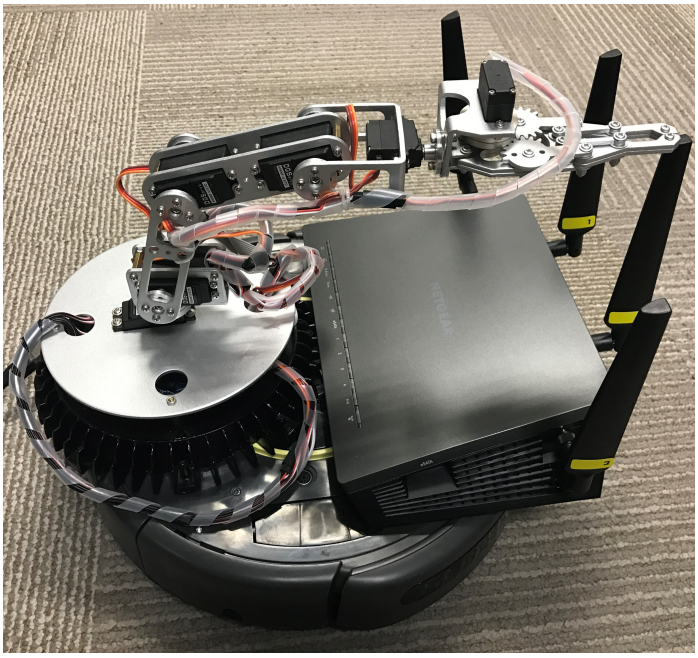

Figure 3.13: **Robotic Platform**

throughput of all 192 configurations over the average throughput for each base orientation. Fig. 3.12 shows that Twirl can deliver network performance improvement of up to 1.8x.

The results show that the network throughput performance can be improved by as much as 1.8x through simply adapting the orientation of the AP. This is comparable to the improvement achieved by AP relocation [8]. This indicates that multipath effects can be mitigated without physically relocating the AP using large-scale movement. The results also indicate the promising potential of orientation adaptation of AP.

Summary: We investigated how *AP position diversity* can improve *Average Gain* in various network scenarios. It was found that *AP position diversity* provides significant network performance improvement, ranging from 1.22x to 5.3x on an average. It is also worth to notice that spectrum efficiency is also improved as *Average Gain* increases. Additionally, the maximum throughput improvement observed is up to 52.8x. Thus, the results clearly motivate further investigation on how to utilize the benefits brought by *AP position diversity*. The experiments presented in this section are conservative (tested with a limited number of locations), and hence the optimum network performance can be even higher. It is also

worth to note that *AP position diversity* is indeed a promising application for mmWave, due to the harsh channel conditions of mmWave.

3.1.4 Problem Statement and Scope

The problem addressed in this paper is to determine the optimal location for a self-positioning AP system where the network performance is optimized, and how to practically reach the optimal location. For the initial study of a self-positioning AP system, the scope of the problem investigated is the following: (i) Non-mmWave spectrum (e.g., 5GHz) is considered. (ii) A single AP scenario is considered.

3.2 Design Basics

3.2.1 A Case for Hierarchical Mobility

WiFi networks have many degrees of freedom with regard to providing different network services based on various network conditions or user requirements, including automatic modulation control and transmission power control, etc. This work seeks to provide current WiFi networks with an additional degree of freedom -*AP position diversity*. The key argument that we make in this paper is that the impact of the AP location on the network performance is actually related to a juxtaposition of two different phenomena - path loss and multipath. *We posit that the search complexity problem can be tackled by decoupling the two phenomena, and solving them independently*. The first step is to find the optimal macro-position of the AP so that the average path loss between AP and client is minimized. Upon reaching the optimal macro-position, the second step involves performing a brute force search to find the optimal micro-position. We now theoretically and quantitatively validate our argument.

Macro-mobility:

Path loss in a network is the attenuation of a transmitted signal as it propagates through a medium. While it happens because of a variety of factors such as penetration loss, absorption, and propagation loss, it is strongly inversely proportional to the distance between

Figure 3.14: **Throughput**

the transmitter and receiver. The goal of this part is to establish that adapting AP based on path loss phenomenon through macro-mobility will improve network performance. To model the path loss between AP and clients, we utilize a widely accepted log-distance based path loss model as shown in Equation 4.11 (the impact of shadow fading on the self-positioning system will be discussed in Section 3.4). Traditional log normal shadowing model and, more recently, advanced practical indoor path loss model [53] are based on the log-distance path loss model. Path loss exponent is a key parameter in this model, which can be roughly estimated based on scenario type or accurately calibrated using the Cayley-Menger determinant based algorithm [54].

$$Path\ Loss = PL_0 * (\frac{d_i}{d_0})^{n_i} \tag{3.2}$$

where, d_i, PL_0, and n_i is the distance between AP and client i, the path loss at the reference distance d_0, and path loss exponent between AP and client i, respectively.

Here, we intend to minimize average path loss between AP and clients which can maximize average link quality. Average link quality is an important metric for WiFi networks because any link in WiFi networks with low-quality consumes extra transmission resources (e.g., time) due to its low modulation and coding rate. Utilizing low modulation and coding

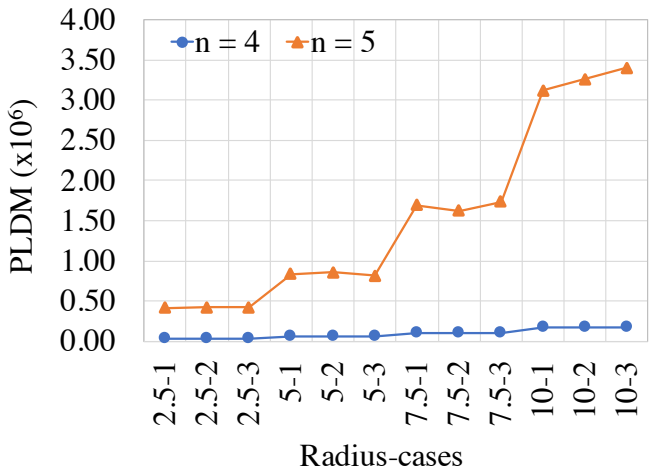

Figure 3.15: PLDM

rate will not impact the distributed coordination function MAC algorithm of WiFi networks. Thus, from the MAC perspective, low-quality WiFi links have the same transmission opportunity as high-quality WiFi links. Also, considering DL transmission in WiFi networks, low-quality links may even need to retransmit due to transmission failure. In such case, AP increases its contention window and waits extra time to complete the transmission which leads to even worse spectrum efficiency (while other high-quality links also need to wait for the completion of the retransmission). Based on the above discussion, we intend to minimize the average path loss between AP and clients to maximize average link quality. To minimize average path loss, we use a simplified metric - path loss distance metric (PLDM) ($\Sigma d_i^{n_i}/k$), where k is the total number of clients. Average path loss between AP and clients are minimized when PLDM is minimized since PL_0 and d_0 in Equation 4.11 are constant parameters.

In the macro-mobility experiment, 3 clients are located on the arc of a circle with 10m radius in the lab scenario. The clients are placed equidistant on the circle. We change the position of the AP from the center of the circle to positions along concentric circles with different radii - 2.5m, 5m, 7.5m, and 10m (3 different AP locations on each concentric circle are tested). The experiment also follows the experimental methodology of Section 3.1. From Fig. 3.14, it can be identified that as the AP moves away from the center, the network

exhibits lower performance. The macro optimal location is the center of the circle, and at that point, the PLDM is also minimized (with the path loss exponent n_i is estimated as 4 for each client). The results indicate the macro-position has a significant impact on the overall network performance, and specifically, minimizing PLDM improves network performance. Fig. 3.15 shows how the PLDM changes across with different path loss exponent for the 3 clients scenario. It can be observed that there is a strong inverse relationship between the PLDM and throughput, thus further motivating the idea of minimizing the average path loss between AP and clients. Fig. 3.14 also shows the minimum and maximum throughput amongst 5 micro-positions (with 2cm granularity between adjacent micro-positions) tests at each of the macro-positions; this shows that further performance improvement can be achieved through micro-adjustments which will be further analyzed in next section.

Micro-mobility: In an effort to encompass micro-mobility of a self-positioning AP system, the granularity by which the AP moves needs to be determined in the first place. Identifying a desired micro search granularity interval is important for reducing the search cost and complexity. Any practical self-position AP would need to find an optimal solution in reasonable time while still ensuring satisfactory network performance improvement.

Related works have suggested that multipath will have an impact if the movement distance is greater than 1/4 to 1/2 of the wavelength of the transmitted signal [14, 7]. In particular, [7] states that when the distance between two locations is greater than 1/4 wavelength, the phase difference between the responses on the two locations changes by $\pi/2$, which causes a significant change in the overall received signal strength. This implies that movement of the AP between 1/4 to 1/2 of the wavelength is sufficient to mitigate multipath. For a 5GHz signal, the movement of an AP between 1/4 to 1/2 of the wavelength translates to movement between 1.5cm to 3cm. To validate this claim, we perform experiments that involved moving the AP by small intervals and measuring throughput between the client and AP. The AP was moved by the granularities of 0.5cm, 1cm, 2cm and 3cm using the *Tolomatic Programmable linear actuator* shown in Fig. 3.18. The actuator system

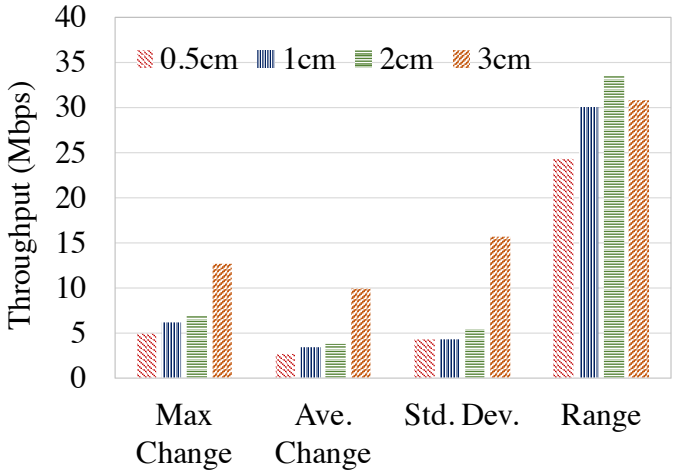

Figure 3.16: **Granularity Statistics**

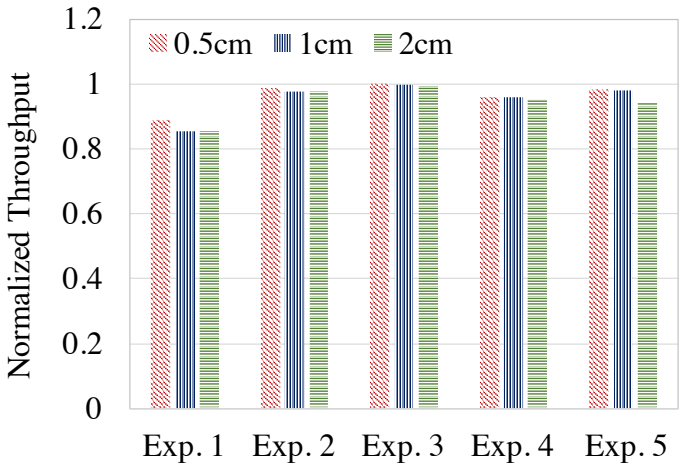

Figure 3.17: **Optimum Throughput**

allows mobility along the x, y, and z axes, and ensures micro-mobility with an accuracy of 3.175 μm. The throughput at each point was evaluated for movements of up to 10cm in x and y axes, and 6cm along the z axis (with a physical limitation of 6cm along the z-axis).

In this granularity experiment, a single client scenario is considered with 5 different client location settings. A 0.5cm interval movement means that the AP moves with an interval of 0.5cm in the x, y and z directions in a $2.5*2.5*2.5\text{cm}^3$ cube, which equates to 216 points. Similarly, for 1cm, the AP moves in a $5*5*5\text{cm}^3$ cube with 216 points. To fairly compare the performance for the different intervals, a rectangular prism with dimensions

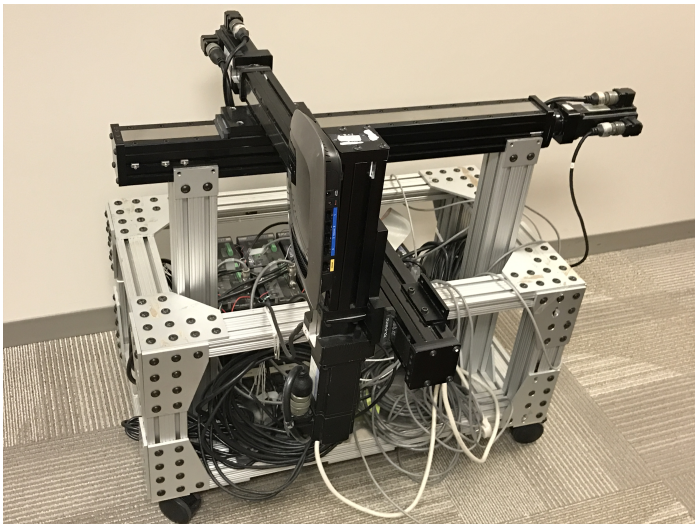

Figure 3.18: Tolomatic Actuator System

$16*10*6\text{cm}^3$ for the 2cm interval, and $24*21*6\text{cm}^3$ for the 3cm was evaluated by moving the actuator. This ensures that there are 216 points in the cube at which measurements can be made for various granularity.

The standard deviation, range, as well as maximum and average changes between adjacent points, are shown for the different intervals of movement in Fig. 3.16. The maximum and average changes as shown in Fig. 3.16 are obtained by calculating the difference in throughput for each point in space and all adjacent points near it. For example, if we imagine a 3D coordinate system, then at point (1,1,1), all adjacent points with a granularity of 1cm is (0,1,1), (2,1,1), (1,0,1), (1,2,1), (1,1,0) and (1,1,2). The range is calculated as the maximum throughput value subtracted by the minimum throughput value obtained within the entire search cube. From Fig. 3.16, the standard deviation increases as the granularity increases. There is, however, a significant increase in the standard deviation for a granularity interval of 3cm, which indicates significant impact by multipath can be observed for 3cm granularity. Also, the range metric can achieve up to 33.6Mbps within a small searching cube with the interval movement of 2cm. The maximum and average change of the throughput between adjacent points for the different intervals further seeks to verify the claim that micro-mobility makes a notable impact on the network performance. The results

shown in Fig. 3.16 effectively substantiate that moving the AP, by intervals of as small as 3cm, has a considerable impact on the throughput performance.

It is obvious that the smaller the interval by which the AP is moved, the larger the likelihood of finding the optimum position. However, there is a trade-off between the time spent searching and the highest throughput obtained. As shown in Fig. 3.16, a movement of 3cm causes a large performance variation which may lead to missing the optimal location. Therefore, movement intervals of less than 3cm should be considered for 5GHz signal. Moving the AP with intervals of 0.5cm, 1cm and 2cm yields the results shown in Fig. 3.17 for 5 different client positions. The highest throughput obtained is for a search space that is exhaustively searched for an interval of 0.5cm. However, the optimum throughput value obtained when searching with a granularity of 0.5cm, is on average approximately 1.03% and 2.08% higher for granularities of 1cm and 2cm, respectively. This means that a micro-search with a granular interval of 2cm reduces the search time by 75% while having a minimal impact in identifying the optimal position. The interval of 2cm is in line with the notion that the movement of the AP of between 1/4 and 1/2 of the wavelength is sufficient for significant impact through multipath.

3.2.2 CC and Brute-force Search

CC: For the macro-search problem, we consider optimizing the path loss phenomenon for WiFi networks. We, therefore intend to minimize the average path loss between an AP and clients. As the average path loss is minimized, the average link quality is then maximized. We term this optimal macro position as *CC*. The CC is related to the geometric centroid in that the latter minimizes the average distance to a given set of vertices. Here, CC is adapted with the path loss exponent. This renders the computation of the optimal location that minimizes average path loss between AP and all the clients as a convex optimization problem which will be discussed in Section 3.3. Here, we consider minimizing the average path losses between the AP and all the clients, where the average path loss can be considered as the path loss of a virtual link between the AP and single virtual client.

Brute-force Search: Once the CC is determined in a particular network, a brute-force micro-search approach can then be used to search a finite number of points in the vicinity to further improve the network performance to combat multipath. As a theoretically good position of the AP has been obtained through the determination of communication centroid, a brute force approach is then applied for searching a finite number of points around the communication centroid to further improve network performance.

3.2.3 Practical System Design and Discussion

To practically enable mobility of an AP, we propose a self-positioning AP system with the following requirements and features: 1) *Robotic platform:* any robotic system has floor movement capability; 2) *Power source of AP:* the robotic platform or the controller can provide port to power the AP in order to eliminate power outlet (e.g., mini APs can be powered by any power sources with micro USB port). 3) *Wireless backhaul:* wireless backhaul can be utilized to eliminate the Ethernet cable. To maintain the performance of such a system, the wireless backhaul communication channel should be different from the front end communication channel. 4) *Movement range:* we assume that the AP can only move in a limited area where no obstacle exists in this region, and we also consider the limited area as a convex set for simplicity, where, for every pair of points within the region, every point on the straight line segment that joins the pair of points is also within the previously defined region (in such case, the path planning problem is simplified as moving in the straight line); 5) *Location calibration:* the AP can utilize localization technique to measure its relative position w.r.t. wireless backhaul to calibrate its position and strictly restrict the system to move in the previously defined limited area.

3.3 Hermes — A Self-Positioning WiFi Access Point

Hermes relies on the notion of a communication centroid to minimize the average path loss from itself to all clients with an adaptively computed path loss exponent; and then uses a brute-force search algorithm at the communication centroid to do fine-grained adapta-

tion to combat multipath. The algorithm proposed in this thesis is designed to minimize the average path loss instead of maximize SNR as proposed in [8]. The main reason is that SNR is not stable (influenced by dynamic environment). However, the advantage of the proposed algorithm is: 1) communication centroid is identified based on theoretical path loss model without impacted by dynamic channel condition; 2) given the communication centroid, fine-grained adaptation is performed to adapt the micro-position based on site-specific channel condition. Based on the design insights of the previous section,, we propose *Hermes*, a self-positioning WiFi AP in this section. The following items are the major components that constitute *Hermes*: 1) localization of Clients; 2) computation of the macro-optimal CC based on clients' positions; 3) brute force micro-search.

3.3.1 Localization of Clients

Localization techniques: Recently, many studies have been done for WiFi-based indoor localization [55]. Specifically, [56] presents $SpotFi$, which is an accurate indoor localization system that can be deployed on off-the-shelf WiFi infrastructure. This system can achieve a median accuracy of $40cm$. $SpotFi$ incorporates super-resolution algorithms that can accurately compute the angle of arrival (AoA) of multipath components and estimate the location of the target by using the direct path AoA estimates and RSSI measurements. As AP is equipped with comparatively large number of antennas, [57] can be applied to *Hermes*, which utilizes multipath suppression algorithm to achieve a median accuracy of $23cm$.

Robotic Trilateration: Typically, localization techniques require at least three receivers to localize clients' position. Given the benefit of movement capability of *Hermes*, localization techniques can be applied to single AP *Hermes*. Trilateration is a process by which the location of a transmitter can be determined by measuring the distance between the transmitter and three different receivers with known locations [58]. Although the target environment for *Hermes* does not have three receivers with known locations, *Hermes* itself has moving capability. Thus, we propose a technique called *robotic trilateration*, in which *Hermes*

moves to m number of positions (with $m \geq 3$) to measure the distance between itself and its clients m times to estimate the clients' positions. Also, given the mobility advantage, *Hermes* can rotate in rn number of directions, and collect average distance estimation to reduce measurement error. As m and rn increase, the estimation accuracy increases, but the time complexity also increases.

[58] proposes an enhanced trilateration algorithm that simplifies the trilateration problem by limiting the receivers locations. Based on the proposed algorithm, by solving quadratic equations, the number of solutions for quadratic equations is reduced to 2. Utilizing the same methodology, we let *Hermes* move to three specific types of coordinates to measure the distance between itself and a client: 1) A1(0,0,0), A2(x_2,0,0), and A3(x_3,y_3,0), where A1, A2, and A3 are non-collinear. *Hermes* relies on a virtual coordinate system where the initial position of the AP is defined as the origin with coordinates (0,0,0), and the initial direction that the AP faces to is defined as the x positive direction. The unit length in the coordinate system should be less than the granularity of micro-positioning. *Hermes* measures the distance between the AP and a given client at the initial position (A1). Then, the AP moves to A2 (x_2,0,0) and A3 (x_3,y_3,0). Then, the following quadratic equations can be formed: Then, the AP moves to m-1 positions, where the positions have coordinates of the form A2 (x_2,0,0) or A3 (x_3,y_3,0), with an additional constraint that at least one position is chosen for each of coordinate types of A2 and A3. At each position, the AP measures the distance between itself and the client. Then, for every combination of three non-collinear positions, one each from A1, A2, and A3, the following quadratic equations are formed:

$$r_1^2 = x^2 + y^2 + z^2 \tag{3.3}$$

$$r_2^2 = (x - x_2)^2 + y^2 + z^2 \tag{3.4}$$

$$r_3^2 = (x - x_3)^2 + (y - y_3)^2 + z^2 \tag{3.5}$$

Where, r_1, r_2, and r_3 are distances measured from positions A1, A2, and A3. x, y, z are the coordinates of the client of interest. The following equations are then used to calculate the location of the client of interest for that set of positions:

$$x = \frac{r_1^2 - r_2^2 + x_2^2}{2x_2} \tag{3.6}$$

$$y = \frac{r_1^2 - r_3^2 + x_3^2 + y_3^2 - 2x_3x}{2y_3} \tag{3.7}$$

$$z = \sqrt{r_1^2 - x^2 - y^2} \tag{3.8}$$

Note that, if $m > 3$, the above equations can be formed for each unique combination of positions of the form A1, A2, A3. For example, if m is 5, and say each coordinate type A1/A2/A3 has 1/2/2 positions, the number of equation sets becomes 4. For each equation set, a corresponding client location can be calculated. The average of all possible client locations is then computed to improve the location estimation accuracy. As can be seen from Equation 3.8, z can be either positive or negative. For a 2D robotic platform, there is no need to calculate the unique client coordinate, since both negative or positive z solution will let the robotic platform converge to the same CC. For a 3D robotic platform, as the robotic platform can move in z direction, the distance between the AP and its client can be utilized to identify unique client location. Specifically, if the robotic platform moves in the positive z direction, and the distance between the robotic platform and its client decreases, it means that the client location has a positive z coordinate.

Monitoring System: In order to adapt for dynamic client scenario, in *Hermes*, we propose the following monitoring system to constantly monitor the clients' mobility status using the localization methods discussed in this section. We categorize clients mobility as 4 types: 1) *Fixed*: client with no change in position, 2) *micro-movement*: client with movement less than *mr* meter, 3) *macro-movement*: with movement larger than *mr* meter , and 4) *con-*

stantly moving: client does not stay still. More specifically, a client will be categorized in each type, when the client is monitored as the specific type for *mt* seconds. The trade-off to set low *mr* or *mt* is higher optimized network performance but more frequent AP movement. The default of *mr* and *mt* are set as 50x of wavelength and 20s.

3.3.2 Computing CC

Given the algorithm to identify locations of the clients, the next step is to identify the CC within the predefined movement range. CC is the position with minimum average path loss between AP and its clients. Thus, we intend to minimize the following equation as discussed in Section 3.2: As minimizing the average of path losses by changing the AP's position is equivalent to minimizing the average of distances between the AP and its clients raised to the power of n.

$$\frac{\sum_{i=1}^{k} w_i |\vec{p}_o - \vec{p}_i|^{n_i}}{k} \tag{3.9}$$

where k is the total number of clients. w_i is the weight for the link between AP and client i which is in the range of [0,1] (the higher the weight is, the higher the QoS is given to client i). $\vec{p}_o$ and $\vec{p}_i$ are the coordinates of the optimum AP position and the coordinates of client i, and n_i is the path loss exponent. If a client is identified as a constantly moving client, a weight 0 is given to such client. We intend to show that this is a convex optimization problem. The mathematical objective is to prove the following statement:

$$\frac{\sum_{i=1}^{k} w_i |\vec{p}_o - \vec{p}_i|^{n_i}}{k} \; is\ a\ convex\ function$$

The first step is to show that the n^{th} power of a non-negative convex function, as the distance is non-negative, is still a convex function, where n is always larger than 1. The second step is to show that the sum of convex functions is still a convex function, and the third step is to show the convex function divided by a non-zero constant is still a convex function. The proof for the second and third steps are trivial and can be found in [59]. The convex function definition is given in Equation 3.10, where c(x) is the convex function and

x_1/x_2 are arbitrary variables of c(x). Then, important proof steps are given below for the first step, where f(x) follows the definition of a convex function.

$$\forall t \in [0,1], c(tx_1 + (1-t)x_2) <= tc(x_1) + (1-t)c(x_2) \tag{3.10}$$

Proof. Assume f(x) = h(g(x)), where $h(z) = z^n$ and g(x) is a non-negative convex function.

$$Since\ g(x)\ is\ non-negative:$$

$$[g(tx_1 + (1-t)x_2)]^n <= [tg(x_1) + (1-t)g(x_2)]^n$$

$$Since\ n > 1\ and\ z\ is\ non-negative:$$

$$h''(z) = n_i(n-1)z^{n_i-2} > 0$$

$$Since\ h(z)\ is\ convex:$$

$$h(tz_1 + (1-t)z_2) <= th(z_1) + (1-t)h(z_2)$$

$$By\ substitution:\ f(tx + (1-t)x) <= f(x) + (1-t)f(x)$$

□

Assume the locations of all clients are given. Algorithm 1 can be utilized to identify the location of the CC. The initial position of the AP is defined in line 1. The sum of n^{th} power of distances between initial AP position and all its clients is calculated in line 2. We define *Step* as the pace to search in line 3. If *Step* is larger than the movement granularity of *Hermes*, defined as *gran*, continue the search in line 4. Search in 6 different directions, and if the sum of *n*th power of distance between the new AP position and all clients are smaller, replace AP's coordinate with the new AP's position as shown in line 5-line 8. Step becomes half of the previous value in each loop (loop is formed in line 4 to line 11) as shown in line 10. Finally, the CC is identified with the minimum average of $n_i{}^{th}$ power of the distance between the new AP position and all clients in line 12. When a new client joins the network or a client is detected with macro-movement using the monitoring system, or if an existing client either becomes active or deactivate, the macro-search will commence

once again.

Algorithm 1 Computing CC

1: $AP = (cx, cy)$
2: $Ave = \sum w_i |AP - clients|^{n_i}/k$
3: $Step = InitialStep$
4: **while** $Step > gran$ **do**
5: $\quad ChangeAPwith \pm Step$ for x, y and z
6: $\quad NewAve = \sum w_i |NewAP - clients|^{n_i}/k$
7: $\quad$ **if** $NewAve < Ave$ **then**
8: $\quad\quad AP = NewAP$
9: $\quad$ **End if**
10: $\quad Step = Step/2$
11: **End while**
12: $CC = AP$

3.3.3 Brute-force Search

After identifying the CC, the next step in *Hermes* is to utilize a brute force search to identify the optimal micro-location. Specifically, *Hermes* considers CC as the center of searching space, and *Hermes* rotates itself in p uniform distributed directions. At each position, AP and clients perform both UL or DL throughput measurement, due to the channel asymmetric issue discussed in Section 3.1.3. The tradeoff of measurement duration is that long duration leads to high reliability but also high time complexity. The throughput measurements from clients are reported to AP. AP utilizes the following T metric to identify the optimal micro position:

$$T = \sum_{i=1}^{k} (w_l * Throughput_{UL_i} + (1 - w_l) * Throughput_{DL_i}) \tag{3.11}$$

where, the weighed factor w_l (in the range of [0,1]) and $1 - w_l$ is used to assign weights for DL and UL measurement. AP identifies the position with maximum T as optimum position. The micro-search will be performed at the initial stage and the measurement at the p micro-positions will be recorded as history data, in particular, the lowest value of T obtained over the p positions will also be noted. Once the AP is moved to the optimal

micro position, the AP will only move to a new micro position when the measured T metric drops to less than half of the sum of optimum and lowest T. The brute force search will then commence once again.

Here, we utilize throughput as the measurement metric, and it can identify the optimum micro position which maximizes the received signal quality (e.g., by maximizing its constructive multipath interference), as well as minimizes interference (by maximizing its destructive interference). If the current throughput performance becomes lower than any recorded throughput, it triggers *Hermes* movement to another micro-position with optimum throughput. Note that the brute force search can also be triggered after a certain period of time.

3.3.4 Navigating with Barriers

Even though *Hermes* has movement capability, it is still likely that there could be barriers that block *Hermes*, and *Hermes* cannot physically reach the CC or the optimum micro-position. To deal with the corresponding problem, it is critical that *Hermes* has barrier circumventing capability. To enable such functionality, *Hermes* can rely on the *Pledge algorithm* [60]. Pledge is a simple barrier circumventing algorithm. As a barrier is encountered, it will move along the barrier and measure the angle that is turned. When the current angle is same as the original angle and the angular sum of turns is 0, the barrier is then circumvented.

3.3.5 Unreachable Target Locations

Besides circumventing any barriers, it is also practical to consider stopping at the location which is closest to communication centroid, if the barrier cannot be circumvented. To enable such capability, if *Hermes* cannot achieve the communication centroid after $utl - t$ seconds, it will move to the location that is closest to communication centroid (the location can be calculated through the virtual coordinate system). The brute-force search algorithm will then be performed at a sub-optimal position.

3.3.6 Robotic Platform Discussion

The robotic platform of Hermes can be a drone, or rail on the cell, etc. Without losing generality, we utilize iRobot Create 2 as the robotic platform for Hermes. Ethernet limitations can be resolved using wireless backhaul as discussed in Sec. 2. For mini APs, power cord limitations can also be resolved as long as the robotic platform or the controller can provide port to power the AP (mini APs can be powered by any power sources with micro USB port). Two specific parameters pertaining to the robotic platform have an influence on the performance of *Hermes*, which are *movement accuracy* and *movement capability*. With higher movement accuracy, a smaller search granularity becomes feasible. If movement accuracy can achieve 1/4 of the signal wavelength, the optimum position is potentially achievable. Another parameter is the movement capability: 1) the space size that the robotic platform can search; 2) the degrees of robotic platform's mobility. Basically, with higher degrees of freedom for mobility, the performance of *Hermes* is likely to increase. Also, the interface that the robotic platform relies on to navigate itself has a large impact on network performance. While *Hermes* significantly reduces the search space from an algorithmic standpoint to improve algorithm efficiency, having additional navigational capabilities (e.g., vision camera) supported by the robotic platform can also help *Hermes* reach the optimum position quickly.

3.4 *Hermes* Analysis

In this section, we utilize simulation-based analysis to study: 1) Impact of dynamic Shadow fading: the impact of obstacles on channel quality while *Hermes* computes CC, and 2) CC vs. Optimal Location: the performance gap of CC versus optimal location.

3.4.1 Impact of Dynamic Shadow Fading

Shadowing effect is an important phenomenon to be considered in the path loss model. For indoor scenarios, there is a very high probability that the link between AP and client is impacted by shadowing and leads to NLoS channel condition. In *Hermes*, to compute CC,

Table 3.2: MATLAB Simulation Configurations

	Settings
Number of Obstacle	33
Minimum Obstacle Size (m)	(0.75, 0.25, 0.1)
Maximum Obstacle Size (m)	(1.75, 1.25, 1.75)
Average Obstacle Size (m)	(1.24, 0.59, 0.47)
Standard Deviation of Obstacle Size (m)	(0.36, 0.32, 0.45)
Size of Room (m)	(9, 6.5, 3)

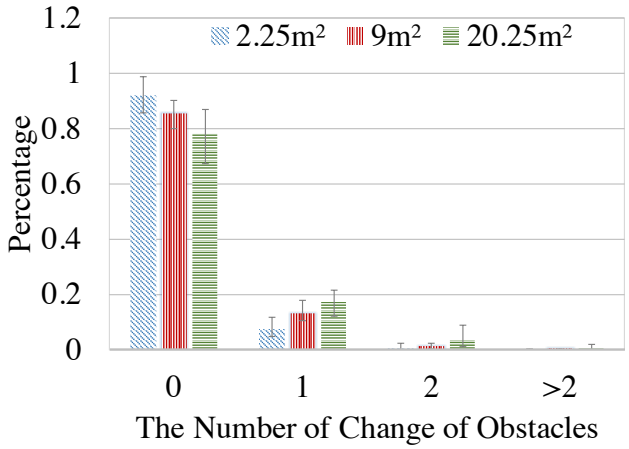

Figure 3.19: Dynamic Shadowing

the shadowing parameter is not considered in Equation 4.11. The reason will be explained herein.

In *Hermes*, as the system will constantly move, the number of obstacle between AP and each client may change. Thus, to accurately identify CC, the exact location, size, and even the material of each obstacle need to be known by the AP, which incurs very high complexity for the AP to collect these parameters. To quantitatively analyze the impact of shadowing effect on *Hermes*, we utilize MATLAB simulations to identify how likely the number of obstacle between AP and each client changes as *Hermes* moves.

The simulation parameters are summarized in Table 3.2. The obstacle information is collected based on the obstacle layout in the lab scenario (only obstacles with large size or high penetration loss are considered). We have run 10 sets of simulations with

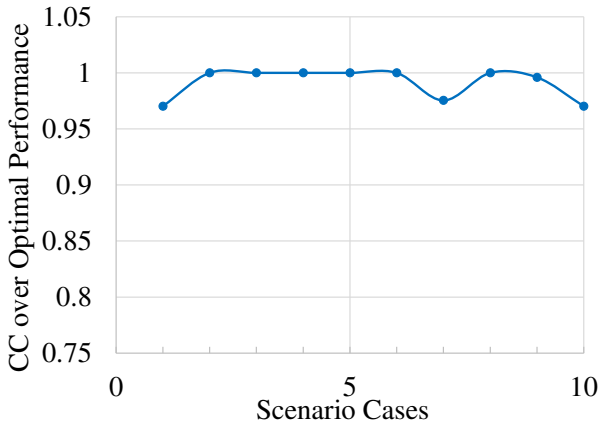

Figure 3.20: **CC Performance Analysis**

different obstacle configurations with obstacle size follows the distribution with average and standard deviation obstacle size shown in Table 3.2, and the size is limited by max and min of obstacle size. In each scenario, the movement range (with the center located at the center of the floor) of AP is configured as 2.25 m^2, 9 m^2, and 20.25 m^2. For each scenario, 1000 clients are simulated. As AP moves in each predefined area, we intend to identify the number of obstacle change between AP and each client. In fig. 3.19, the results show how the number of obstacle changes while the AP moves. To be noticed, the higher the number of obstacle change is, the larger the impact it has on the CC computing algorithm. We categorize the number of change of obstacle of 0, 1, and 2 or above as *no impact*, *low impact* and *high impact* cases, respectively. As the movement range changes between 2.25 m^2, 9 m^2, and 20.25 m^2, the high impact cases appears in 1%, 1.4% and 4.4% of overall cases, respectively. Thus, it can be seen that the high impact cases rarely happen. Thus, we conclude that the impact of shadowing effect on computing CC algorithm is very limited. Also, due to the extremely high complexity and cost to consider shadowing effect in *Hermes*, we intend to eliminate the shadowing parameter in CC computing algorithms. For cases with the number of obstacle changes is 2 or above takes account 0.5%, 1%, and 3.9% as AP move range from 2.25 sq. m, 9 sq. m, and 20.25 sq. m, respectively.

Table 3.3: ns-3 Simulation Configurations

	Settings
Client Number	3
Distance between AP and client	10m
Traffic Direction	Dl
Transport Protocol	UDP
WiFi Spectrum	5GHz
Experimental Duration	20s

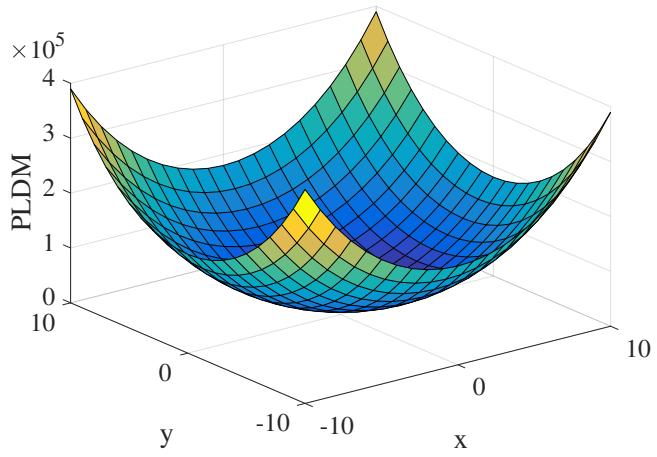

Figure 3.21: Path Loss Distribution

3.4.2 CC vs. Optimal Location

In this work, CC is defined as the position with minimized average path loss (to maximize average link quality), which does not directly lead to maximal throughput performance. Here, we utilize ns-3 [61] simulations to study the performance gap of CC versus optimal location. The simulation scenario is configured as shown in Table 3.3. Each client is randomly distributed around the AP. The default log-distance path loss model is utilized (without modeling the multipath effect).

We have run the simulation 10 times with random clients location configurations. As shown in Fig. 3.20, the normalized aggregate throughput performance of CC ranges from 0.97 to 1 compared with optimal location. This further validates that minimizing average

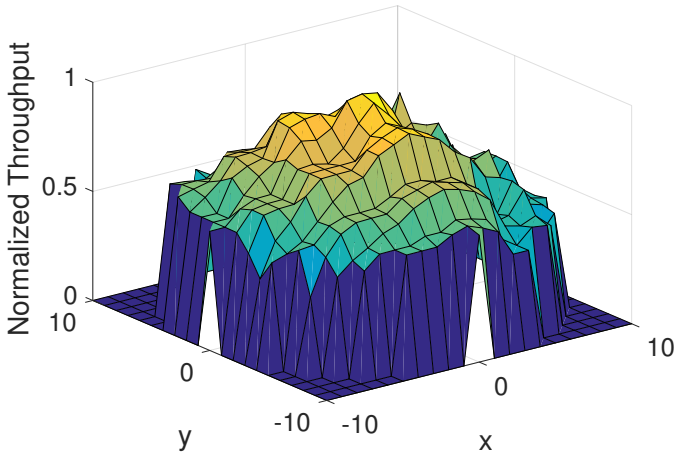

Figure 3.22: **Throughput Distribution**

path loss can almost achieve optimal network performance. To further illustrate the performance of CC, fig. 3.21 and 3.22 show the average path loss distribution and aggregate throughput performance distribution of a specific scenario, where AP is located at (0, 0), and three clients are located at (9.8, 0), (-5, 8.5) and (-4.8, -8.8). In this example, the CC is located at (0, 0). The normalized aggregate throughout performance within 10m of AP ranges from [0.33, 1]. As the AP is located at any location where the link quality of a specific link has bad channel quality, the aggregate performance of the network becomes extremely bad due to the bad quality link consuming extra transmission resources. More specifically, as AP is located at (10, 0), the aggregate performance is 0.48 (each client contributes 0.18, 0.16, and 0.14). In this example, it is clear that even one of the client has extremely good link quality, it only performs 0.18, since it has to share the channel with the other two low-quality links. If modulation, coding, and transmission success rate of each link can be predicted at each AP location, the network performance can be further improved.

3.5 Hermes Evaluation

In this section, the performance of *Hermes* is experimentally evaluated in different environments with varying restrictions. The throughput is measured over a period of 20s, and an average result is obtained over three 20-second periods. Algorithms of *Hermes* follow specifications in Section 3.3. For client localization, the distance between the client and AP are assumed to be known to the AP. For communication centroid, the number of positions *Hermes* moves to, m, is chosen as 3, path loss exponent n_i is chosen as 4 for each client based on the scenario type, and weighted factor w_i is set as 1 for each client. To determine the micro-optimal position, the brute force search technique is used in which, the possible number of locations to search, p is chosen as 9. DL traffic is assumed for the experiments, so w_l is set as 1. For simplicity, a wired backhaul system is configured for performance evaluation. Experimental results are also compared with the *iMob* system proposed in [8]. The system in [8] searches for an optimal position in a 4ft.^{2} region using the OST to find the position of the AP such that the aggregate throughput is maximized in real-time without having the AP to retrace its path. In essence, if there are N total number of points that the AP can be positioned within the 4ft.^{2} plane, OST specifies that the AP finds the maximum aggregate throughput in the first $\frac{N}{e}$ points. It further stipulates that the AP should stop at the first point after the $\frac{N}{e}$ points that yields a greater aggregate throughput than the maximum throughput found in the first $\frac{N}{e}$ points. In case the OST is unable to find a point that yields a higher aggregate throughput, the expectation is reduced in proportion to the number of points it has already traversed. We utilize the actuator system as the platform for the *iMob* system.

3.5.1 Number of Clients

In this experiment, the starting position of the AP is located in the circle with 10m distance to the CC. The optimal aggregate throughput obtained for 1, 2 and 3 clients of *Hermes* is compared to the results obtained through the implementation of the *iMob* [8].

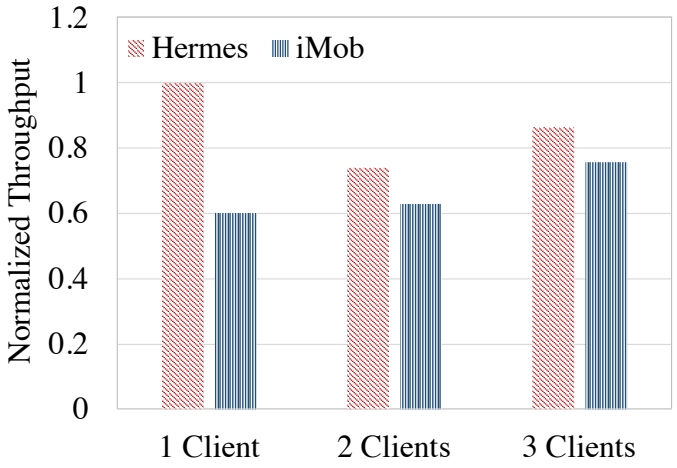

Figure 3.23: **Number of Clients**

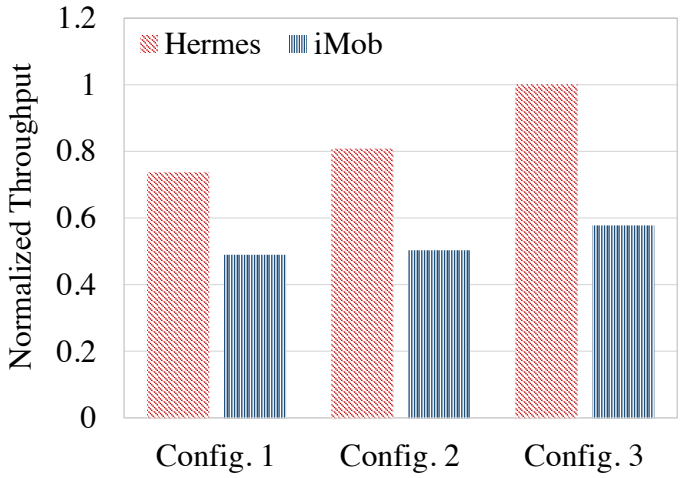

Figure 3.24: **Clients Configurations**

The aggregate throughput for 1, 2 and 3 clients over three different configurations are shown in Fig. 3.23. As can be seen, there is a significant aggregate throughput improvement of 66%, 17%, 20% of *Hermes* compared with *iMob* for 1, 2 and 3 clients scenarios, respectively. It reveals the benefit of the macro optimization algorithm of *Hermes*. Furthermore, it is important to mention that there are on average over 110 points that *iMob* needs to traverse before it stops at a position that it considers optimal. For *Hermes* however, there are on average 10 micro-position stops it makes before finding the position that results in the highest aggregate network throughput.

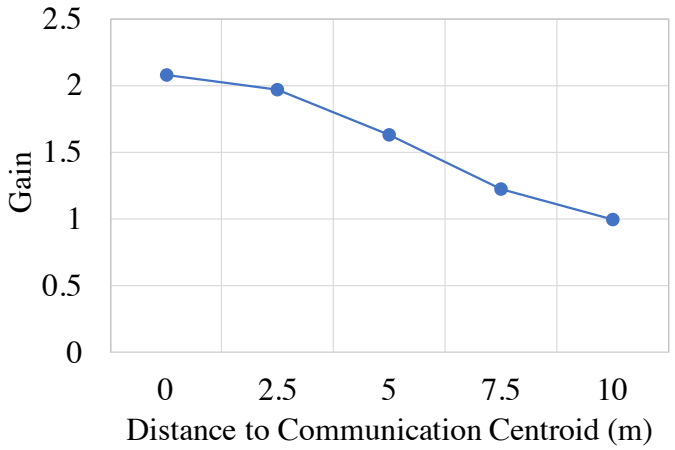

Figure 3.25: Constrained Mobility

3.5.2 Location of Clients

To further evaluate the performance of *Hermes* in a multi-client scenario, the optimal positions obtained by *Hermes* and *iMob* are analyzed for three different topology configurations where three clients are randomly placed around a circle with a radius around 10m. For configurations *1* and *2*, the starting position of the AP is randomly located inside the circle. For configuration *3*, the starting position of the AP is located on the circle with 10m distance to CC.

In Fig. 3.24, the performance improvement of *Hermes* over *iMob* is up to 73% for configuration *3*. In configuration *3*, the starting position of the AP is on the circle along which the clients are placed on. As *Hermes* performs both macro-positioning to identify CC and micro-positioning to identify the optimal micro position, *Hermes* can optimize both path loss and multipath phenomenon. *iMob* mainly considers micro-positioning to benefit from mitigating multipath but not from path loss phenomenon. Also, the efficient micro-searching algorithm in *Hermes* at the CC reduces the search complexity. The results further indicate the promising improvement achieved by macro-mobility of *Hermes*. To be noticed, the performance improvement of *Hermes* compared with *iMob* increases as the distance between starting point and CC increases.

3.5.3 Constrained Mobility

In real-life environments, various constraints can limit the movement of *Hermes*, and it needs to be taken into account. This can prevent *Hermes* from moving towards the CC. Following the same experimental configurations of macro-mobility experiments in Section 3.2.1, the impact on the aggregate network throughput of various distances the AP is away from the CC is shown in fig. 3.25. It shows the network throughput performance as the AP is away from CC with distance ranging from 0m to 10m with a step size of 2.5m.

From fig. 3.25, the overall network performance is approximately less than a half when it is placed as far as 10m from CC. It exhibits a nearly linear relationship in terms of the overall network throughput degradation as the AP is moved away from the CC. This implies that if the AP is not able to precisely move to the CC due to barriers, *Hermes* will still exhibit acceptable performance improvement compared with an arbitrary starting position of the AP.

3.5.4 Summary of Experimental Results

The results obtained seek to effectively evaluate the proposed *Hermes* under various network conditions. The performance of the system in tested configurations are analyzed and also compared to [8]. It was found that *Hermes* outperforms the *iMob* system for a single AP with different number of clients. An improvement of over 66% was obtained for a single client scenario. An improvement of *Hermes* over *iMob* was obtained for multi-client scenarios achieves an increase of 17% and 20% for 2 and 3 client configurations, respectively. Even though *iMob* exhaustively searches a larger area than *Hermes*, the additional macro-search of the *communication centroid* results in a lower search space and a higher aggregate throughput of the system. This is further validated by location of clients experiment where 3 clients are randomly placed around a 10m circle. An improvement of up to 73% is observed for *Hermes* in this multi-client scenario. In addition, *Hermes* is also able to deliver acceptable performance even under constrained mobility situations as shown in

Fig. 3.25.

3.6 Summary

In this chapter, we present a self-positioning AP system - *Hermes*. *Hermes* performs positioning by sequentially solving two related, but independent problems which aim to improve network performance. The first problem is to find the CC so that path loss phenomenon is optimized from the network perspective. The second problem involves finding an optimal micro position around the CC to optimize the multipath phenomenon. In addition, the notions of finding a CC and using brute force search can be directly applied to multiple APs scenario, as long as the optimum pairing set of APs and clients are given. Other than expanding the scope of this work, the following are the most important future work to be considered: 1) self-positioning time complexity analysis, 2) leveraging network fairness utilizing AP mobility, and 3) mitigating interference utilizing AP mobility.

CHAPTER 4

INFRASTRUCTURE MOBILITY IN EXTREMELY HIGH FREQUENCY

The mmWave WiFi standard (e.g., IEEE 802.11ad) operates in the 60GHz unlicensed frequency band. It can deliver multi-gigabit ($\sim$7Gbps) performance primarily by virtue of using a large bandwidth (greater than 2GHz). Specifically, the bandwidth supported by 802.11ad is 12.5x larger than the bandwidth supported by the latest non-mmWave WiFi standard 802.11ax. While the potential performance is quite promising, mmWave is vulnerable to unreliable wireless channel conditions (especially non-line-of-sight (NLOS)) compared to conventional WiFi operating in 2.4GHz or 5GHz. The communication performance drops significantly when the wireless link has an obstacle such as a wall or a cabinet in its way. Given the fickle nature of mmWave communication, it is expected to be predominantly used in a dual-band (or a tri-band) configuration that works along with conventional WiFi.

In this context, it is likely that mmWave WiFi can deliver considerably better performance, but that the performance cannot be assured since it is dependent on the existence of LOS conditions. As for LOS condition, it is a function of the physical environment, but communication technologies hitherto have had no ability to improve the conditions when necessary. In recent years, related works have started exploring *infrastructure mobility* as a degree of freedom in the WiFi framework that can be exploited to improve the physical environmental conditions for wireless communications [8, 25, 21, 11]. Considering the strategy of infrastructure mobility, a WiFi AP with mobility can discover an optimal location for itself and move to that location to offer the best possible performance for the network. Given that mmWave WiFi has a critical requirement on wireless channel conditions, infrastructure mobility becomes an especially attractive degree of freedom for mmWave WiFi, where the creation of LOS conditions can have a profound impact on the overall network performance.

In this chapter, the primary focus is to identify the potential of enabling mobility for the mmWave network. First, we explore the strategy of infrastructure mobility to alter the location of an access point (AP) in order to provide LOS connectivity to stations (STAs) in indoor mmWave WiFi networks. Through both simulation-based studies and theoretical analyses, we make a detailed case for infrastructure mobility by identifying the impact of AP mobile platforms configurations on network performance and propose a ceiling-mounted mobile (CMM) AP model. Then, we compare the performance of a CMM AP with multiple static APs, and we identify that the throughput and fairness performance of a CMM AP is better than as many as 5 ceiling-mounted static APs. Afterwards, we present a LOS prediction algorithm based on machine learning (ML) that addresses the *LOS discovery problem* within a CMM AP framework. The algorithm relies on the available network state information (e.g., LOS connectivity between STAs and the AP) to predict the unknown LOS connectivity status between the reachable AP locations and target STAs. We show that the proposed algorithm can predict LOS connectivity between the AP and target STAs with an accuracy up to 91%. Based on the LOS prediction algorithm, we then propose a systematic solution *WiMove*, which can decide if and where the AP should move to for optimizing network performance. Using both ns-3 based simulation and experimental prototype implementation, we show that the throughput and fairness performance of *WiMove* is up to 119% and 15% better compared with other approaches.

4.1 Experimental Analysis

Following the same experimental methodology in Sec. 3.1, we investigate the performance benefits of *AP position diversity* when WiFi carrier frequency varies among 2.4GHz, 5GHz, and 60GHz. For 2.4GHz and 5GHz bands, we follow the default devices configurations given in Table 3.1. For the 60GHz experiment, we utilize a *Tp-link AD7200* as AP and an *Acer TravelMate P648* laptop as client. Fig. 4.1 shows 2x, 2x, and 5.3x *Average Gain* as a result of *AP position diversity* for 2.4GHz, 5GHz, and 60GHz, respectively. There is

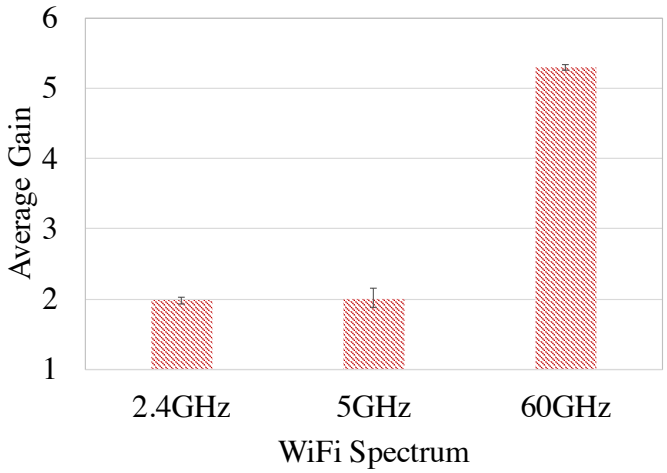

Figure 4.1: Spectrum

no difference between the *Average Gain* of 2.4GHz and 5GHz. Since 2.4GHz and 5GHz spectrum are close to each other, there is no significant difference in signal propagation characteristics. However, *AP position diversity* is able to provide 5.3x performance improvement for 60GHz. The major reason is that both propagation loss and penetration loss of mmWave signals are significantly higher than that of 2.4GHz and 5GHz. It reveals the fact that location matters substantially for mmWave. *The key observation here is* AP position diversity *is a significantly promising application for mmWave.*

4.2 Statistical Analysis

4.2.1 Simulation Methodology

To evaluate the performance of AP mobility quantitatively, we use the ns-3 simulator [61]. To incorporate the features of indoor configurations and 802.11ad, we make the following modifications to the default ns-3 simulator.

Simulation of Indoor Scenarios

Due to the lack of an indoor scenario model (especially an obstacle model) in ns-3, we implemented the following indoor scenario features. A room is simulated as a specific three-dimensional space with a given obstacle distribution model. To simplify the simu-

lations, we assume that the obstacles are modeled as cuboids, and they are placed on the floor, where the overlapping of obstacles is allowed to mimic complex cuboids-based obstacles. Typically, when an STA is communicating with an AP, it is located on the top of an obstacle (e.g., laptop on the desk) or attached to the side of an obstacle (e.g., TV on the wall). To simulate such practical scenarios, we consider that the placement of the STA follows an obstacle dependent distribution, where an obstacle is uniformly selected as the base location for the STA, and the STA is uniformly distributed on top or sides of the selected obstacles.

To accurately simulate the indoor obstacles, the implemented obstacle model has the following features:

- The center of the obstacles follows a Poisson point process (PPP) as shown in Eq. 4.10. The probability distribution for the number of obstacles to be uniformly placed in an indoor scenario is given as:

$$P\{N = n\} = \frac{\lambda^n * e^{-\lambda}}{n!} \tag{4.1}$$

  where, the expected number of obstacles per unit area is defined as λ and n is the number of obstacles to be distributed.

- The x, y, and z dimension of obstacles follow a truncated normal distribution to constrain the maximum and minimum of obstacle dimension.

- The material of the obstacle is uniformly chosen from [62] to represent materials with various penetration losses.

We show the default parameters used in the simulation in Table 4.2. The parameters are derived by using a real-life physical space (a lab environment) as a guiding example. To build a cuboid-based obstacle model, the x, y, and z dimensions are collected based on the largest dimensions of a measured obstacle. We then collect the number of obstacles in the lab space as n. To calculate the x, y, z dimension distribution parameters, we use the distribution fitter in MATLAB to calculate the best fit normal distribution with mean

Table 4.1: Default Simulation Parameters

Parameter	Setting
Size of room (m)	(9, 4, 3)
λ	4.7
(μ_x, μ_y, μ_z) (m)	(0.54, 0.28, 0.61)
$(\sigma_x, \sigma_y, \sigma_z)$ (m)	(0.18, 0.08, 0.21)
Platform location	Center of the ceiling
Platform orientation	Parallel to shorter edge
Platform shape	Straight line
Platform length (m)	3
P	30
STA number	1
n_{pl}	2
σ_m	2.24

μ_x, μ_y, μ_z, and standard deviation $\sigma_x, \sigma_y, \sigma_z$. The maximum and minimum of x, y, and z dimensions of obstacles are utilized as the range limits in the truncated normal distribution.

Simulation of 802.11ad

We use the 802.11ad model based on [63]. The simulator provides all techniques that are essential for 802.11ad, such as beamforming training and steering, hence providing an accurate simulation environment for 802.11ad. The mmWave channel is another essential component of simulating the performance of 802.11ad. To incorporate shadow fading based on information of mmWave WiFi devices and obstacles, we consider the impact of shadow fading and multipath separately. Specifically, we modified the widely accepted log-distance based path loss model as follows:

$$L(d) = L(d_0) + 10 * n_{pl} * log_{10}(\frac{d}{d_0}) + X_s + X_{\sigma_m} \tag{4.2}$$

where, $L(d_0)$ is the path loss at a reference distance d_0, n_{pl} is the path loss exponent, d is the distance between two communication devices, X_s represents shadow fading where the penetration loss is calculated based on the obstacles' location, dimension and material

between mmWave WiFi devices, and X_{σ_m} represents the normally distributed multipath fading with σ_m as the standard deviation. Particularly, X_s is 0 when the communication link is in LOS connectivity. We collected the average of 5 sets of experimental estimations of the log-distance based path loss model to collect n_{pl} and σ_m based on [64], which are presented in Table 4.2.

Consider an LOS connection between two communication devices, where the path loss exponent represents the channel attenuation for the LOS condition and X_σ only represents the distribution of fast fading (due to no shadowing fading at LOS connection). Therefore, we collected 5 sets of experimental estimations of the path loss model (n and σ_{fading}), where all of the experiments are performed with LOS connections between communication devices in the lab environment [64]. Similarly, for the impact of multipath, the average of 5 sets of path loss parameters are calculated and shown in Table 4.2. The reason why we do not utilize NLOS based path loss model estimation is that penetration loss of various obstacles introduces uncertainty in the path loss model. Thus, we believe that LoS based path loss estimation is more accurate than NLOS-based path loss estimation.

Based on the aforementioned ns-3 models, we can evaluate the performance of the CMM AP under scenarios with different configurations. The basic simulation steps are: 1) generate an indoor environment with specific size and obstacle distribution, 2) place the STA and AP at specific location in the aforementioned scenario, and 3) measure the performance between AP and STAs for multiple runs. If not otherwise mentioned, the parameters of simulation are shown in Table 4.2.

4.2.2 Simulation-Based Statistical Analysis

In this section, we use simulation analysis to identify the potential impact and benefits of AP mobility using the simulation platform described in the previous section. Specifically, considering the case of AP mobility, to evaluate the performance of a specific STA i with the mobile AP, we utilize the optimal LOS ($Max_p(LOS_{i,p})$) and optimal throughput ($Max_p(Thpt_{i,p})$), which represents the maximum LOS and throughput performance

that can be achieved while AP is at location p on the mobility platform. In this context, we investigate 1) the impact of different AP mobile platform configurations on network performance, and 2) the performance of a CMM AP and multiple static APs.

AP Mobility Platform Configurations

AP Mobility - Floor vs. Walls vs. Ceiling: Intuitively, as the platform is located on the ceiling, the expected LOS and throughput performance of the platform should be the best compared to the platform placed on the walls or the floor. We use quantitative simulation analysis to validate the above hypothesis and identify the corresponding performance gain of a CMM AP.

Fig. 4.2 illustrates the optimal LOS probability when the AP platform is located on the floor, the walls, and the ceiling. The expected optimal LOS probability of the CMM AP performs 88%, 100%, 137%, 60%, and 540% better compared with AP located on the left wall, the right wall, the front wall, the rear wall, and the floor, respectively. Clearly, the floor-based platform has the worst LOS performance due to the high probability of blockage. In this set of simulations, because of the specific randomly generated layout of obstacles, the AP mobile platform has relatively high performance when it is located on the rear wall compared with other walls. Similarly, Fig. 4.3 illustrates the throughput performance [1]. The expected optimal throughput of the CMM AP is 101%, 116%, 139%, 54%, and 460% better compared with AP located on the left wall, the right wall, the front wall, the rear wall, and the floor, respectively. The maximum achieved throughput performance is nearly 4Gbps. We observe that LOS performance is proportional to throughput performance. It is interesting to observe that the throughput performance is mostly either maximum or minimum. The reasons are that NLOS connectivity is likely to result in minimum performance due to high penetration loss, and LOS connectivity is likely to result in maximum performance due to the limited room size. In Section **??**, we use theoretical

[1]The STA index in all figures is sorted in ascending fashion with respect to the metric being plotted for easier interpretation.

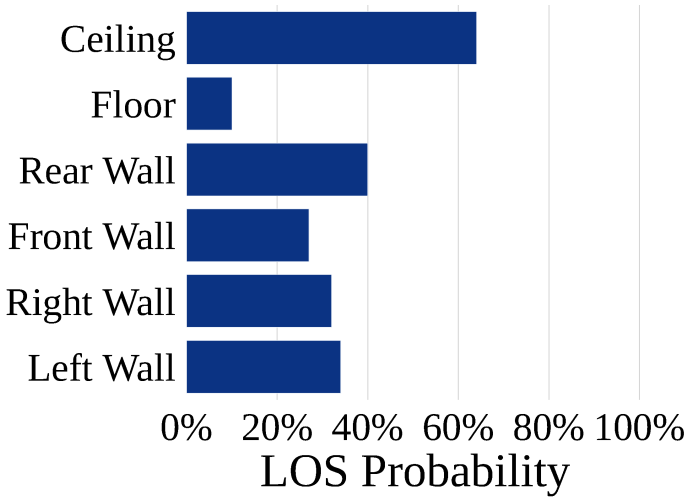

Figure 4.2: LOS - AP Location

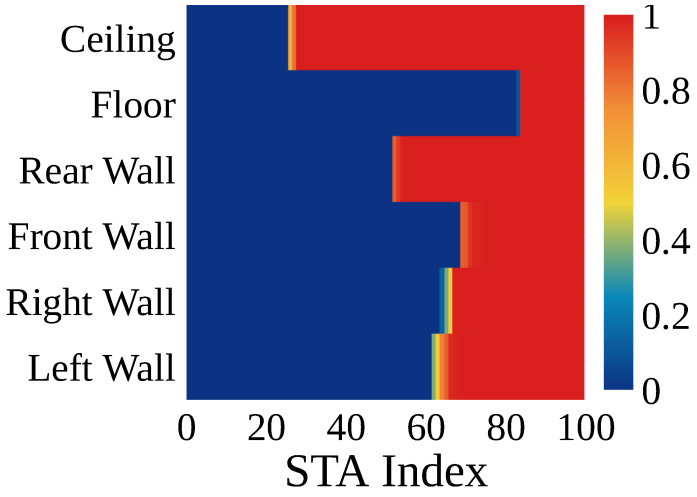

Figure 4.3: Throughput - AP Location

analysis to validate the relationship between LOS probability and the AP's height. Also, LOS performance improvement is more significant than the throughput performance. The reason is that there are cases when there are obstacles only marginally blocking the LOS connection between AP and STA. As the AP moves and channel changes from NLOS to LOS, throughput may not improve significantly due to the relatively small penetration loss change.

The performance of a CMM AP is significantly better than that of floor-based or wall-based AP mobility.

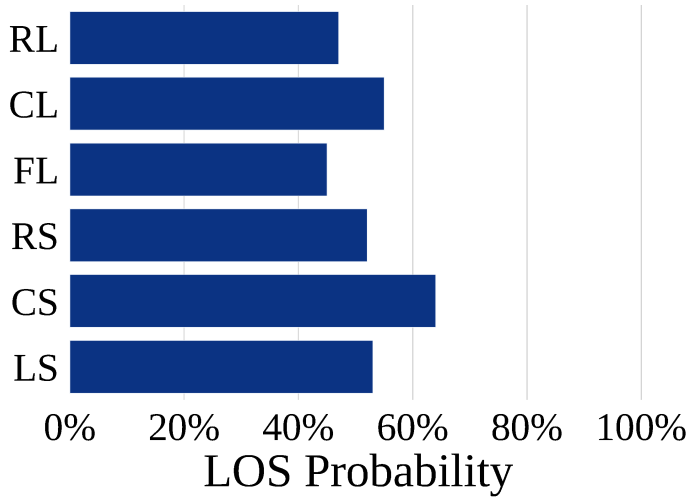

Figure 4.4: LOS - Ceiling Location

Ceiling Location: Based on the above simulation analysis, it is clear that a CMM AP achieves the best performance compared with other types of AP mobility. However, considering the default linear robotic platform, the orientation and location to place the platform is still an interesting problem to investigate. We use simulations to validate the expected optimal LOS and throughput performance when the platform is located on the edges and the center of the ceiling with the direction of the platform either parallel to the shorter edge or the longer edge. The specific instances of ceiling locations considered are: on the left shorter edge (LS), right shorter edge (RS), center parallel to the shorter edge (CS), front longer edge (FL), rear longer edge (RL), and center parallel to the longer edge (CL).

Fig. 4.4 and 4.5 show the optimal LOS probability and optimal throughput performance as the AP platform is located at the edges or the center of the ceiling with orientation parallel to the shorter edge or longer edge. Clearly, the CS based AP platform has optimal performance. There are 21%, 23%, 42%, 16%, and 36% LOS probability improvement of the CS based platform compared with LS, RS, FL, CL, and RL based platform, respectively. The throughput performance gain is observed to be proportional to LOS performance and follows a similar trend. Since the obstacles follow a PPP and the STAs follow an obstacle dependent distribution, the center-based CMM AP is more likely to have the largest LOS

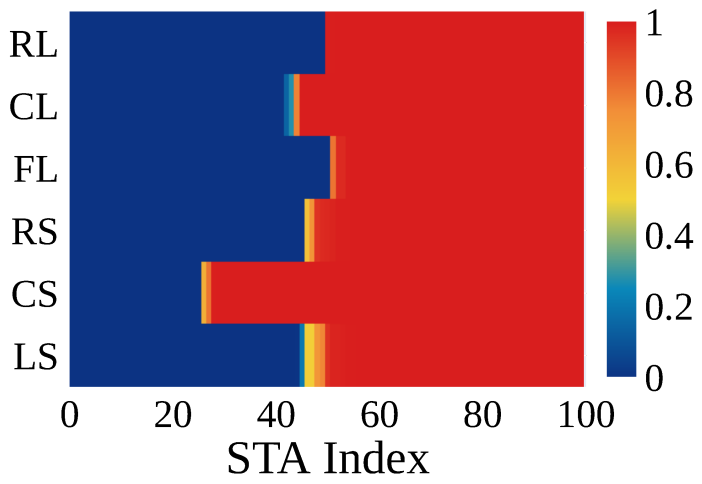

Figure 4.5: Throughput - Ceiling Location

coverage area. Even considering the case with NLOS connectivity between the AP and STAs, the AP platform located at center benefits from shorter expected distance w.r.t. STAs. Thus, it leads to less expected propagation loss providing a higher margin at the receiver to compensate for the additional penetration loss. It is also interesting to observe that when the platform is parallel to the shorter edge, the performance is better than when the platform is parallel to the longer edge. We will validate that higher LOS probability can be achieved while the platform is parallel to the shorter edge of the room using theoretical analysis in Section **??**.

> The performance of CS based CMM AP is better than that of other locations based CMM APs.

Platform Shape: The major advantage of AP mobility is the diversity in AP locations provided by the AP mobile platform. As the shape of the AP mobility platform can dramatically change the AP diversity locations, it can have significant impact on network performance. We herein investigate the impact of different AP mobility platform shapes on the network performance. As 2D platform is considered, there are two essential parameters of the shape: furthest x and y dimension in the shape. We consider 4 different platform shapes: 1) straight line (SL), where AP location diversity is along a single dimension, 2)

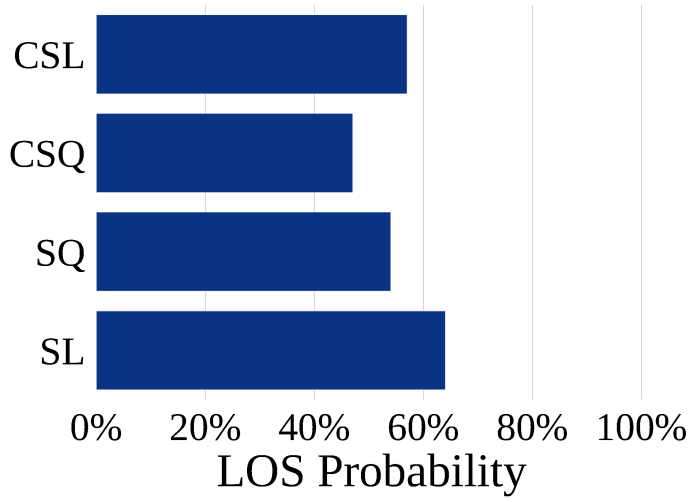

Figure 4.6: LOS - Platform Shape

cross straight line (CSL), with two perpendicular lines with the same length, 3) compressed square (CSQ), where the AP mobile platform has continuous movement range in a given square area, 4) Square (SQ), where the AP mobile platform can only move on the boundary of a given square area. Specifically, the total length for the AP mobile platform is fixed as 3m for all the platform shapes, and the width of the platform segment is 0.65m.

Fig. 4.6 and 4.7 present the optimal LOS and throughput performance of different platform shapes. The expected optimal LOS probability of the SL based CMM AP performs 19%, 36%, 12% better than SQ, CSQ, and CSL based CMM AP, respectively. Similarly, the throughput performance gain is proportional to LOS performance. Clearly, SL based CMM AP performs the best and CSQ based CMM AP performs the worst. If the diversity of AP locations is maximized, the overlapping coverage area of all the AP locations is minimized. For the CSQ based CMM AP, the AP mobile platform provides continuous movement range in a given square area, where the AP location diversity is minimized, which leads to a limited performance gain. On the other hand, the SL based CMM AP maximizes the AP location diversity in a linear fashion, which leads to significantly better performance gain compared with other platform shapes.

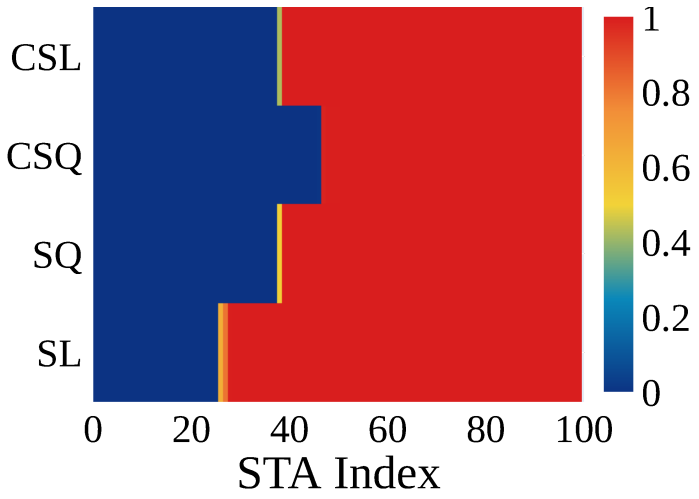

Figure 4.7: Throughput - Platform Shape

The performance of a SL based CMM AP is better than that of the other shapes based CMM AP.

Platform Length: Clearly, the larger the CMM AP platform is, the higher the potential AP location diversity can be provided, which can lead to a higher performance gain. The question we would like to investigate here is the performance gain when the platform length varies. Specifically, we change the platform length from 1m to 4m with steps of 1m.

Fig. 4.8 and 4.9 show the optimal LOS probability and throughput performance of different platform lengths. The performance of the CMM AP increases as the platform length increases. It is interesting to observe that the performance gain is not linearly proportional to the platform length. Specifically, the performance gain varies from 35%, 17%, and 12% when the platform length increases from 1m/2m/3m to 2m/3m/4m, respectively. As we identified within the ceiling location-based simulations, the AP mobile platform located at the edge of the ceiling leads to lower performance compared with the mobile AP located at the center of the ceiling. As the platform length increases towards the edge of the room, the performance gain per additional unit additional length decreases. This indicates the performance improvement is saturated after the platform size reaches the around 3/4 of the shorter dimension.

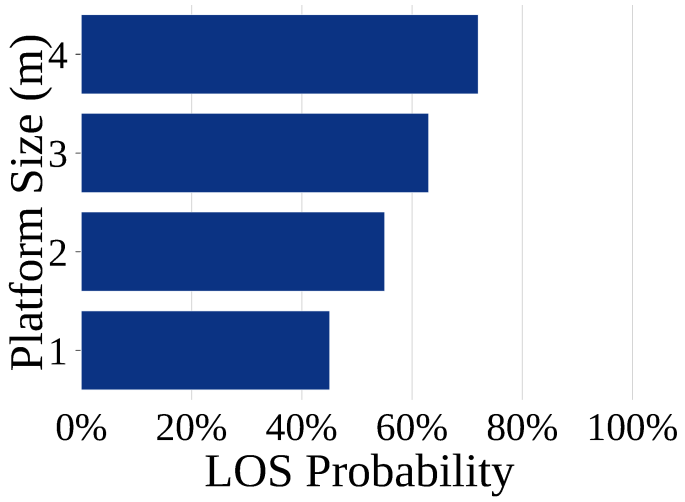

Figure 4.8: LOS - Platform Length

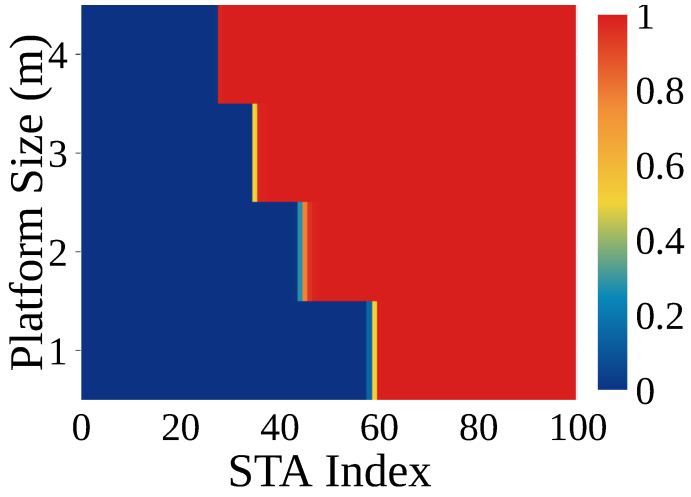

Figure 4.9: Throughput - Platform Length

As the CMM AP platform length increases, the performance gain per additional unit length decreases.

A CMM AP vs. Static APs

Single STA scenario: After identifying that the platform configurations of a CMM AP can have a significant impact on network performance, we compare the performance of a CMM AP with ideal configurations with multiple static APs. The ideal CMM AP configurations follow the definition in Table 4.2. A linear placement methodology is applied to place static

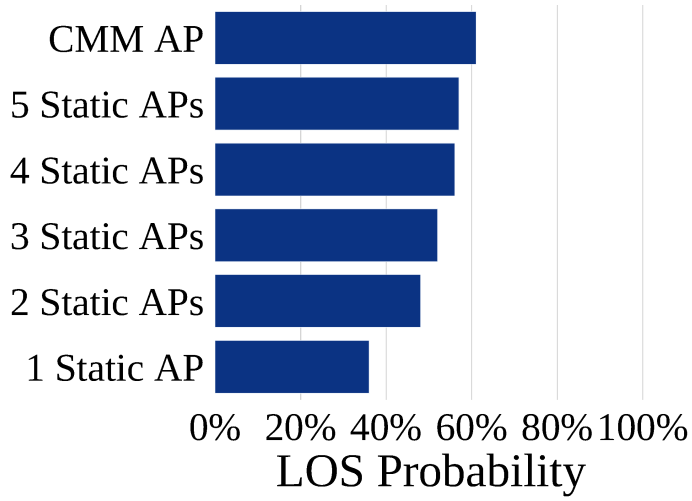

Figure 4.10: LOS - Static vs. CMM AP

APs on the ceiling. For a specific STA, we consider the maximum LOS and throughput performance achieved by one of the multi-AP as the performance of the multi-AP case. The number of static AP is set to be 1 to 5.

Fig. 4.10 and 4.11 show the expected optimal LOS and throughput performance of the CMM AP and static APs. We can observe that on an average the expected optimal LOS performance of CMM AP performs 92%, 44%, 33%, 23%, and 21% better than 1∼5 static APs, respectively. Similarly, we can observe that on average expected optimal throughput performance of CMM AP performs 72%, 38%, 19%, 15%, and 12% better than 1∼5 static APs, respectively. Specifically, among 5 configurations, the throughput performance of CMM AP is upto 72% and 17% better than 1 and 5 ceiling mounted static APs, respectively. Clearly, both LOS and throughput performance of the CMM AP are better than 1∼5 static APs. Specifically, the LOS and throughput performance of static APs increase as the number of static AP increases due to the improved AP location diversity. It is interesting to observe that the throughput performance of static APs increases by 25%, 16%, 3%, and 3% when the number of static APs increases from 1/2/3/4 to 2/3/4/5. We can observe that after the number of static AP reaches 3, the performance of static AP saturates due to the limited improvement of AP location diversity. Thus, the performance of the CMM AP with

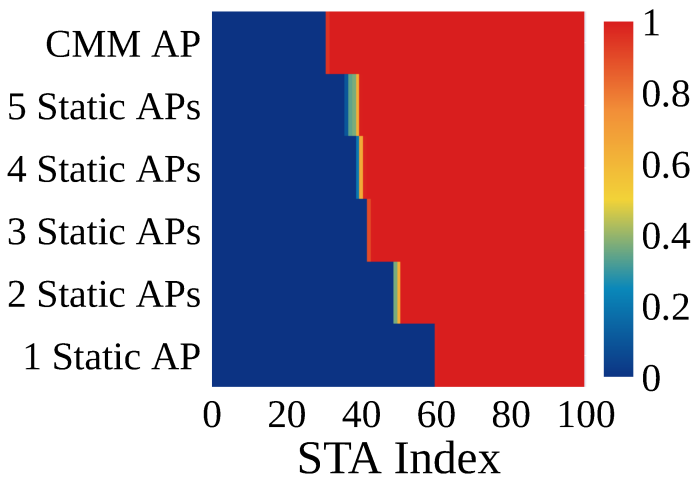

Figure 4.11: Throughput - Static vs. CMM AP

higher AP location diversity is better than as many as 5 static APs. LOS performance of the CMM AP is comparable to 5 static APs scenario, and throughput performance is still 12% better than 5 static APs scenario. To sum up, the results indicate that CMM AP achieves promising performance compared with multiple static APs. It is also obvious that the performance improvement when the AP number increases from 1 to 3 is significant. For more than 3 APs, the performance improvement is not very significant.

The performance of a CMM AP is better than that of 1∼5 ceiling mounted static APs.

Obstacle Density: As obstacle densities will also impact the network performance, we simulate 9 sets of obstacle densities configurations where the expected number of obstacles ranges from 12 to 108, which in turn corresponds to 10% to 90% of the coverage area of the entire floor.

Fig. 4.12 and 4.13 show the expected optimal LOS and throughput performance of the CMM AP and static APs. Each block of data represents the expected performance of 100 STAs. From the simulation results, we can identify that as the obstacle coverage percentage increases, both the LOS and throughput performance are likely to decrease for both CMM AP and static APs. The intuitive reason is that as the number of obstacle increases, there

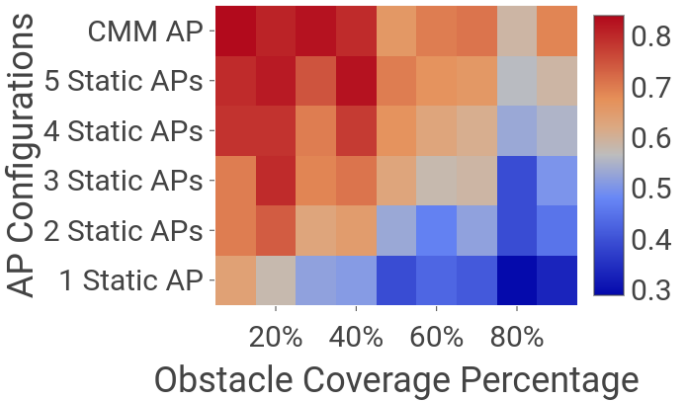

Figure 4.12: LOS - Obstacle Coverage

is a higher probability of obstacles blocking the LOS between AP and STAs. Also, it can be observed that the CMM AP generally has the best performance. The LOS performance of CMM AP over 1∼5 static APs are 171%, 119%, 111%, 101%, and 96% on an average considering all obstacle coverage configurations. Similarly, the throughput performance of CMM AP over 1∼5 static APs are 184%, 143%, 127%, 113%, and 106% on an average. Although LOS performance of CMM AP is 4% worse than 5 static APs case, the throughput performance of CMM AP is 6% better than 5 static APs case due to optimal platform configurations leads to lower expected propagation loss. These simulation results indicate the promising application of CMM AP in various obstacle coverage configurations.

Multi-STA scenario: Other than throughput performance, network fairness is another essential metric for WiFi networks considering a multi-STA scenario. Fairness becomes even more critical in mmWave WiFi networks. Considering a 2-STA scenario, if the first STA is in NLOS with the AP and the second STA is in LOS with the AP, the aggregate network throughput performance will still be high. However, the STA in NLOS is likely to experience severely bad service quality. Thus, network fairness becomes a challenging issue to solve in mmWave WiFi as it is hard to guarantee the LOS connectivity between AP and all STAs. We will analyze both the throughput and fairness performance of the CMM AP and static APs in a multi-STA scenario. For simplicity, we assume only single AP is ac-

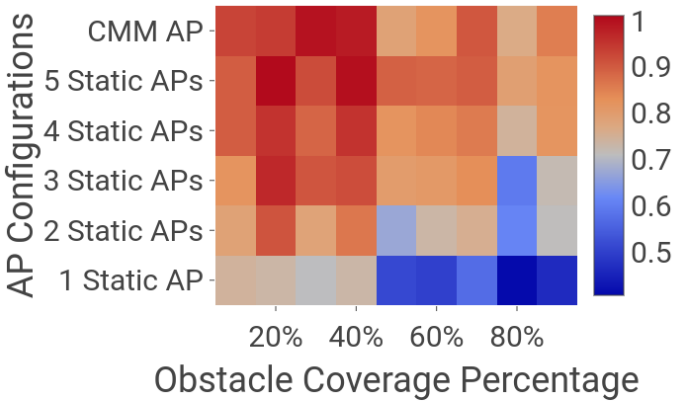

Figure 4.13: Throughput - Obstacle Coverage

tively serving Multi-STA at a time without considering the problem of MAC sharing and optimum pairing between multi-AP and multi-STA. Specifically, we consider both optimal throughput and optimal Jain's fairness index ($(Max_p(fairness_{i,p}))$) [65] for evaluations. For Jain's fairness index, it ranges from $1/n_s$ (single STA has aggregate network throughput) to 1 (each STA has equal throughput), where n_s is the number of STA. n_s is set as 5.

Fig. 4.14 shows the aggregate optimal throughput performance of the CMM AP and static APs. The throughput performance of CMM AP outperforms 1∼5 static APs are 76%, 35%, 7%, 4%, and 5%, respectively. The throughput performance of CMM AP is significantly better than static APs when the number of static AP is smaller than 3. As the number of static AP becomes larger than 3, the CMM AP performance gain is not significant. The reason is that as long as one STA among all STAs is in LOS with the AP, the throughput performance will be high. Thus, as the number of AP increases, it is likely that at least one STA is in LOS connectivity with one of the AP. There are 50% of chance for single static AP that there is at least one STA is in NLOS condition. On the other hand, there is 28% of chance there is at least one STA in NLOS for CMM AP. It means there is additional 80% of NLOS cases of single static AP compared with CMM AP. To further analyze the network fairness, Fig. 4.15 presents the Jain's fairness index for CMM

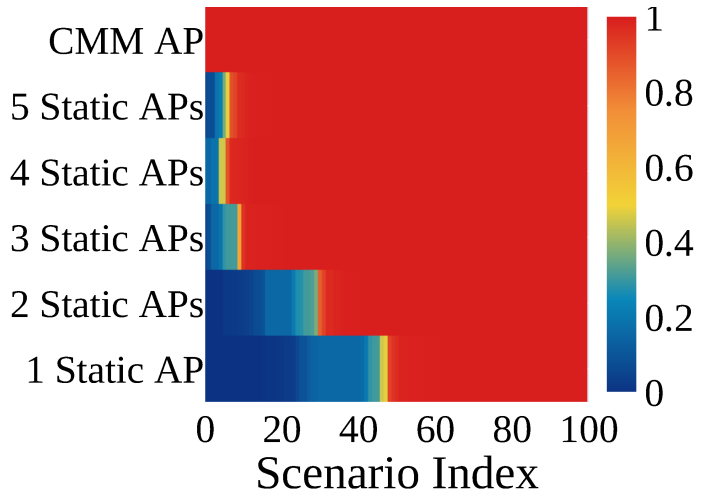

Figure 4.14: Throughput - Multi-STA

AP and static APs. The fairness performance of the CMM AP is 91%, 69%, 35%, 26%, and 28% better than 1∼5 static APs, respectively. Although the throughput performance of the CMM AP is comparable to 4∼5 static APs, the CMM AP can achieve better network fairness compared with static APs for the multi-STA scenario. The reason is that the CMM AP can provide the highest number of LOS connectivity with STAs due to the higher AP location diversity provided by the AP mobile platform.

A CMM AP can perform better than 1∼5 static APs in the perspective of throughput and fairness.

Cost Analysis: After identifying the potential benefits of the CMM AP, we will evaluate the cost of both CMM AP and static APs in the perspective of cost-to-build and energy consumption. We first perform a one-time cost-to-build comparison between the CMM AP and static APs. For the CMM AP, we consider the following substantial equipment: a 3m linear actuator costs $599.99 by estimation [66], and TP-Link Talon AD7200 AP at $350 [67]. This makes the total one-time cost as $949.99 for the CMM AP. For static APs, the only substantial equipment is the AP itself. Based on the one-time cost comparison plot given in Fig. 4.16, we see that the CMM AP is lower in cost than the 3 static APs while the performance of CMM AP is higher than 3 static APs based on the previous quantitative

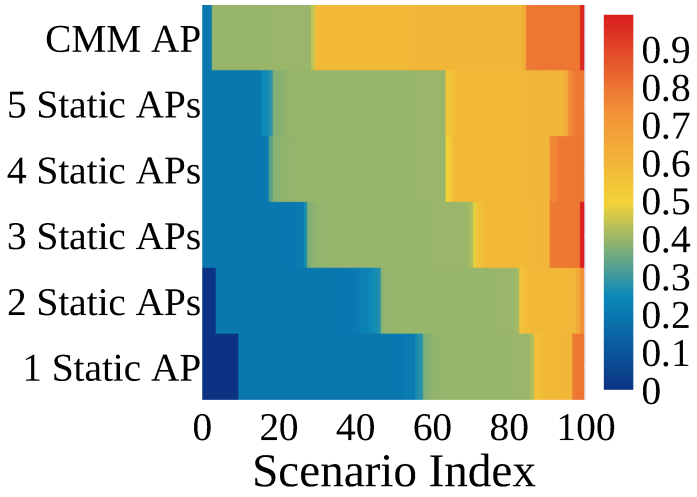

Figure 4.15: Jain's Fairness Index - Multi-STA

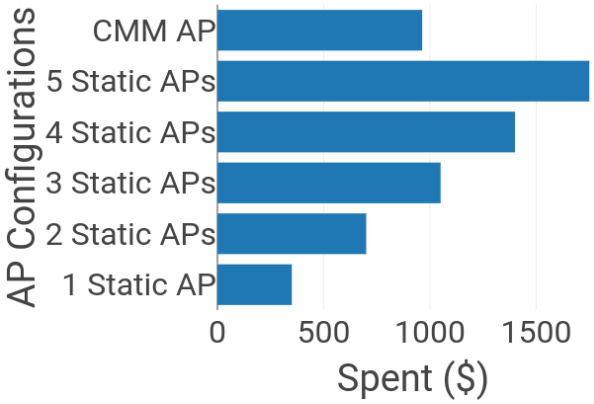

Figure 4.16: Cost-to-build

analysis.

To compare the energy cost for the CMM AP and static APs, we consider a single STA scenario connected with TP-Link Talon AD7200 AP. For the CMM AP, in the worst case scenario, we consider the power consumption of the linear actuator as it is moving with a load of the AP and while the AP is actively transmitting. We also consider an optimal case for the CMM AP in which the linear actuator is not moving, but the AP is transmitting. For static APs, we consider the case where only 1 static AP is transmitting, and the remaining are in idle mode. Based on the measurements conducted using a power monitoring meter,

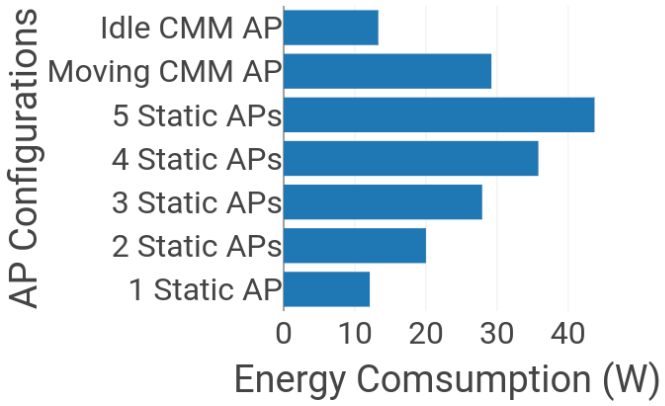

Figure 4.17: Energy Cost

the linear actuator consumes 17.1W when it is moving with the AP, and 1.2W when it is still while holding the AP. The AP was found to consume 12.1W during transmission, and 7.9W during idle time. Using these power consumption measurements, we compare the power consumption of CMM AP and static APs as shown in Fig. 4.17. We see that the power consumption for the optimal case of CMM AP is only slightly higher than single static AP case, and the worst case CMM AP performs similar like 3 static AP configurations. Thus, the power consumption of CMM AP is not expensive compared with static APs.

4.2.3 Summary

In this section, we explore the use case of infrastructure mobility to provide the LOS connectivity to STAs within indoor mmWave WiFi networks. We make a detailed case for a CMM AP by comparing its performance with other types of AP mobility and multiple static APs. Through both simulation and theoretical analyses, we identified that the CMM AP is a promising strategy to improve the performance of mmWave WiFi. Given the benefits of infrastructure mobility, the following are the essential future work to be considered: 1) analyzing benefits of AP mobility in case of dynamic environment (e.g., moving STAs),2) designing a systematic algorithm to leverage the benefits of AP mobility, and 3) AP mobility cost analysis.

4.3 *WiMove*: A Practical System Toward Infrastructure Mobility in mmWave WiFi

Line-of-sight (LOS) is a critical requirement for mmWave communications. In this section, we explore the use of access point (AP) infrastructure mobility to discover and optimize LOS connectivity to stations (STAs) within indoor mmWave WiFi networks. We consider a ceiling-mounted mobile (CMM) AP as the infrastructure mobility framework. Within this framework, we present a LOS prediction algorithm based on machine learning (ML) that addresses the *LOS discovery problem*. The algorithm relies on the available network state information (e.g., LOS connectivity between STAs and the AP) to predict the unknown LOS connectivity status between the reachable AP locations and target STAs. We show that the proposed algorithm can predict LOS connectivity between the AP and target STAs with an accuracy up to 91%. Based on the LOS prediction algorithm, we then propose a systematic solution *WiMove*, which can decide if and where the AP should move to for optimizing network performance. Using both ns-3 based simulation and experimental prototype implementation, we show that the throughput and fairness performance of *WiMove* is up to 119% and 15% better compared with other approaches.

Related works have mainly explored a floor-based mobile AP that navigates its way around obstacles for conventional WiFi networks due to the robotic framework simplicity [8, 25, 11]. In this work, we explore a more effective framework for mmWave WiFi - *a ceiling-mounted mobile (CMM) AP that moves on an actuator platform*, where the CMM AP can potentially achieve higher LOS probability to STAs compared with floor-based AP mobility. Within this framework, we focus on the *LOS discovery problem*. Explicitly, we define the *LOS discovery problem* as how to figure out the LOS connectivity between all available AP locations and target STAs. An idealized solution to this problem is to calculate the optimal location based on a geometric problem formulation, assuming that the locations of the STAs and the locations, shapes, and even materials of the obstacles in the physical space are known. Then, it is trivial to identify the LOS connectivity between target STAs with all possible locations of AP on the actuator platform. However, discovering the

physical attributes of STAs and the physical attributes of obstacles (especially the material of obstacles) is either non-trivial or expensive.

In this context, we present a machine learning (ML) based solution to solve the *LOS discovery problem*. Given it is likely that multiple active WiFi devices exist in a WiFi network and there is rich network state information (e.g., LOS connectivity between the AP and STAs) available, we utilize the network state information as the input to the ML algorithm. [2], *WiMove* utilizes a machine learning (ML) based solution to estimate the LOS connectivity between AP and STAs by relying solely on the LOS connectivity matrices between STAs and the AP in the network. The algorithm trains itself to predict the desired LOS connectivity information more specific LOS estimation techniques, simply based on the network state information. When network dynamics happen (e.g., when a new STA joins the network), the algorithm can identify whether the target STA (e.g., the new STA) is likely to have LOS connectivity to all possible AP positions. We evaluate the LOS connectivity prediction accuracy of the ML-based algorithm in different network scenarios, and it achieves prediction accuracy by up to 91%. Then, we incorporate the LOS prediction algorithm in a systematic solution, *WiMove*, which is designed to maximize the number of LOS connectivity between AP and STAs given the LOS prediction results. *WiMove* can decide whether repositioning the AP is required and, if so, where to move to. Similarly, when STAs leave the network, the decision as to whether to move and where to move to depends on LOS connectivity objectives. Using both ns-3 based simulation and experimental prototype implementation, we show that the throughput and fairness performance of *WiMove* is up to 119% and 15% better compared with other approaches. Finally, for obstacle dynamics (obstacles added or removed), the AP recalculates the connectivity matrices based on which LOS links have been compromised, and which LOS links have been newly created. Having these capabilities precludes the AP from having to perform the expensive (and noisy) process of localization of the STAs and the obstacles in the network

[2] According to WiFi statistics [68], the number of WiFi devices is predicted to achieve 27 billions in 2022.

that would otherwise be required for recalculation.

The following is a summary of our key contributions:

- We present a LOS prediction algorithm for a CMM AP to determine the LOS connectivity between all available AP locations on the actuator platform and target STAs. The algorithm uses a novel ML-based methodology to recalculate the LOS connectivity when network condition changes by purely relying on network state information (e.g., LOS connectivity between STAs and the AP).

- We then incorporate the ML-based LOS prediction algorithm into a systematic solution, *WiMove*, which is able to identify the optimal AP location with a maximized number of LOS connectivity between AP and STAs. Then, we present the evaluation results for *WiMove* using both simulations and experimental prototypes. We show that the throughput and Jain's fairness index of *WiMove* performs up to 119% and 15% better compared with other approaches. Based on our knowledge, we are the first work to leverage the benefits of infrastructure mobility in the context of mmWave WiFi.

4.3.1 Background Overview

mmWave WiFi

The essential advantage of the mmWave WiFi as compared to conventional WiFi is the availability of a large amount of unlicensed spectrum. Taking advantages of the large spectrum available, the bandwidth supported by mmWave WiFi standard 802.11ad is 12.5x larger than the bandwidth supported by the latest non-mmWave WiFi standard 802.11ax. However, achieving the multi-gigabit performance in mmWave WiFi networks is not a trivial problem, since the mmWave signal propagation characteristics significantly differ from that of the conventional spectrum. The major difference is that mmWave communication has *extremely high signal attenuation* [17] generally caused by: 1) high propagation loss: there is an additional signal attenuation of 22dB at 60GHz compared to that of 5GHz based on the free space path loss model and the properties of the propagation media can also

significantly increase the signal attenuation (e.g., oxygen absorption or rain attenuation); 2) high penetration loss: the attenuation impact is amplified when there is shadow fading or NLOS between the transmitter and receiver pair; and 3) sparse multipath diversity: multipath components propagating through objects tend to have low signal power due to longer propagation paths and additional reflection loss. Due to these features of mmWave communication, NLOS can have a severe impact on mmWave WiFi performance. Note that a consequent advantage of mmWave communication compared with the ultra high and super high frequency is that the high signal attenuation naturally lowers the probability of interference.

LOS in mmWave Networks

Based on the harsh mmWave signal propagation characteristics, it is likely that robust receiver signal quality is hard to achieve. While beamforming can be utilized to combat the severe propagation loss in mmWave communication, the additional loss caused by NLOS can lead to severe performance degradation (e.g., a human blocking LOS could lead to $\sim$30dB additional loss [69]) more solid reference on LOS/NLOS rx power difference. Note that for 802.11ad [70], a 2dB additional loss could cause a 1Gbps performance drop when the modulation and coding schemes drop from 23 to 22. Thus, providing high and robust receiver signal quality is an essential problem for mmWave WiFi. In this context, in order to achieve multi-gigabit performance, LOS connectivity is highly critical in mmWave networks. In a simple experiment to observe the impact of NLOS in mmWave WiFi, we build a mmWave link using a TP-Link Talon AD7200 AP and an Acer Travelmate P648 laptop. We observe that obstacles such as a wall, a metal cabinet, and a cardboard box can degrade the performance of an ideal link with LOS connectivity from 1Gbps to 0Gbps, 0Gbps, and 0.52Gbps, respectively. Even though LOS connectivity provides critical benefits for mmWave communication, achieving LOS connectivity is not trivial. Consider typical indoor scenarios consisting of randomly located obstacles with various dimensions and materials that could potentially block the mmWave link. Also, both mmWave STAs

and the obstacles can be dynamic, which prevents the possibility of predetermining the ideal AP location with optimized LOS connectivity to STAs.

LOS and Infrastructure Mobility To optimize LOS connectivity in a mmWave network adaptively, we consider infrastructure mobility as a promising candidate solution, as infrastructure mobility allows for changing the location of the AP adaptively. Fig. 4.18 shows a scenario with a CMM AP and randomly distributed obstacles, where the obstacle density and dimension follows distribution based on real-world measurements. The gray cuboids, white cuboids, and black circle represent the CMM AP with its platform, obstacles, and the STA, respectively. For simplicity, the presented actuator platform is a 1D linear actuator [3]. In Fig. 4.18, the CMM AP initially located at the center of a linear actuator platform can't provide LOS connection to the STA. Given the degree of freedom of AP mobility, the AP can move to a location on the side of the platform where LOS connectivity can be provided. On a more generalized note, using simulation-based statistical analysis, we identify that a CMM AP operating on a 3m long linear actuator provides a 70% increase in LOS probability coverage compared with a static ceiling-mounted AP. This translates to a 60% increase in throughput performance. It should be noted that this work investigates the application of infrastructure mobility in the context of mmWave WiFi due to the critical impact of LOS connectivity for mmWave communication. This approach is also generally applicable to other types of wireless networks (e.g., wireless sensor networks, conventional WiFi, and robotic wireless networks), since wireless link performance generally benefits from LOS connectivity.

4.3.2 The *LOS discovery problem*

The network scenario considered in this work is a single room with a single CMM AP serving multiple STAs, where the CMM AP platform is mounted on the center of the ceiling parallel to the shorter edge. The AP can move to P discrete available positions on the

[3] With larger movement range provided by the actuator platform, higher LOS connectivity probability can be achieved, but the cost also becomes more expensive.

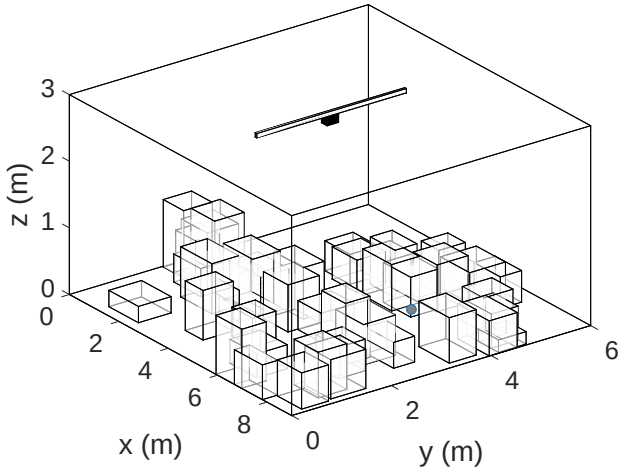

Figure 4.18: Infrastructure Mobility Providing LOS

platform [4]. There are M STAs in this network scenario at a specific time instance t. For both the AP and STAs, it is assumed that both 5GHz and 60GHz WiFi radios are available. At $t+1$, there is an $(M+1)^{th}$ STA intending to connect to the AP through mmWave. At time instance $t+1$, we assume that the STA-STA LOS connectivity matrix between $M+1$ STAs and AP-STA LOS connectivity matrix between AP and first M STAs are given (the data collection methods are described in Section 4.3.5). The LOS connectivity of the new STA with all available AP locations is unknown. The information on STA's intention to connect to the AP and the connectivity information of the AP are communicated through the 5GHz band.

LOS connectivity is defined as a binary variable with 1 representing LOS and 0 representing NLOS. We define $los_{i,j}$ representing the LOS connectivity between device i and device j. For example, for AP at location p (with $p \in [1,P]$) on the actuator platform, $los_{p,m}$ represents LOS connectivity status between the AP at location p and STA m (with $m \in [1,M+1]$ at $t+1$). Specifically, we consider the LOS connectivity matrices with two pieces of information: 1) $LOS_{(ss,t+1)}$: it represents the LOS connectivity status between all

[4] We assume the power and the Ethernet cords of the AP are delivered through the actuator platform.

STAs at time instance $t+1$:

$$LOS_{(ss,t+1)} = \begin{bmatrix} los_{1,1} & los_{1,2} & \dots & los_{1,M+1} \\ los_{2,1} & los_{2,2} & \dots & los_{2,M+1} \\ \vdots & \vdots & \ddots & \vdots \\ los_{M+1,1} & los_{M+1,2} & \dots & los_{M+1,M+1} \end{bmatrix}$$

and, 2) $LOS_{(as,t+1)}$: it represents the LOS connectivity status between all available AP locations with all STAs at a time instance $t+1$:

$$LOS_{(as,t+1)} = \begin{bmatrix} los_{1,1} & los_{1,2} & \dots & los_{1,M} \\ los_{2,1} & los_{2,2} & \dots & los_{2,M} \\ \vdots & \vdots & \ddots & \vdots \\ los_{P,1} & los_{P,2} & \dots & los_{P,M} \end{bmatrix}$$

Within this scope, as network dynamics changes (e.g., a new $(M+1)^{th}$ STA joins the network), the objective is to identify AP-STA LOS connectivity vector $\vec{as}_{(M+1,p,t+1)}$ between AP and $(M+1)^{th}$ STA at time instance $t+1$, where

$$\vec{as}_{(M+1,p,t+1)} = [los_{M+1,1}, los_{M+1,2}, ..., los_{M+1,P}] \tag{4.3}$$

Given the AP-STA LOS connectivity vector $\vec{as}_{(M+1,p,t+1)}$, the AP can then optimize the LOS connectivity to the targeted STA. With this network problem definition, we restrict the scope of this work to the following: (i) we only consider a single WiFi network where a CMM AP serving multiple STAs in a single room; and (ii) we assume the actuator platform of CMM AP as a 1D linear actuator.

4.3.3 LOS Prediction Algorithms

Given the potential benefits that can be achieved by leveraging LOS connectivity in mmWave WiFi, we propose an ML-based algorithm to address the *LOS discovery problem* in this section.

Heuristic Intuitive Approach

Based on our observations, a deterministic solution for the *LOS discovery problem* is not feasible. We intend to solve the *LOS discovery problem* using heuristic methods from a probabilistic perspective. At a single time instance t, the obstacle map (location and dimension of obstacles) is fixed but unknown. The set of LOS connectivity information of $LOS_{(ss,t)}$ and $LOS_{(as,t)}$ can reveal the information about unknown obstacle map to some extent. Assuming that $LOS_{(ss,t)}$ and $LOS_{(as,t)}$ are given, we intend to identify the LOS connectivity between the target $(M+1)^{th}$ STA with the AP at time instance t. Similar to AP-STA LOS connectivity vector $\vec{as}_{(M+1,p,t)}$, we define the STA-STA LOS connectivity vector of $(M+1)^{th}$ STA to all STAs as $\vec{ss}_{(M+1,m,t)}$ at time instance t:

$$\vec{ss}_{(M+1,m,t)} = [los_{M+1,1}, los_{M+1,2}, ..., los_{M+1,M+1}] \tag{4.4}$$

Specifically, the connectivity vector $\vec{ss}_{(M+1,m,t)}$ can be collected from the connectivity matrix $LOS_{(ss,t)}$. Intuitively, if the $(M+1)^{th}$ STA has similar LOS connectivity vector $\vec{ss}_{(M+1,m,t)}$ with another m'^{th} STA ($m' \in [1,M]$), the location of these two STAs is likely to be closed to each other. Given the location similarity between these two STAs, the AP-STA LOS connectivity matrix $LOS_{(as,t)}$ is also likely to be similar to each other. Given the objective is to estimate $\vec{as}_{(M+1,p,t)}$, we propose the following heuristic algorithm based on the previous intuitive observation. We first identify the most similar STA-STA connectivity vector of m'^{th} STA and the target $(M+1)^{th}$ STA, and then match AP-STA LOS connectivity vector $\vec{as}_{(M+1,p,t)}$ with $\vec{as}_{(m',p,t)}$. Specifically, to identify the maximum similarity of STA-STA LOS connectivity vector between the target $(M+1)^{th}$ STA and other STAs, we identify m'^{th} STA with minimum Euclidean distance between the STA-STA LOS connectivity vectors with target $(M+1)^{th}$ STA. The equation to calculate the Euclidean distance between STA-STA LOS connectivity vectors is shown in the following equation:

$$d(M+1,m) = ||\vec{ss}_{(M+1,m,t)} - \vec{ss}_{(m,m,t)}|| \tag{4.5}$$

There is a possibility that multiple STAs have the same minimum Euclidean distance. We collect the set of STAs, V, with maximum similarity with the target STA. Then, we calculate the expected AP-STA LOS connectivity vector E[$\vec{as}_{(m,p,t)}$] of the set of STAs. We consider E[$\vec{as}_{(m,p,t)}$] as the predicted result for $\vec{as}_{(M+1,p,t)}$ of the target $(M+1)^{th}$ STA. The pseudo code for this heuristic algorithm is presented in Algorithm 1.

Algorithm 2 Connectivity Similarity

$LOS_{(ss,t)}$ and $LOS_{(as,t)}$ at time instance t $\vec{as}_{(M+1,p,t)}$ of $M+1^{th}$ STA $\vec{ss}_{(M+1,m,t)}$ = Target STA-STA LOS connectivity vector

while Traverse all $\vec{ss}_{(m,m,t)}$ other than $M+1^{th}$ **do** d($\vec{ss}_{(M+1,m,t)}, \vec{ss}_{(m,m,t)}$) ¡ minimum distance minimum distance = d($\vec{ss}_{(M+1,m,t)}, \vec{ss}_{(m,m,t)}$) Initialize V to a empty set Add m to V; d($\vec{ss}_{(M+1,m,t)}, \vec{ss}_{(m,m,t)}$) == minimum distance Add m to V; $\vec{as}_{(M+1,p,t)}$ = E[$\vec{as}_{(m,p,t)}$] of V

The above algorithm requires only $LOS_{(ss,t)}$ and $LOS_{(as,t)}$ at a single time instance t. In fact, the $LOS_{(ss,t)}$ and $LOS_{(as,t)}$ can be continuously monitored and collected. Here, we leverage the benefits of a total of T data samples to further improve the performance of the heuristic algorithm. To utilize T data samples, it is important to notice that not all historical data samples provide useful information for LOS prediction. The key methodology is that we first identify the most similar $LOS_{(ss,t)}$ from T data samples with the current $LOS_{(ss,t')}$. Ideally, if $LOS_{(ss,t)}$ of two data samples are similar, it is likely that the location of STAs from different data samples are also similar to each other. Thus, we utilize $LOS_{(ss,t)}$ as a representation for scenario features. We can then utilize Algorithm 1 to find the best matched $\vec{ss}_{(M+1,m,t)}$ from the most matched $LOS_{(ss,t)}$ and the current $LOS_{(ss,t')}$. Specifically, to achieve such an objective, we calculate the Euclidean distance between $LOS_{(ss,t)}$ of the target data sample with that of T data samples using equation 4.6. Then, we find the set of $LOS_{(ss,t)}$ with minimum Euclidean distance with the current $LOS_{(ss,t')}$.

$$d(LOS_{(ss,t')}, LOS_{(ss,t)}) = ||LOS_{(ss,t')} - LOS_{(ss,t)}|| \tag{4.6}$$

Having identified a set of $LOS_{(ss,t)}$ with maximum similarity with the target $LOS_{(ss,t')}$, S, we perform Algorithm 1 to identify the most matched STA-STA LOS connectivity vectors

from the set of best matched set of $LOS_{(ss,t)}$ to identify the expected E[$\vec{as}_{(m,p,t)}$] as Algorithm 1. The pseudo code for the identify most similar scenario is presented in Algorithm 2.

Algorithm 3 Scenario Similarity

T sets of $LOS_{(ss,t)}$ and $LOS_{(as,t)}$ most matched STA-STA LOS connectivity matrix set S $LOS_{(ss,t')}$ = Target LOS STA STA connectivity matrix

while Traverse all $LOS_{(ss,t)}$ other than the target **do** $d(LOS_{(ss,t')}, LOS_{(ss,t)}))$ ¡ minimum distance minimum distance = $d(LOS_{(ss,t')}, LOS_{(ss,t)})$ Initialize S to a empty set Add t to S $d(LOS_{(ss,t')}, LOS_{(ss,t)}))$ == minimum distance Add t to S

ML Framework

We identify three limitations in the heuristic algorithm that can be addressed with intelligent approaches. 1) Performance optimality: the heuristic algorithm is only capable of identifying the most similar scenario or STA-STA LOS connectivity vector. The second, third or other similar STA-STA LOS connectivity vectors may also provide valuable information that can be captured to improve the LOS prediction performance; 2) Given there is a rich set of network state information other than LOS, it is not trivial for the heuristic algorithm to jointly consider multiple types of input data (e.g., LOS connectivity and location of STAs); 3) When data samples are limited, the data set may not provide enough information for the algorithm to achieve reasonable prediction accuracy. It is possible to permute the STA-STA LOS connectivity matrix $LOS_{(ss,t')}$ of the target scenario to identify similar matrices with STAs in different orders. However, the time complexity of such a heuristic algorithm will be high O((M+1)!), considering the permutations of the training set. Hence, with a large number of STAs and data samples, the heuristic algorithm is infeasible to operate in a real-time manner.

To further improve the prediction accuracy and reduce time complexity, we consider a Machine Learning (ML) based approach. The proposed ML approach can take into account multiple network state information as input, and the time complexity will be constant for an offline trained model. The problem to predict the LOS connectivity of the $(M+1)^{th}$

STA with the AP is represented and solved in a supervised fashion. Thus, keeping the fact in mind that the underlying relationship between input and output is actually a skewed representation of the fixed obstacle map, we utilize parametric function approximation approaches to learn this latent structure. While we are aware that it might not be possible to learn the full obstacle map, we aim to extract as much possible information in an attempt to maximize the prediction accuracy. In our ML-based LOS connectivity prediction framework, we use Artificial Neural Networks (ANNs) as a recipe for parametric function approximation.

Input Features and the Output: We consider the availability of LOS connectivity information, which can be collected using [71], which explores space and antenna diversity to identify LOS connectivity. We also utilize the localization information of STAs that can be obtained with reasonable accuracy based on [72], which utilizes RSSI-based location-clustering techniques. The input data is present in the format of 1) LOS connectivity matrix between STAs, $LOS_{(ss,t)}$, LOS connectivity matrix $LOS_{(as,t)}$ between AP and STAs, and 2) the localization matrix of STAs in the form of three dimensional cartesian coordinates. The input data is generated in accordance to practical estimation techniques for both LOS and localization prediction and hence accounts for the uncertainty involved. Specifically, we incorporate the error model of LOS estimation and localization based on the prediction cumulative distribution function (CDF) presented in [71] and in [72], respectively. The labels (ground truth) for training are present in the format of $\vec{as}_{(M+1,p,t)}$ i.e., the LOS connectivity matrix of $(M+1)^{th}$ STA with the P possible locations of the AP.

As we can see, the $LOS_{(ss,t)}$ matrix is symmetric and diagonal elements are always 1. We extract only the $(M+1)*M/2$ informative bits from this matrix. Given the network has $M+1$ STAs, the $LOS_{(ss,t)}$ matrix has total $(M+1)*(M+1)$ features and the $LOS_{(ss,t)}$ matrix has $M*P$ features. The localization matrix for $(M+1)$ STAs consists of $3(M+1)$ features. The input feature vector X is obtained by concatenating these three feature vectors into a single vector of size $(M^2+(5+P)M+4)$. The network outputs $\hat{Y} \in [0,1]^P$, a P sized

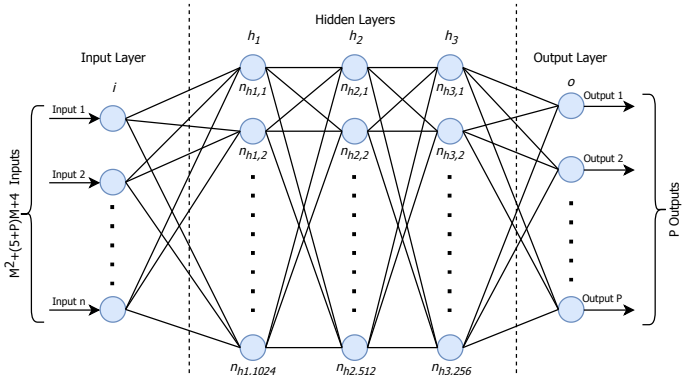

Figure 4.19: Neural network architecture

probability vector representing the probability of LOS connectivity of $(M+1)^{th}$ STA with P locations.

Network: We use a Multi-Layer perceptron network [73] with the number of hidden layers and neurons configured to work across different network scenarios. The flattened input feature vector of size $(M^2+(5+P)M+4)$ is fed to a fully connected network as shown in Fig 4.19 with 3 hidden layers. The l^{th} hidden layer has a total of n_{H_l} neurons. The k^{th} neuron in $(l-1)^{th}$ layer is connected to j^{th} neuron in l^{th} layer with a weight of w^l_{jk}. b^l_j represents the bias of the j^{th} neuron in the l^{th} layer. The activation of the j^{th} neuron in the l^{th} layer, i.e. a^l_j, is calculated through the forward propagation rule as below,

$$a^l_j = \sigma(\sum_k w^l_{jk} a^{l-1}_k + b^l_j) \tag{4.7}$$

where, σ applies the non-linearity in the model using the ReLU activation function,

$$\sigma(h) = max(0,h) \tag{4.8}$$

Finally, we use softmax layer [74] before the output layer to transform the output logits to the probability vectors. The model is trained through the backpropagation rule, using weighted cross-entropy loss, defined as:

$$H_y(p) = \sum_i^P -(y_i \log(p_i) * w + (1-y_i)\log(1-p_i)) \tag{4.9}$$

Here, p represents the softmax probability of output logits, and w is calculated as the ratio

of NLOS vs. LOS connectivity using training data. As the ratio of NLOS to LOS connectivity in the data samples is imbalanced, the weighted cross entropy loss with weight w, balances the loss function to avoid any local minima. Using the available training data bank, $DB = \{(X_1, Y_1), (X_2, Y_2), \ldots (X_N, Y_N)\}$, of N samples, the loss function is minimized using stochastic gradient descent (SGD) with momentum optimizer [75]. In SGD, a batch of B training samples is randomly selected out of N training samples, and the weights and biases are updated through the backpropagation rule. A fraction of the gradient in the previous iteration is retained with the "coefficient of momentum". At each learning iteration, the learning rate is decreased over time to optimize performance and to increase the convergence rate [76] of the algorithm. While training, we also augment the training set by a random permutation over the sequence order of the STAs in the input features. This not only increases the training set size but also improves the convergence of gradient descent by avoiding any STA-order based local minima. The random permutations prevent the ML architecture to extract features based on the STA ordering.

As mentioned previously, more network information can be collected and feed into ML model. Here, we consider STA location as another metric, which can be estimated using localization techniques [72]. Similar to the extracted features of the LOS connectivity input matrix, we obtain an additional location feature vector of size $3M + 3$, which is appended to the LOS features. In this fashion, with given LOS and location input, our feature size increases to $M^2 + (5 + P) * M + 4$. Other network architectural parameters remain intact as explained before.

It should also be noted that while the AP is moving towards the estimated optimal location, it will continue to gather the ground truth for the traversed locations. This information can be provided as the ground truth for LOS prediction matrix and can be utilized to augment the existing training data feedback to the ML models to further boost the prediction performance. We leave the feedback based adaptive improvements for future work.

4.3.4 LOS Prediction Evaluation

In this section, we evaluate the performance of both heuristic and ML-based LOS prediction approach through simulations. We utilize ns-3 simulator to generate the network scenarios to collect required data samples. By tuning network scenarios, we are able to generate a large number of data samples and measure corresponding network performance.

Simulation Platform

To incorporate the features of indoor configurations and 802.11ad, we make the following modifications to the default ns-3 simulator.

Simulation of Indoor Scenarios: Due to the lack of an indoor scenario model in ns-3, we implemented the following indoor model. A room is simulated as a specific three-dimensional space with a given obstacle distribution model. To simplify the simulations, we assume that the obstacles are modeled as cuboids and that they are placed on the floor. Typically, when an STA is communicating with an AP, it is located on the top of an obstacle (e.g., laptop on the desk) or attached to the side of an obstacle (e.g., TV on the wall or human using a mobile phone). To simulate such practical scenarios, we consider that the placement of the STA follows the following distribution: an obstacle is uniformly selected as the base location for the STA, and the STA is uniformly distributed on top or sides of the selected obstacles.

To accurately simulate indoor obstacles, the implemented obstacle model has the following features:

- The center of the obstacle follows a Poisson point process (PPP) as shown in Eq. 4.10. It defines the probability for obstacles to be uniformly placed in an indoor scenario.

$$P\{N = n\} = \frac{\lambda^n * e^{-\lambda}}{n!} \tag{4.10}$$

  where, the expected number of obstacles per unit area is defined as λ and n is the expected number of obstacles to be distributed.

Table 4.2: Default Simulation Parameters

	Settings
Size of room (m)	(9, 4, 3)
(μ_x, μ_y, μ_z) (m)	(1.08, 0.28, 0.61)
$(\sigma_x, \sigma_y, \sigma_z)$ (m)	(0.46, 0.08, 0.21)
Platform location	Center of the ceiling
Platform orientation	Parallel to shorter edge
Platform length (m)	3
P	30
M	20
n_{pl}	2
σ_{fading}	2.24
T	10,000
Network dynamics	instant STA dynamics

- The x, y, and z dimension of obstacles follow a truncated normal distribution to constrain the maximum and minimum of obstacle dimension.
- The material of the obstacle is uniformly chosen from [77] to represent materials with various penetration losses.

We show the default parameters used in the simulation in Table 4.2. The parameters are derived by using a real-life physical space (a lab environment) as a guiding example. To build a cuboid-based obstacle model, the x, y, and z dimensions are collected based on the largest dimension of a measured obstacle. We then collect the number of obstacles in the lab space as n. To calculate the x, y, z dimension distribution parameters, we use distribution fitter in MATLAB to calculate the best fit normal distribution with mean μ_x, μ_y, μ_z, and standard deviation $\sigma_x, \sigma_y, \sigma_z$. The maximum and minimum of x, y, and z dimensions of obstacles are utilized as the range limitation in the truncated normal distribution.

Simulation of 802.11ad: We use the 802.11ad model based on [63]. The simulator provides all techniques that are essential for 802.11ad, such as beamforming training and steering, hence providing an accurate simulation environment for 802.11ad. The mmWave

channel is another essential component of simulating the performance of 802.11ad. To incorporate shadow fading based on information of mmWave WiFi devices and obstacles, we consider the impact of shadow fading and multipath separately. Specifically, we modified the widely accepted log-distance based path loss model as follows:

$$L(d) = L(d_0) + 10 * n_{pl} * log_{10}(\frac{d}{d_0}) + X_s + X_{\sigma_m} \tag{4.11}$$

where, $L(d_0)$ is the path loss at a reference distance d_0, n_{pl} is the path loss exponent, d is the distance between two communication devices, X_s represents shadow fading where the penetration loss is calculated based on the obstacles' location, dimension and material between mmWave WiFi devices, and X_{σ_m} represents the normally distributed multipath fading with σ_m as the standard deviation. Particularly, X_s is 0 when the communication link is in LOS connectivity. We collected the average of 5 sets of experimental estimations of the log-distance based path loss model to collect n_{pl} and σ_m based on [64], which are presented in Table 4.2.

Data Sample Generation: To generate data samples using the above ns-3 model, we initialize the network scenario by generating a random network scenario like Fig 4.18. Then we deploy M STAs following the STA distributions mentioned above. At each time step, network dynamics (e.g., STAs join or leave the network) happens based on the Poisson distribution with an expected rate of one unit per time step. We then collect network state information (i.e., STA-STA LOS connectivity matrix, AP-STA LOS connectivity matrix, and STA location matrix) for each time instance t. The default parameters of the number of STAs M, the number of data samples T, the number of available AP locations P are described in Table 4.2.

ML Network Configurations

We use Tensorflow [78] to implement and run the ML models. We use three hidden layers in the model with 1024, 512 and 256 neurons, respectively. We use a default batch size of 256 except for the cases where the total training sample size is smaller than 256. The

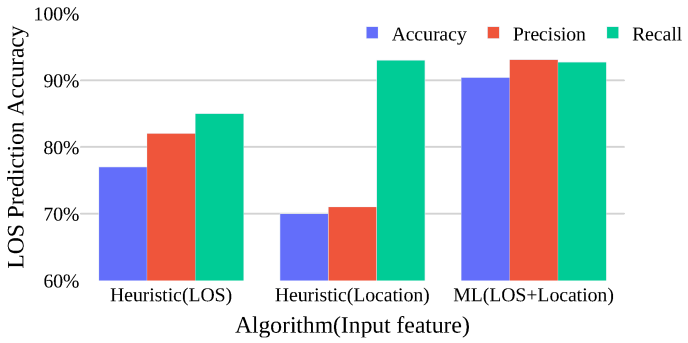

Figure 4.20: Comparison of heuristic and ML

learning rate is initialized as 0.15, and decreased with a factor of 0.9 every 5000 steps. For the LOS connectivity prediction of all AP locations, the performance metrics are found very similar with insignificant variance. Hence, in subsequent analysis, we only present the average performance over all the AP locations.

We split the available data into two sets: 1) the training set comprises of 70% of the data and is used to learn the network weights, and 2) the remaining 30% set is used for testing. We use three different metrics to evaluate algorithm performance, namely overall accuracy, precision and recall for LOS connectivity. Precision for LOS connectivity is defined as the fraction of actual LOS connections out of total predicted LOS connections. Recall informs how accurately the model can predict LOS connections out of actual LOS connections. For each configuration, we ensure the evaluation correctness through random permutation tests [79]. It is to be noted that this is a binary classification problem (predicting the presence of LOS connection) and hence, a random classifier will have an accuracy of 50%. As LOS connectivity and NLOS connectivity are not equally distributed, an evaluation based only on accuracy will represent biased results. Hence, we provide precision and recall along with accuracy. Additionally, we also randomly permute the labels of test set to validate that the ML model is learning meaningful latent structure in terms of the relationship between inputs features and output labels.

Comparison of ML and Heuristic

In this section, we evaluate the performance of both heuristic and ML algorithms. In a 6 STAs scenario, we test 2 different input features, LOS and location, separately with heuristics algorithm, and we consider both inputs as the ML inputs. From Fig.4.20, we can see that accuracy of three settings achieves 77%, 70%, and 90%, respectively. Overall, we identify that ML performs significantly better than the heuristic algorithm described. These results validate that ML can take advantage of multiple input features and gain more insightful information from jointly considering LOS and location input features. Specifically, LOS connectivity matrices provide network-level relative information of each STA and location matrices provides the physical information of each STA. Even with prediction error, ML model is able to jointly learn the location of each STA and identify the corresponding LOS connectivity with all available AP locations. In case of the heuristic algorithm, the introduction of error in data in accordance with error models reduces the performance since it only tries to identify the AP-STA LOS connectivity vector based on the best matching metrics. In the following section, we will mainly evaluate ML performance due to its high prediction accuracy.

Impact of Number of STAs

Here, we test the ML performance with different number of STAs. Specifically, the number of STAs $M+1$ is configured as 6, 11 and 21. Surprisingly, from Fig 4.21, we identify that the prediction accuracy saturates when the number of STA is as low as 6. The prediction accuracy is 90%, 91%, and 90% for 6, 11, and 21 STAs, respectively. It indicates the ML performance is invariant with the number of STAs. However, we identified that as the number of STA increases, the minimum required network size also increases. If the minimum required network complexity is not used, the performance drops. Therefore, we conclude that ML performance is largely invariant with the number of STAs as long as the network size is large enough.

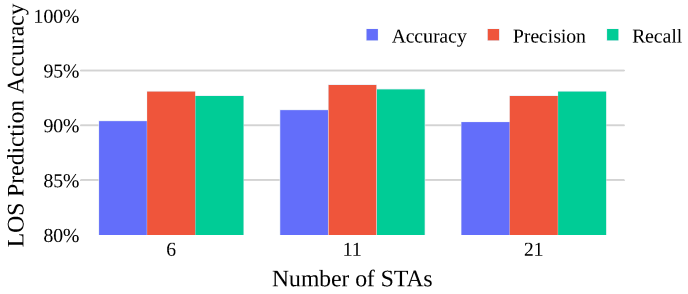

Figure 4.21: ML with different number of STAs

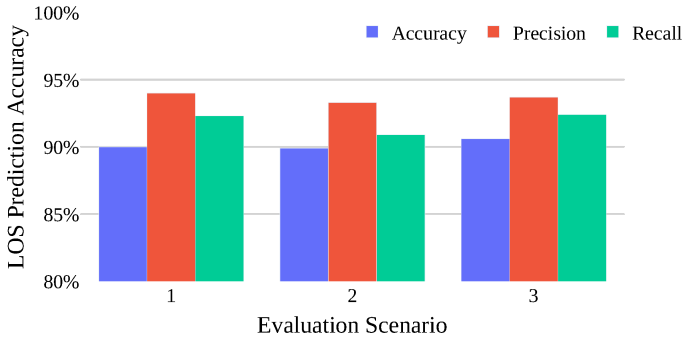

Figure 4.22: ML with different Obstacle maps

Impact of Obstacle Maps

To analyze the impact of different obstacle maps, and hence quantize the applicability of the ML algorithm to different indoor scenarios, we obtain the performance metrics for 3 different obstacle maps for default scenarios. From Fig. 4.22, we observe that the mean accuracy is 90% with a standard deviation of 0.4%. The low variance demonstrates that the proposed algorithm is generalizable to different scenario instances (i.e., different STA locations within different obstacle maps).

Dynamic Environments

The ML framework presented above requires the environment to be static (i.e., fixed obstacle map). In practice, however, the obstacle maps or STA locations are dynamic, as the obstacle and STA locations could change at every time step t. We consider a discrete dynamic scenario, where obstacles or STAs can be different at every time step. We first classify dynamic scenarios and evaluate ML in different dynamic scenario settings.

Specifically, we classify network dynamics into three types: 1) instant STA dynamics: it is defined as when fixed STA becomes active or fixed active STA drops out of the network, 2) continuous STA dynamics: a active STA changes its location, and 3) continuous obstacle dynamics: obstacle in target scenario moves to another location. These dynamics can be identified based on network state information available. Instant STA dynamics can be identified by the connected STA MAC address change. Continuous STA dynamics can be identified by the change of STA location and the connectivity matrix to other static connected STAs. Continuous obstacle dynamics can be identified by the change of STA LOS connectivity matrix without changes in STA location. Instant STA dynamics and continuous STA dynamics do not skew ML model prediction accuracy as the underlying obstacle map is unaffected. However, obstacle dynamics change the obstacle map, which can lead to decreased performance of ML model. Thus, we will target obstacle dynamics in the rest of this section. Considering the case in which the ML model is retrained after an obstacle movement is detected, the performance is now limited by the frequency of obstacle movements. On average, if there is an obstacle movement every k time steps, then the achievable performance of the ML model after training from data of k time steps is of interest. The methodology to study the continuous obstacle dynamics scenarios is to train using the data set collected at each k time steps. Specifically, we change the number of data sample collected k from 100 through 10000.[5].

The neural-network presented in the previous section is an offline learning method, where the network weights are learned based on the data collected before deployment. Once the network is deployed for application usage, the network weights are not updated. This offline training methodology cannot be applied as-is in the case of dynamic scenarios due to the two major challenges: (1) no fixed latent structure in the data points: as the obstacle map is changing with each time step, the underlying input and output relationship is no longer fixed; (2) data availability: with the environment changing at each time step

[5]As the number of samples are less than 100, heuristic algorithm can be utilized as the baseline for prediction

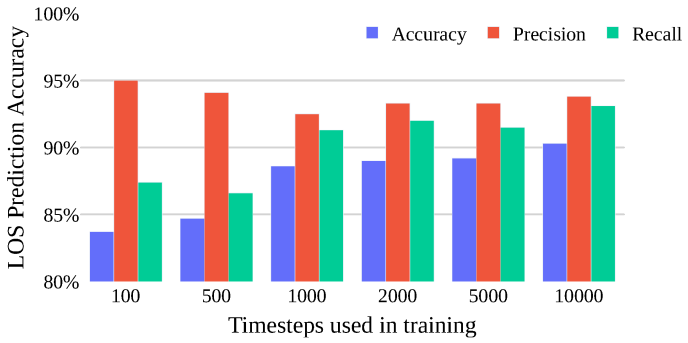

Figure 4.23: ML in Dynamic Scenarios

t, it is possible to obtain only a few training labels per time step which makes it really challenging to learn with the data-hungry models.

Fig. 4.23 shows the prediction accuracy when the number of samples increases from 100 to 10,000. Clearly, we can observe that there is a tendency that the prediction accuracy increases as the number of data sample increases. Specifically, the prediction accuracy increases from 84% to 90% as the number of data samples increases from 100 to 10000, respectively. Similarly, the recall rate also increases with the number of timesteps. However, increasing the timesteps does not have significant impact on the precision metric. The precision varies in the range of 93% to 95%. We also observe that the prediction accuracy for dataset from as low as 100 time steps is reasonably accurate.[6]

4.3.5 *WiMove*: A Systematic Solution

In this section, a systematic solution of *WiMove* is first discussed. In this solution, we intend to maximize the mmWave WiFi network performance in the perspective of throughput and fairness. We assume STAs with NLOS with AP can be served using 5GHz band (the joint 5GHz and 60GHz network optimization is considered as future work). The objective function for AP to identify the optimal location is to *maximize the number of LOS connectivity links between AP and STAs*. Given this objective function, we will then evaluate *WiMove* using both simulations and experiments.

[6]Note that, as the number of network status data samples are small, the prediction accuracy will be low.

Trivial Solutions

Before we introduce the solution of *WiMove* for the CMM AP in mmWave WiFi, we will first briefly discuss two trivial approaches to provide mmWave service to STAs and the corresponding trade-offs:

- *Single static AP:* The static AP is mounted at the center of the ceiling to maximize the overall LOS probability with randomly deployed STAs. This approach has simplest strategy and minimum cost, but the non-adaptive solution can only achieve limited performance. For example, if a STA is in NLOS with the AP, the AP can't provide LOS to the STA unless the STA moves to a location with LOS connectivity with the AP.

- *Brute-force:* Another trivial but adaptive approach is brute-force solution which enables the AP periodically traversing the entire platform in order to collect network status information. At each available AP location, the AP utilizes LOS or localization techniques to collect network status information. The time complexity to perform LOS or localization is generally much smaller than actuator movement speed, as mechanical movement speed in typically in granularity of meters per seconds but LOS or localization can be done in granularity of milliseconds. Thus, it is feasible that the AP can collect network status information for each desired AP locations. Based on the collected global knowledge, the location with maximum number of LOS STAs can be identified and then the AP moves to the optimal location. This approach is straight forward, but it introduces a significant amount of time complexity.

WiMove *Overview*

Given the LOS prediction algorithm presented in Section 4.3.3, we intend to employ the algorithm in a practical system to evaluate the overall system performance. To perform such ML algorithm, we assume there is a cloud server available which connects with AP

using WiFi [7]. The cloud server can collect network status information from the AP and train the ML model and inform the AP about AP-STA LOS connectivity vector with a target STA. In this context, to achieve the objective of maximizing the number of LOS connectivity between AP and STAs, the overall systematic solution of *WiMove* is presented as follows:

- *Initialization brute-force:* The AP uses the brute-force discovery to collect global data of network status information through 5GHz band. The AP then informs the cloud server with the collected network status information at current time instance. The collected network status information is then fed to the ML model for training. If network dynamics happens, the algorithm goes into the phase of *Network dynamics*.

- *Network dynamics:* As discussed in Section 4.3.3, there are three types of network dynamics: 1) instant STA dynamics, 2) continuous STA dynamics, and 3) continuous obstacle dynamics. The system deals with each dynamic scenario in the following manner: 1) instant STA dynamics: when an STA becomes active, the AP collects LOS prediction results from cloud server and then identifies the closest optimal location and goes into *AP Movement* phase. When a fixed active STA drops out of the network, the AP will stay at the current location; 2) continuous STA dynamics: the AP collects LOS prediction results from cloud server and then identifies the closest optimal location and goes into *AP Movement* phase; 3) continuous obstacle dynamics: re-initialization of the ML algorithm is required, it goes into *Initialization brute-force phase* to retrain the ML model.

- *AP movement*: AP moves to the identified target location and goes into the *Reach Target* phase. Note that, the AP will collect ground truth network status information with the target STA during movement [8]. If the current location satisfies the objective function due to false negative prediction, the AP will stop at the current location.

[7] Based on computation power of the cloud server, the ML model can be trained for every k sets of network status information.

[8] When the percentage of ground truth data is smaller then a threshold of 50%, the *WiMove* goes into the *Initialization brute-force* phase.

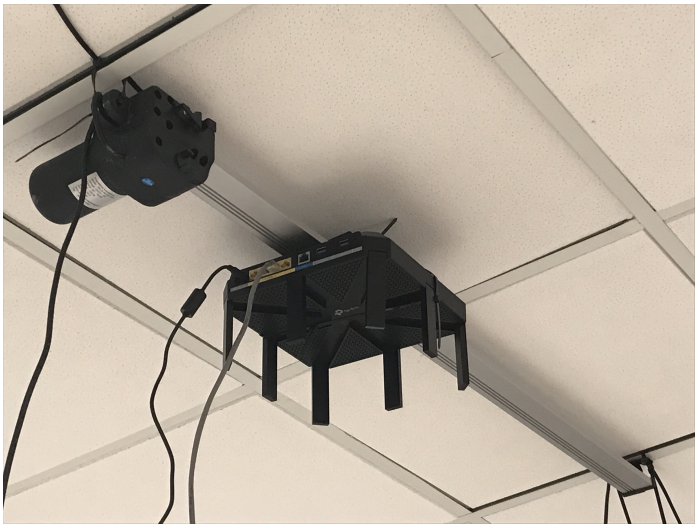

Figure 4.24: Experimental Platform

- *Reach Target*: If the AP reaches the target location with correct prediction, *WiMove* goes into idle phase. If the prediction is wrong, *WiMove* goes into *AP movement* phase with a new nearest optimal location.

Evaluation Methodology

Consider a room with the CMM AP platform mounted at the default location on the ceiling with parameters following the configurations in Table 4.2. There are M STAs in the scenario at a specific time instant. We consider instant STA dynamics in the evaluation. STAs join or leave the network based on a Poisson distribution with an expected rate of one unit per minute. The overall evaluation time is 5 minutes. Similar like LOS prediction evaluation, we incorporate LOS estimation and localization error in the network status collection phase.

We evaluate three different approaches for providing 802.11ad service in the network: 1) static AP, 2) brute-force, and 3) *WiMove*. For *WiMove* and brute-force, the goal is to identify the nearest location on the platform that maximizes the number of LOS STAs connectives. The metrics to be studied are 1) the number of LOS STAs, 2) aggregate throughput performance, and 3) Jain's fairness index. Specifically, for Jain's fairness index,

it ranges from $1/M$ (single STA has aggregate network throughput) to 1 (each STA has equal throughput).

Simulation configurations: We evaluate the performance of the aforementioned 3 approaches through ns-3 simulations. *WiMove* approach decides whether to adapt the AP location at every time instance when the network dynamics happens. We consider the number of STAs to be 10 at the first time step. The ML prediction accuracy achieves 91% in this specific configuration.

Experimental configurations: In order to evaluate the performance of *WiMove*, brute-force, and single static AP experimentally, we mounted a 1m long Progressive Linear Actuator PA-18 [66] on the optimal location of the ceiling in a lab environment utilizing cable zips. This unit is controlled by a central controller through Arduino UNO [80] and Mega Moto Plus [81]. The AP mounted on the actuator is Tp-link Talon ad7200 [67]. The experimental platform is shown in Fig. 4.24. We use 3 Acer Travelmate P648 laptops [82] as STAs. To collect training data for ML, the LOS and distance matrices of all possible locations are hard-coded. For *WiMove*, the controller controls the location of the AP in the discrete dynamic scenario based on the ML feedback. The ML prediction accuracy achieves 90% in this specific configurations.

Simulation Evaluation

Initially, 10 STAs are active. Based on the Poisson distribution of STA events, the STA number changes at each minute as $\{$-1, -2, +1/-1, +1$\}$, where +1 means a new STA joins the network and -1 means an active STA drops off.

Fig. 4.25a, 4.26a, and 4.27a show the number of LOS STAs, aggregate throughput and Jain's fairness index for the aforementioned three approaches at various time instants. For the initial 60s, the average performance of the three approaches is very similar. From 120s to 240s, the throughput performance and Jain's fairness index of *WiMove* is 115% and 33% better compared with single static AP case. This time period clearly reveals the drawback of static AP, which has very limited performance when AP does not have good channel

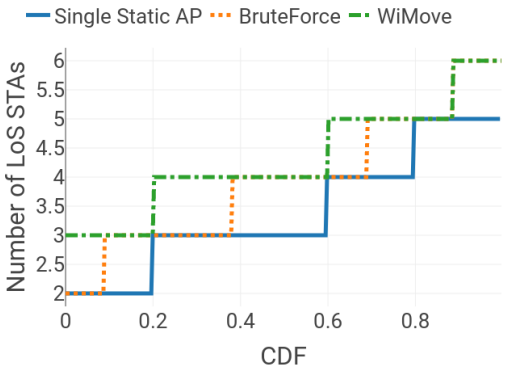

(a) Simulation

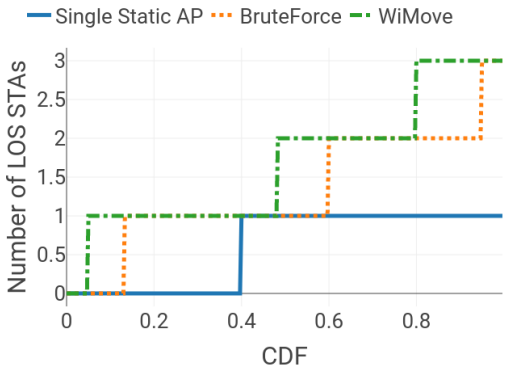

(b) Experiment

Figure 4.25: Number of LOS STAs

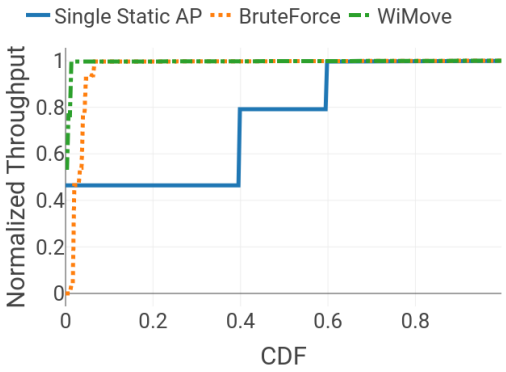

(a) Simulation

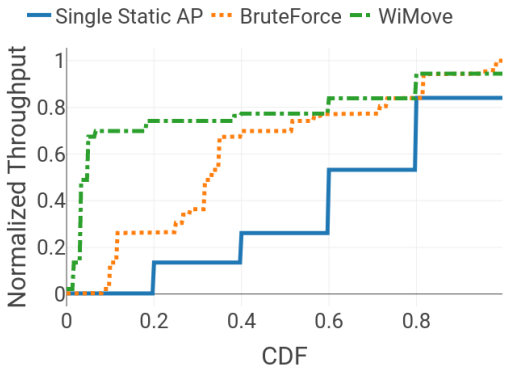

(b) Experiment

Figure 4.26: Throughput

connection with STAs. Overall, *WiMove* throughput performance is 30% and 110% better compared with brute-force and single static AP, and Jain's fairness index is 14% and 7% better compared with single static AP and brute-force. Since neighboring LOS locations are highly correlated (appears as a group), the AP moves toward the correct location as long as *WiMove* predicts the single correct location connectivity in one of the grouped locations.

Experimental Evaluation

For the environment setup for experimental evaluation, initially there are 2 STAs in the network and the STA numbers change at each minute as {+1, -2, +1/-1, +1}.

Fig. 4.25b, 4.26b, and 4.27b illustrate the number of LOS STAs, throughput and Jain's fairness index for the aforementioned 3 approaches at various time instants. For *WiMove* and brute-force with an initial location at the edge of the platform, there is 1 STA in LOS condition. For the single static AP case, the 2 STAs are both in NLOS condition. Initially, *WiMove* tries to explore the entire platform to collect network information (same as brute-force). In the first 60s, *WiMove* and brute-force take 25s to reach the location that has LOS w.r.t. to both STAs. Clearly, at the location with maximum LOS STAs, the network has high fairness and throughput. The network performance might drop during the movement phase, but the performance gain can be considerable when *WiMove* reaches the optimal location. For example, during the first 60s for *WiMove*, the number of LOS STA is increased by 50%, the throughput is increased by 10%, and Jain's fairness index is also increased by almost 50%. For the period between 180s to 240s where only 1 STA is active, single static AP is in NLOS with that specific STA which leads to no throughput. With mobility advantage, severe cases such as this can possibly be avoided. From this set of experiments, the throughput performance of *WiMove* is 119% and 29% better compared with brute-force and single static AP, and Jain's fairness index is 15% and 8% better compared with brute-force and single static AP. Overall, we can observe *WiMove* dynamically adapts to network conditions and achieves the best performance among brute-force and single static AP.

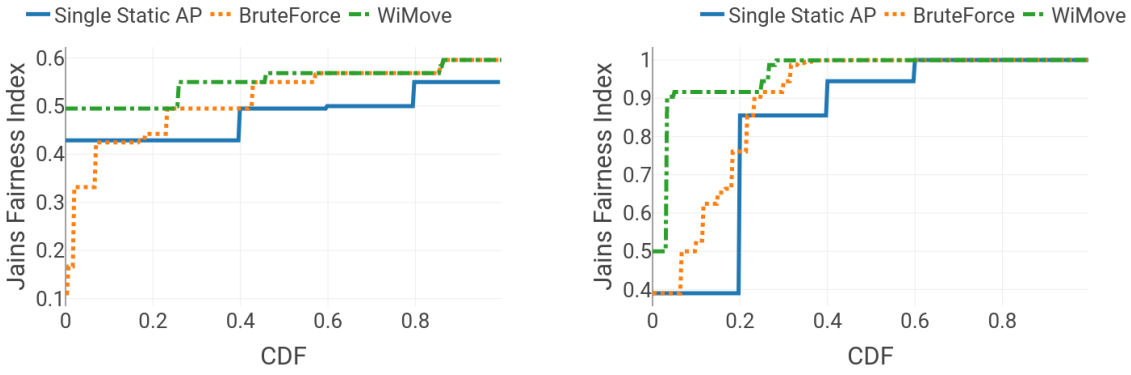

(a) Simulation **(b) Experiment**

Figure 4.27: Jain's Fairness Index

4.3.6 Summary

In this section, we present *WiMove* which uses ML techniques that, upon a network state change, predicts the location that maximizes the number of LOS connections. Using a simulation and prototype evaluation, we show that *WiMove* can perform up to 119% and 15% better than other specific intuitive approaches. The following are the essential future work to be considered: 1) AP mobility cost analysis, 2) jointly optimization of mmWave and conventional WiFi.

CHAPTER 5
INFRASTRUCTURE INTERFERENCE MITIGATION

Coexistence issue is an important research area in wireless communications. By mitigating the interference between various types of wireless networks, the overall network performance can be significantly improved. The coexistence issue exists in various important scenarios. For example, the coexistence issue between Bluetooth and WiFi in unlicensed band and the coexistence issue between 5G NR and WiFi in unlicensed band. In this chapter, we consider the problem of enabling the coexistence between a wireless network with centralized MAC (e.g., LTE-U) and a wireless network with distributed MAC (e.g., WiFi) from the perspective of a centralized manner. LTE in Unlicensed band (LTE-U) has gained intensive attention recently due to its capability to offload mobile data to unlicensed bands. In order to use unlicensed band, LTE-U has to coexist with WiFi - another wireless technology that operates in unlicensed bands. This coexistence is riddled with several challenges as these technologies use different core networks, backhauls and deployment plans. Within this broad paradigm, we present *Duet*, a Medium Access Control (MAC) layer solution that enables both LTE-U and WiFi nodes to operate fairly and efficiently, with the following properties: (1) no changes in WiFi framework, (2) high performance of LTE-U and WiFi networks within static and dynamic load scenarios, and (3) robustness to fully and partially connected networks. Using ns-3, we simulate *Duet* in various scenarios and show that *Duet* can improve the overall network throughput by up to 74%.

The global mobile data usage is expected to grow 53% annually from 2015 to 2020. The huge mobile data usage requirement drives the mobile industry to embrace the formidable challenge and invent next-generation mobile technologies. Long-Term Evolution (LTE), as a successful mobile technology, has gained enormous importance in recent years because it brings higher data rates as well as lower latency to mobile communication systems. Despite recent advances, LTE still may not be able to meet the mobile data challenge due

to the spectrum scarcity in licensed bands. To tackle this problem, Qualcomm introduced LTE-U focusing on operation in unlicensed bands [83], aiming at assisting cellular operators to offload cellular data to unlicensed bands. Due to the maximum power limitation in unlicensed bands, small cell is an ideal application to operate LTE-U. Small cell technology is a promising solution to offload cellular traffic as it can provide better local channel capacity compared with macro cell [38]. Thus, combining LTE-U with small cell can further relieve the traffic burden of overloaded cellular networks.

In order to operate in the unlicensed spectrum, LTE-U has to compete with other wireless technologies that operate in the same unlicensed spectrum. Among these, WiFi is widely popular with high density deployment. It is not trivial for LTE-U and WiFi to coexist as-is due to the differences in their MAC protocols. LTE-U uses a centralized MAC protocol, while WiFi uses a distributed MAC protocol. The distributed nature of MAC in WiFi makes the traffic patterns of individual clients random and unpredictable. Also, LTE-U and WiFi transmissions can interfere with each other. Therefore, it is hard for LTE-U to coexist with WiFi without communication guidelines at system level that ensure fair access to the spectrum for both of these technologies while maintaining high efficiency of the channel.

The context of this paper is the coexistence between a wireless network with centralized MAC (e.g. LTE-U) and a wireless network with distributed MAC (e.g. WiFi). There are several solutions proposed in related literature to solve the coexistence problem. However, they either require extra time resources for sensing the channel, thereby leading to less channel efficiency [47] or they do not consider fairness metrics, different load conditions and hidden terminal problems [83]. In this context, we present *Duet*- an algorithm that triggers the coexistence between LTE-U and WiFi networks, while ensuring fair resource allocation and high channel efficiency in both LTE-U and WiFi networks.

Specifically, the main contributions of this paper are: 1) We propose *Duet*, an algorithm to adaptively tackle the coexistence problem of LTE-U and WiFi through an enhanced

ON/OFF duty cycle mechanism, in which LTE-U transmissions are allowed during the LTE-U ON period and WiFi transmissions are allowed during the LTE-U OFF period. *Duet* can be applied to both fully and partially connected networks with either static or dynamic network load; 2) we evaluate *Duet* through ns-3 simulations in various scenarios and show that it can improve the overall network throughput up to 74% while maintaining good channel utilization and fairness between LTE-U and WiFi networks.

5.1 A primer on LTE-U/WiFi coexistence

LTE-U uses a centralized MAC protocol, where the small cell base station schedules time and frequency resources among all User Equipment (UE). By assigning resources using a scheduling algorithm such as a proportional fair scheduler, the small cell ensures maximum channel efficiency without starvation of UEs.

The most popular WiFi MAC, Distributed Coordination Function (DCF), is a contention based distributed MAC protocol. Fig. 5.1 shows the mechanism of DCF. DCF is based on Carrier Sense Multiple Access with Collision Avoidance (CSMA/CA), in which a WiFi station only transmits when the channel is sensed idle. More specifically, DCF includes a backoff mechanism in the WiFi station that generates a random backoff number from [0,*cw*], where *cw* is the contention window size. The backoff counter decreases as long as the channel is sensed idle after a time period DIFS. When the backoff counter reaches zero, it triggers the corresponding WiFi station to transmit a packet. Upon successful reception of the packet, the receiver transmits an ACK back to the sender after a time period SIFS. However, it is possible that more than one station chooses the same backoff number. In this case, stations transmit at the same time and lead to a collision. If collision happens, *cw* will be doubled and the process repeated from channel sensing.

If LTE-U and WiFi networks operate in the same spectrum as-is, throughput of the WiFi network will be significantly reduced. (as shown in Section 5.5). This is because the LTE-U controller, in an effort to maximize the channel efficiency of the LTE-U network,

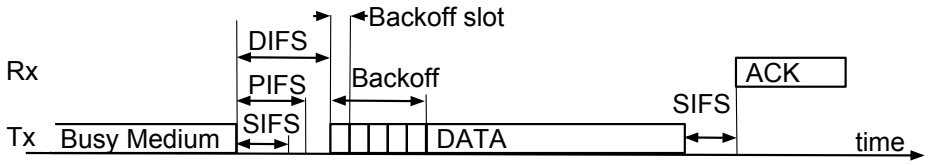

Figure 5.1: DCF Mechanism

always allows the small cell and UEs to transmit, keeping the channel busy and thus the WiFi stations cannot transmit. Even in the case when a WiFi node transmits, there is a chance of collision with LTE-U packets, since LTE-U small cell and UEs do not listen to the channel before transmitting. Therefore, if WiFi and LTE-U nodes were to operate in the same spectrum, a good coexistence algorithm is required to achieve high channel efficiency and fair resource allocation of LTE-U and WiFi nodes.

5.2 Experimental Analysis on LTE-U/WiFi coexistence

In this chapter, we study the interference impact of LAA on WiFi under various network conditions using purely experimental analysis in indoor environments (as LTE-U and LAA utilize the same physical features, we use only LAA for convenience in this experimental analysis section). The following three questions are specifically considered in this chapter: (1) What are the implications of LAA usage on WiFi? (2) How should LAA or WiFi be configured for WiFi to be less impacted? (3) How should the LAA MAC protocol be designed to be gracefully co-exist with WiFi? To answer the above questions, we present comprehensive experimental results and give insights based on the results.

Evaluation setup for both LAA and WiFi will be introduced first, including the platforms of LAA and WiFi, scenario, experimental parameters and experimental evaluation methodology. Then, the experimental results and analysis will be discussed. The perspective on LAA MAC designs from the experimental evaluation results will be illustrated in the end of this chapter.

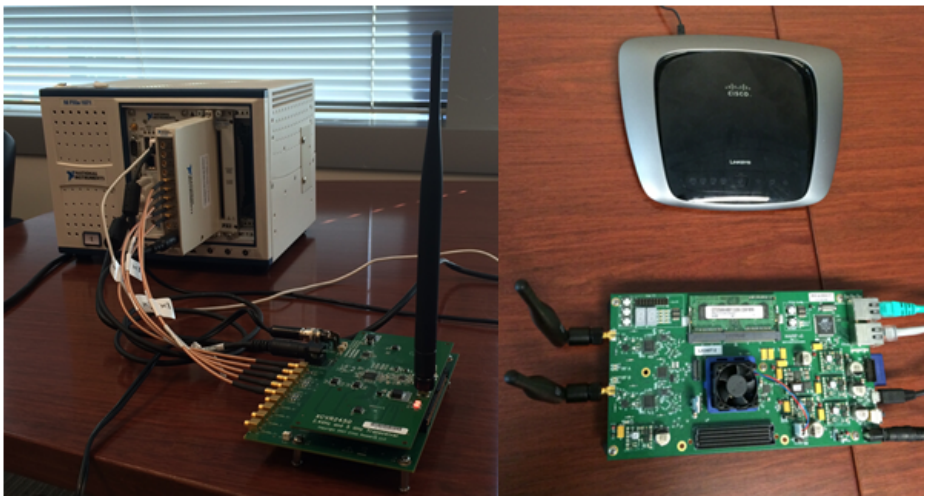

Figure 5.2: Left: LAA platform; Right: WiFi platform (WARP and Router)

5.2.1 Experimental Evaluation Setup

Experimental platforms

In this section, we describe the experiment platforms that are used to evaluate the impact of LAA interference on WiFi performance.

1) *LAAplatform*: The NI PXI testing system [84] was used as LAA testbed as shown in *Figure 5.2*. The standard-based PHY of LTE-A (release 10) is implemented on the NI PXI system. The equipment details are listed in *Table 5.1*. The system is able to provide many advanced and user-defined operability on signal transmission and reception, such as subcarrier modulation scheme, OFDM parameters, carrier frequency offset, and timing offset estimation.

2) *WiFiPlatform*: The Cisco-Linksys WRT320N router and Wireless open-Access Research Platform (WARP [85]) v3 are used for the WiFi testbed (see *Figure 5.2*). The off-the-shelf WiFi routers, supporting both 802.11a and 802.11n in 5GHz band, can represent typical commercial WiFi nodes. On the other hand, since WARP supports modification and monitoring of parameters and functions in both the MAC and PHY layer of WiFi, it provides ways to gain detailed information and evaluation. WARP is capable of communicating with off-the-shelf WiFi nodes, but only 802.11a in 5GHz band is implemented in

Table 5.1: Experimental testbed for LAA

Equipment	Model	Specification
Chassis	PXIe-1071	
Controller (Host)	PXIe-8133RT	1.73GHz Quad Core
FPGA	7965R FlexRIO	Virtex 5; 512MB DRAM; P2P streaming with other modules
Baseband Transceiver	NI-5781	ADC; 14bit DAC; 40 MHz BW
RF Frontend	XCVR 2450	2.4-2.5GHz & 4.9-5.9GHz

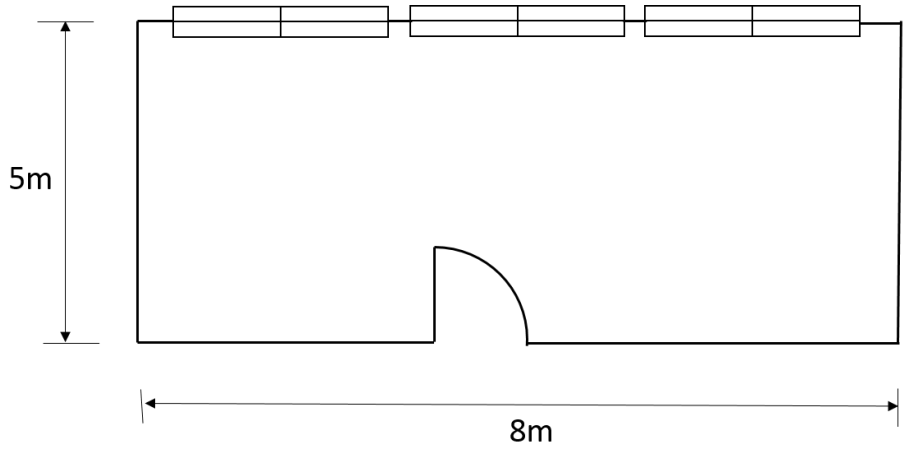

Figure 5.3: Experimental scenario

WARP.

5.2.2 Evaluation scenarios and parameters

All experiments are carried out in a typical indoor office with size 8x5x2.7m^3, and the logical graph for the office is shown in *Figure 5.3*. *Table 5.2* lists the default settings of LAA and WiFi parameters. We mainly use throughput of WiFi as a metric to evaluate the impact of LAA's interference on WiFi performance. Other metrics, such as number of packets transmitted in the PHY layer, can also be collected using WARP, for cases that requires detailed evaluation. In our experiments, the LAA Tx always transmits, which is similar to the transmission of LTE-A in licensed bands. Also, the LAA transmission PSD is chosen such that LAA interference power is around CCA threshold of WiFi communications.

Table 5.2: Default Experimental Settings

Parameters	Default settings
Center frequency	5.18 GHz
WiFi bandwidth	20MHz
WiFi standard	802.11a/n
WiFi ARC	On
WiFi transport protocol	UDP
LAA bandwidth	20MHz
LAA modulation scheme	16-QAM
LAA transmission PSD	-108/-106/-104/-102/-99.5dBm/Hz
Antenna gain	3dBi
Antenna type	Isotropic
Number of Tx/Rx antenna	1/1
Distance between two links	4m
Distance between WiFi Tx/Rx	2m
WiFi throughput testing tool	Iperf

Evaluation Methodology

We design **five** experiments to explore LAA interference effects on WiFi performance:

1) *LAA bandwidth*: LTE-A supports different bandwidths for DBA and spectral efficiency in license bands. Since LAA uses the same technology as LTE-A, it is possible that LAA also supports different bandwidths. While most WiFi nodes use bandwidth of 20MHz, possible bandwidths of LAA can be 1.4/3/5/10/15/20MHz. The bandwidth change can affect the crosstalk interference. Thus, we would like to explore how LAA interference with different bandwidth affects WiFi performance.

2) *LAA center frequency*: Since LAA supports smaller bandwidth than WiFi, it is possible for an LAA channel to use different center frequencies and overlap with different portion of a WiFi channel. Since different sub-carriers in a WiFi channel has different functionalities (some with pilot signals, and no signal is transmitted on the center carrier [70]), overlapping with different portion of the channel can have different effects. Thus, we would like to know how WiFi performance changes when different portions of its channel overlaps with an LAA channel.

3) *CCA threshold*: In WiFi networks, nodes perform CCA before transmissions. If

CCA indicates channel busy, nodes do not transmit. It is possible for LAA interference to trigger channel busy indication during CCA and make WiFi nodes not transmit, which causes throughput degradation. Thus, we would like to explore how LAA interference impacts WiFi CCA under different situations.

4) *WiFi MIMO*: Since MIMO has become an important element in WiFi network, it is important to understand how LAA interference affects MIMO transmissions of WiFi. Since LAA is a competitive technology with relatively large bandwidth and power, the impact can be much severe compared to other unlicensed technologies. Thus, we would like to examine the impact of LAA on WiFi with and without MIMO.

5) *Distance and Obstacles*: Distance between two networks changes the impact of interference. In open space, the interference effect decreases as distance increases. However, this property does not always hold in indoor environment due to heavy multipath fading. Other than distance, existence of obstacles can also change the signal propagation and interference condition. Thus, we study the impact of distance and existence of obstacles between LAA and WiFi networks on WiFi performance.

5.2.3 Evaluation Results and Analysis

In this section, we present results of the five experiments described in Section 3.1.3. The experiment configurations are presented in Section 3.1.2. Each experiment is performed for a duration of 20s and repeated 3 times.

LAA bandwidth

Since it is possible for LAA to support different bandwidths, we investigate the impact of LAA bandwidth on WiFi performance. In this experiment, we set up an LAA transmission using the same center frequency as a WiFi transmission, and change the bandwidth of the LAA transmission. *Figure 5.4* (a) and (b) show the WiFi throughput vs. LAA bandwidth when the WiFi transmission operates 802.11a and 802.11n respectively with different LAA transmission PSD.

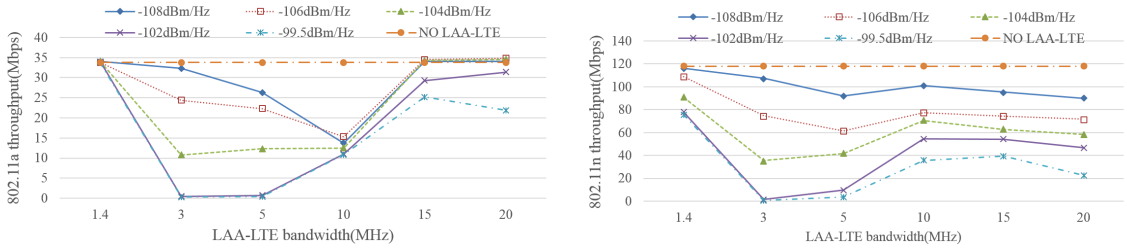

(a) 802.11a throughput vs. LAA bandwidth **(b) 802.11n throughput vs. LAA bandwidth**

Figure 5.4: LAA bandwidths impact on WiFi throughput

Results in *Figure 5.4* indicate that different LAA bandwidths have different impacts on WiFi throughput. *Surprisingly, the impact is NOT proportional to LAA bandwidth.* There is almost no impact when the bandwidth is 1.4MHz. When the bandwidth is 15/20MHz, WiFi throughput gradually decreases as LAA transmission PSD increases. When the bandwidth is 3/5/10MHz, the impact is surprisingly much larger than that of 15/20MHz. When the LAA transmission PSD grows to -102dBm/Hz, there is almost no throughput for 3/5MHz.

The unexpected degradation of WiFi throughput when the interfering LAA bandwidth is 3/5/10MHz (especially 3/5MHz) is consistently observed in all the experiments. Later in the 3rd experiment, WiFi CCA, we will be able to see more insights into this phenomenon with help from an instrumented WARP platform.

Comparing *Figure 5.4* (a) and 2(b), one can observe that the throughput of 802.11a and 802.11n have a similar trend, and LAA interference has larger impact on 802.11n. A more detailed evaluation of the difference in impact between 802.11a and 802.11n will be presented later in the 4th experiment, WiFi MIMO.

We conclude results from this experiment with the following insight:

> *WiFi throughput can be heavily degraded by LAA transmissions with 3/5/10MHz bandwidth (especially 3/5MHz)*

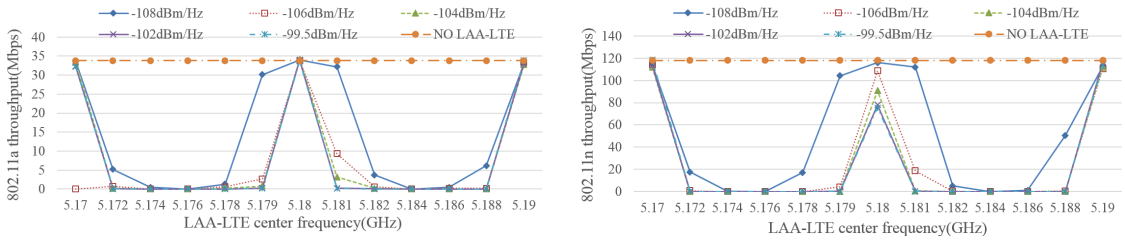

(a) 802.11a throughput vs. LAA center frequency

(b) 802.11n throughput vs. LAA center frequency

Figure 5.5: LAA center frequency impact on WiFi throughput

LAA center frequency

Since different sub-carriers in a WiFi channel have different functionalities (some with pilot signals, and no signal is transmitted on the center carrier [70]), we investigate the impact of an LAA channel overlapping with different portions of a WiFi channel. In this experiment, we set up an LAA transmission with 1.4MHz (we use the smallest bandwidth for the best resolution) and change its center frequency to overlap with different channel portion of a WiFi transmission. The LAA center frequency is varied from 5.17 to 5.19GHz and the WiFi channel is located in 5.17∼5.19GHz. The measured WiFi throughput vs. LAA center frequency is shown in *Figure 5.5* (a) and (b) when the WiFi transmission operates 802.11a and 802.11n respectively with different LAA transmission PSD.

Results in *Figure 5.5* indicate that overlapping in different channel portion does have different impact on WiFi throughput. There is almost no impact when the 1.4MHz LAA channel is located in the guard band of the WiFi channel. The impact is much smaller when the LAA channel is located in the center frequency of the WiFi channel, where no WiFi signal is transmitted, compared to that of other channel portions. The WiFi throughput is almost zero when the LAA channel allocates around middle part of each sideband (5.174∼5.176GHz, and 5.184∼5.186GHz), even when the transmission PSD of LAA is relatively small (-108dBm/Hz).

Again, comparing *Figure 5.5* (a) and (b), similar trend of the throughput of 802.11a and 802.11n can be observed.

We conclude results from this experiment with the following insight:

> *LAA transmissions can have small impact on WiFi throughput when using a 1.4MHz channel with center frequencies located on the guard bands or the center frequencies of WiFi channels.*

WiFi CCA

To figure out the cause of throughput degradation in the previous two experiments, we investigate the impact of LAA bandwidth on WiFi CCA. CCA indicates channel busy in the following two conditions: 1) CS/CCA: the PHY layer detects a WiFi preamble successfully; 2) CCA threshold: the PHY layer detects signal power above a predefined CCA threshold. In this experiment, we set up an LAA transmission using the same center frequency as a WiFi transmission, and change the bandwidth of the LAA transmission. Two WARP v3 nodes carry out the WiFi transmissions. In order to prevent the ACK timeout from increasing the backoff CW, we make the WiFi Tx transmit broadcast packets, which does not trigger ACK transmissions. The application layer of the WiFi Tx sends down to the MAC layer 100 broadcast packets per second with packet size of 168Bytes. The total number of packets transmitted by the PHY layer of WiFi vs. LAA transmission PSD is shown in *Figure 5.6* with different LAA bandwidth. *Figure 5.6* (a), (b), and (c) shows the results when WiFi CCA works normally, when the CCA threshold (-62dBm) is disabled (only CS/CCA is functioning), and when CCA is totally disabled respectively.

Results in *Figure 5.6* (a) indicate that different LAA bandwidths have different impacts on WiFi CCA. The impact is severe when LAA bandwidth is small, such as 1.4/3/5MHz. This indicates that the LAA interference impact on WiFi CCA is an essential cause of the throughput degradation in previous experiments.

Comparing *Figure 5.6* (a) and (b), one can clearly observe that the LAA interference impacts on WiFi CS/CCA. Theoretically, LAA interference should not trigger channel busy indication when only CS/CCA is functioning. In *Figure 5.6* (b), when the LAA bandwidth

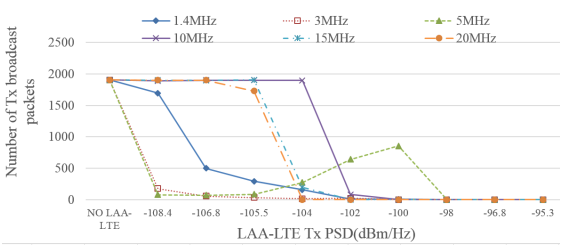

(a) Number of transmitted broadcast packets vs. LAA Tx PSD (CCA works normally)

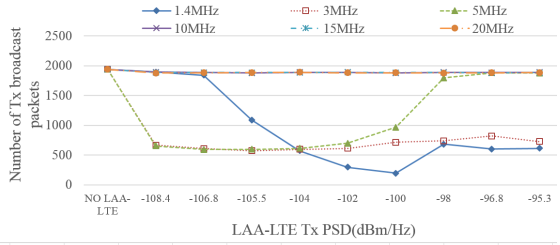

(b) Number of transmitted broadcast packets vs. LAA Tx PSD (Only CS/CCA is functioning)

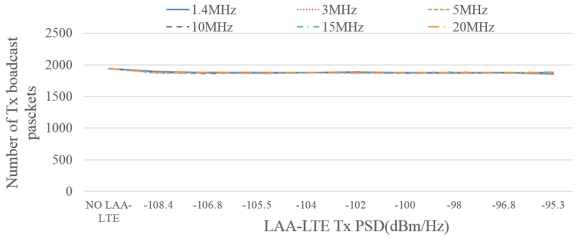

(c) Number of transmitted broadcast packet vs. LAA Tx PSD when CCA is totally disabled

Figure 5.6: LAA impact on WiFi CCA

is 10/15/20MHz, the channel busy indication is not triggered, and the number of transmission keeps the same; we can infer that the decrease in *Figure 5.6* (a) when the LAA Tx PSD is around -103dBm/Hz is caused by CCA threshold. However, surprisingly, the number of transmitted packets decreases severely when the LAA bandwidth is 1.4/3/5MHz in *Figure 5.6* (b). When the bandwidth is 5MHz, this anomalous condition occurs only when the LAA Tx PSD is smaller than -98dBm/Hz; and we can infer that the second decrease of 5MHz bandwidth in *Figure 5.6* (a) around -98dBm/Hz is due to CCA threshold. The anomalous situation when the LAA bandwidth is 1.4/3/5MHz indicates that LAA can trigger CS/CCA of WiFi and cause throughput degradation. However, since WARP implements cross-correlation in CS/CCA for preamble detection, the probability of false alarm is expected to be very small. Currently, we cannot explain this specific anomaly and our ongoing work is exploring potential reasons.

In *Figure 5.6* (c), when CCA is totally disabled, LAA interference cannot impact the transmission of WiFi, and thus the number of transmitted packets remains the same. Com-

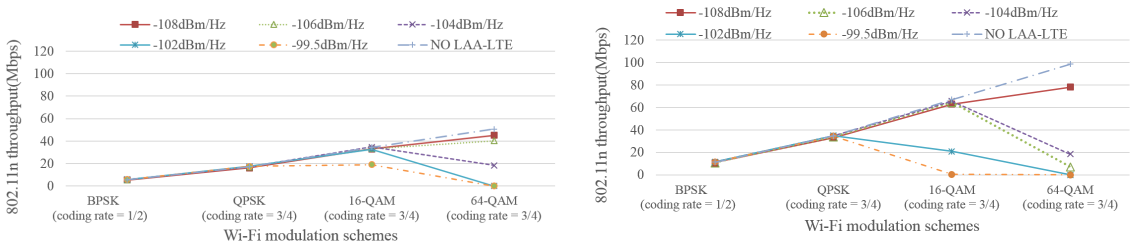

(a) 802.11n throughput vs. MCSs without MIMO

(b) 802.11n throughput vs. MCSs with MIMO

Figure 5.7: LAA impact on WiFi MIMO

paring *Figure 5.6* (b) and (c), we can further confirm that the impact on the number of transmitted packets in *Figure 5.6* (b) is caused by CS/CCA.

We conclude results from this experiment with the following insight:

> *LAA transmissions with 1.4/3/5MHz bandwidth can trigger WiFi CS/CCA and thus heavily impact WiFi performance.*

WiFi MIMO

Since MIMO has become an essential element of WiFi standards, we examine the impact of LAA interference on MIMO transmissions of WiFi nodes. In this experiment, Cisco-Linksys WRT320N routers are used as WiFi nodes. We set up a LAA transmission using the same center frequency and bandwidth as a WiFi transmission, and change the MCSs of the WiFi transmission. *Figure 5.7* (a) and (b) shows WiFi throughput vs. WiFi MCSs when the WiFi transmission operates without and with MIMO respectively with different LAA transmission PSD.

As shown in *Figure 5.7* (a) and (b), WiFi throughput degrades faster for higher modulation rates as the LAA interference power increases. This indicates that higher modulation rates are more sensitive to interference.

Comparing the results in *Figure 5.7* (a) and (b), one can observe that 802.11n throughput with MIMO is even lower than the throughput without MIMO when the LAA inter-

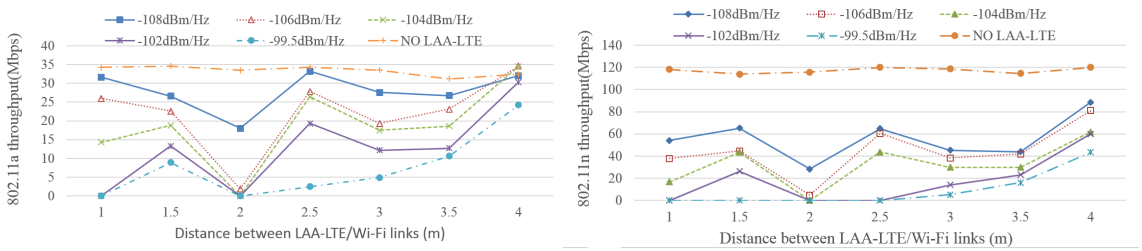

(a) 802.11a throughput vs. distance **(b) 802.11n throughput vs. distance**

Figure 5.8: Impact of distance between LAA and WiFi

ference power is high and the modulation rate is high. This implies that MIMO is more vulnerable to interference, and may degrade the performance of WiFi when interference is strong. Although this throughput degradation can also be caused by other unlicensed wireless transmission (e.g. 802.15), LAA has relatively large bandwidth and transmission power, which makes it easier to cause severe impact to MIMO transmissions of WiFi.

We conclude results from this experiment with the following insight:

> *WiFi with MIMO can perform worse than WiFi without MIMO when LAA interference is strong.*

Distance and Obstacles

Distance and obstacles between two networks changes the impact of interference. In this experiment, we set up an LAA transmission using the same center frequency and bandwidth as a WiFi transmission, and move the WiFi link to change the distance between the LAA and the WiFi link. The distance is varied between 1m to 4m in step of 0.5m. *Figure 5.8* (a) and (b) shows the WiFi throughput vs. distance for 802.11a and 802.11n respectively. To test the effect of obstacles, a 1.07x0.57x1.04m^3 metal desk is placed in the LOS of the 2 links. The WiFi throughput with the obstacle vs. distance is shown in *Figure 5.9* (a) and (b) for 802.11a and 802.11n respectively.

As shown in *Figure 5.8* and *Figure 5.9*, WiFi throughput is not inversely proportional to the distance between the LAA and the WiFi link. This is due to heavy multipath fading

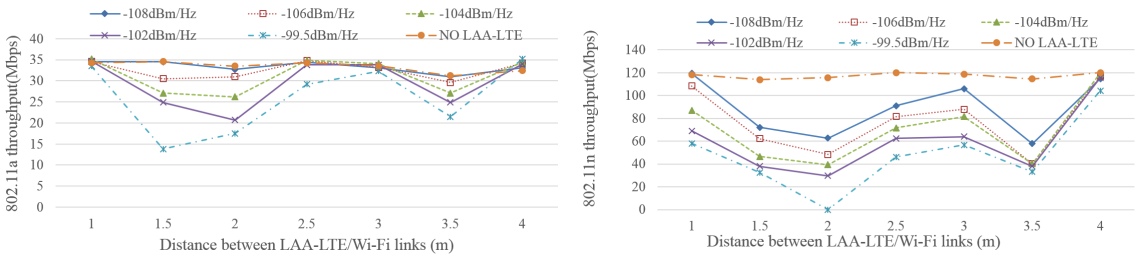

(a) 802.11a throughput vs. distance with obstacle

(b) 802.11n throughput vs. distance with obstacle

Figure 5.9: Impact of a obstacle between LAA and WiFi

in indoor environment. Even when there is no interference from LAA, WiFi throughput slightly changes with distance due to different multipath condition in different location.

Comparing *Figure 5.8* (a) and *Figure 5.9* (a) or *Figure 5.8* (b) and *Figure 5.9* (b) respectively, one can observe that as LOS between LAA and WiFi is blocked by obstacles, throughput of WiFi increases.

We conclude results from this experiment with the following insight:

> *Increasing distance between LAA and WiFi links does not necessarily decrease the impact of interference in indoor environment. On the other hand, blocking LOS between LAA and WiFi links can effectively help decrease the impact of interference.*

5.2.4 Perspectives on LAA MAC design

Since the MAC protocol for LAA is still under development, we present below a few perspectives based on our experimental results that could guide the design of the MAC protocol: 1) In the *LAA bandwidth* experiment, we concluded that LAA with smaller bandwidths can cause severe performance degradation of Wi-Fi. Special care is thus required when simulating the coexisting channel model and designing mechanisms for channel/bandwidth selection. 2) As shown in the *LAA center frequency* experiment, LAA with a 1.4MHz bandwidth does not have a big impact on Wi-Fi transmissions when the center frequency is set

to the center or guard bands of Wi-Fi channels. This observation can be utilized for the design of coexisting mechanisms. 3) Indicated by the *Wi-Fi CCA* experiment, Wi-Fi nodes may interpret LAA signals as Wi-Fi signals and become too conservative when contending for transmission. When designing LAA MAC, this situation needs to be considered, so that LAA and Wi-Fi networks can fairly share the unlicensed band. Based on above experimental analysis, we will formulate LAA and WiFi coexistence problem in next section.

5.3 Problem Definition and Scope

In this section, we formally define the LTE-U and WiFi coexistence problem.

5.3.1 Problem definition

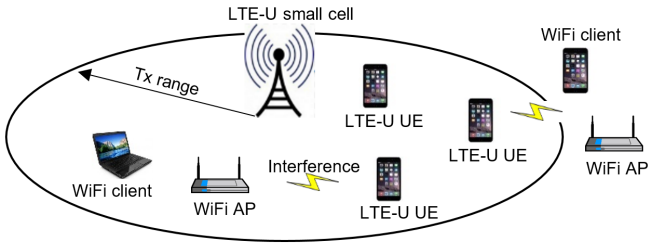

Figure 5.10: LTE-U - WiFi coexistence

Consider the scenario shown in Fig. 5.10, with one LTE-U small cell, N_{lteu} UEs and N_{wifi} wifi nodes. For the LTE-U network, all LTE-U UEs are connected to the LTE-U small cell. For the WiFi network, all WiFi nodes can hear each other. The connectivity between each LTE-U UE i and WiFi node j is represented by connectivity matrix M:

$$M = \begin{bmatrix} x_{11} & x_{12} & x_{13} & \dots & x_{1n} \\ x_{21} & x_{22} & x_{23} & \dots & x_{2n} \\ \vdots & \vdots & \vdots & \ddots & \vdots \\ x_{m1} & x_{m2} & x_{m3} & \dots & x_{mn} \end{bmatrix}$$

where $x_{i,j}$ is defined as below:

$$x_{ij} = \begin{cases} 1 & \text{if LTE-U UE } i \text{ can hear WiFi node } j \\ 0 & \text{if LTE-U UE } i \text{ can't hear WiFi node } j \end{cases}$$

Given the matrix M, the goal is to find a solution to the coexistence problem that results in high overall network throughput while maintaining fairness between LTE-U and WiFi networks. Without a condition on fairness, LTE-U and WiFi networks can selfishly grab more resources for its own transmission, and harm the overall network throughput.

In this paper, we evaluate fairness through a proportional fair defined at link-level granularity. We choose proportional fair metric over other fairness metrics, because it allocates the same amount of time resources to each active WiFi and LTE-U link[1]. Note that, the solution in this paper can be easily extended to other fairness metrics discussed in [86]. Also, as allocating time resources is technology agnostic, proportional fairness criterion is assumed to be reasonable in most scenarios. Proportional fairness between LTE-U and WiFi is reached when the $Lteu_{proportional}$ (average airtime of LTE-U network) is equal to $Wifi_{proportional}$ (average airtime of WiFi network):

$$Wifi_{proportional} = Lteu_{proportional} \tag{5.1}$$

The airtime of a WiFi link is defined by the sum of successful transmission time, contention time (e.g. DIFS, SIFS and backoff time), collision time and transmission delay. The airtime of a LTE-U link is defined by the sum of transmission time and transmission delay. The average airtime of WiFi a network is defined as:

$$Wifi_{proportional} = \frac{C_{wifi}}{L_{wifi}} \tag{5.2}$$

The average airtime of a LTE-U network is defined as:

$$Lteu_{proportional} = \frac{C_{lteu}}{L_{lteu}} \tag{5.3}$$

[1]Note that uplink and downlink can be assigned with different weighted factor for specific scenario.

where, L_{lteu} and L_{wifi} are the number of links in the LTE-U and WiFi networks, respectively. C_{lteu} and C_{wifi} represent the time usage of LTE-U and WiFi networks, respectively.

To summarize, the goal of this paper is to propose an algorithm that allocates time resources to WiFi and LTE-U networks to maximize overall network throughput while achieving the fairness condition in Equation 5.1.

5.3.2 Scope

The scope of this paper is limited to the following constraints: 1) Each LTE-U UE is equipped with a WiFi interface and it is always turned on[2]; 2) Unlicensed spectrum is used as LTE-U supplemental downlink capacity; 3) There is no hidden terminal problem in the WiFi network[3].

5.4 Duet: Adaptive Coexistence Algorithm for LTE-U and WiFi

In this section, we describe the *Duet* algorithm. *Duet* achieves coexistence through an ON/OFF duty cycle mechanism. We first consider a fully connected network where all WiFi nodes can be heard by all LTE-U nodes. In this scenario, we propose Duet-*baseline* where the LTE-U ON/OFF period is linearly or proportionally adapted based on the channel utilization of LTE-U and WiFi networks. We later relax the connectivity constraints and consider a partially connected network. We propose Duet-*SCU (Slotted Channel Utilization)* in partially connected scenarios, where channel utilization is estimated based on slotted time block, and LTE-U ON/OFF period is linearly or proportionally adapted based on the slotted channel utilization of LTE-U and WiFi networks.

5.4.1 Baseline Algorithm

We first consider a fully connected network topology ($x_{i,j}$ equals to 1 for all i and j) and introduce the *Duet-Baseline* algorithm. *Duet-Baseline* involves the following two parts: 1)

[2]Most of devices with LTE-U interface have WiFi interface, e.g. cell phone.

[3]The priority of this work is to investigate hidden terminal between LTE-U and WiFi. Also, hidden terminal problem between WiFi nodes has been widely investigated in related literature [87]-[41].

Channel utilization estimation, and 2) Duty cycle adaptation.

Channel Utilization Estimation

Accurate channel utilization estimation is the core to the *Duet-Baseline* algorithm. In this section, we describe how channel utilization is estimated in both LTE-U and WiFi networks. Since LTE-U uses a centralized MAC protocol, LTE-U transmission time can be easily estimated by the LTE-U small cell. More specifically, LTE-U network information (L_{lteu} and $D_{lteu,i}$, where $D_{lteu,i}$ denotes the airtime of LTE-U packet i) is gathered in LTE-U small cell. WiFi channel utilization is measured by the WiFi interface of LTE-U UE. More specifically, the WiFi interface of LTE-U UE gathers WiFi network information ($D_{wifi,i}$ and L_{wifi}, where $D_{wifi,i}$ denotes the airtime of WiFi packet i), and LTE-U UE reports corresponding information to LTE-U small cell. Let T_e represent the estimated time usage of WiFi transmission, and Bk_e represent the estimated backoff number, which is calculated through a Markov chain based model for contention window size [88]. In order to calculate Bk_e, each WiFi interface of the LTE-U UE overhears and maintains a list of active MAC addresses of WiFi links and updates it periodically. Let D_{packet} and D_{ack} represent the packet duration of the packet and the ACK, respectively. These terms can be accessed by decoding the preamble or through Clear Channel Assessment (CCA) measurement. In Algorithm 1, T_e is estimated by the WiFi interface of LTE-U UE in three different conditions: 1) receiving a data packet in line 3[4]; 2) receiving an ACK in line 5; 3) packet collisions in line 7. The details for estimating channel utilization time can be referred to Algorithm 1.

Channel utilization is defined by T_e divided by LTE-U OFF period for each duty cycle. The estimated WiFi channel utilization is in the range of [0,1], and it is piggybacked on the LTE-U packet and reported to LTE-U small cell at the start of LTE-U ON period.

[4]We ignore the propagation delay (D_{prop}), as it is negligible compared to other delays due to the limited transmission range of a small cell.

Algorithm 4 WiFi Channel Utilization Time Estimation

1: $T_e = 0$
2: **if** Receive a data packet **then**
3: $\quad T_e += DIFS + Bk_e + D_{packet} + D_{prop}$
4: **else if** Receive an ACK **then**
5: $\quad T_e += SIFS + D_{ack} + D_{prop}$
6: **else if** Collision happens **then**
7: $\quad T_e +=$ Channel utilization time of largest packet
=0

Duty Cycle Adaptation

The LTE-U ON/OFF period is linearly or proportionally adapted based on the channel utilization of LTE-U and WiFi in *Duet*. LTE-U small cell allocates time resources to LTE-U and WiFi networks by defining LTE-U ON and OFF period. The small cell sends packets to the UEs through LTE-U links only in LTE-U ON period. Simultaneously, the small cell will track the actual transmission time of LTE-U traffic in LTE-U ON period. WiFi transmissions are allowed during the LTE-U OFF period. To prevent WiFi transmissions during the LTE-U ON period, we can let the WiFi interface of LTE-U UE broadcast CTS-to-self during the LTE-U ON period with a specific Network Allocation Vector (NAV). The WiFi interface of LTE-U UE estimates the time usage of WiFi traffic in LTE-U OFF period. The sum of a LTE-U ON and OFF period is defined as a duty cycle. Based on the time usage of LTE-U and WiFi links and the corresponding LTE-U ON/OFF period, the LTE-U small cell can calculate the channel utilization of LTE-U and WiFi networks. The LTE-U small cell can assign an ON/OFF period to both LTE-U and WiFi traffic of the next duty cycle according to the channel utilization of the current cycle.

The coexistence algorithm of *Duet-Baseline* consists of two phases - linear adaptation and proportional adaptation. In the proportional/linear adaptation phase, the LTE-U ON/OFF period are proportionally/linearly adapted towards maximizing channel utilization/fairness based on the measured channel utilization of LTE-U and WiFi. We illustrate these phases through an example. Consider a scenario where in L_{lteu} is equal to L_{wifi}.

Let $Wifi_{cu}$ (channel utilization of WiFi in the previous duty cycle) and $Lteu_{cu}$ (channel utilization of LTE-U in the previous duty cycle) be 50% and 100%, respectively. Also, assume C_{wifi} and C_{lteu} to be 100ms and 80ms, respectively. If the LTE-U ON/OFF period is proportionally adapted, C_{wifi} and C_{lteu} will be set to 50ms (100*50%) and 130ms (80+100*50%), respectively, for the current duty cycle. Then, maximum channel utilization can be achieved using *Duet*. On the other hand, if the duty cycle length is linearly adapted, C_{wifi} and C_{lteu} will be 99ms (100-1) and 81ms (80+1), respectively, in the current duty cycle. Then, the LTE-U ON/OFF period is adapted towards achieving the fairness between LTE-U and WiFi.

We define *Thres* as channel utilization threshold to trigger linear or proportional adaptation mechanism. The range of *Thres* is [0,1]. As shown in Algorithm 2, if $Wifi_{cu}$ and $Lteu_{cu}$ are both lower or higher than *Thres*, linear adaptation is utilized to let C_{wifi} and C_{lteu} converge to the proportional fairness in line 6 and 8. Otherwise, proportional adaptation is utilized, and C_{wifi} and C_{lteu} can be proportionally adapted to maximize channel utilization in line 2 and 4. If *Thres* is set closer to 1, proportional adaptation is triggered more frequently and the LTE-U ON/OFF period are adapted more aggressively. Linear Adaptation and Proportional Adaptation (LAPA) algorithm of *Duet* can be referred to Algorithm 2.

Algorithm 5 Linear Adaptation and Proportional Adaptation

1: **if** $Wifi_{cu} >= Thres$ **and** $Lteu_{cu} < Thres$ **then**
2: Proportionally adapt C_{lteu} and C_{wifi}
3: **else if** $Wifi_{cu} < Thres$ **and** $Lteu_{cu} >= Thres$ **then**
4: Proportionally adapt C_{lteu} and C_{wifi}
5: **else if** $Wifi_{cu} >= Thres$ **and** $Lteu_{cu} >= Thres$ **then**
6: Linearly adapt C_{lteu} and C_{wifi} towards fairness
7: **else if** $Wifi_{cu} < Thres$ **and** $Lteu_{cu} < Thres$ **then**
8: Linearly adapt C_{lteu} and C_{wifi} towards fairness

5.4.2 Partially connected scenario

In this section, we expand the constraints of *Duet-Baseline* and consider a partially connected scenario (viz. scenario with hidden terminal between LTE-U and WiFi networks),

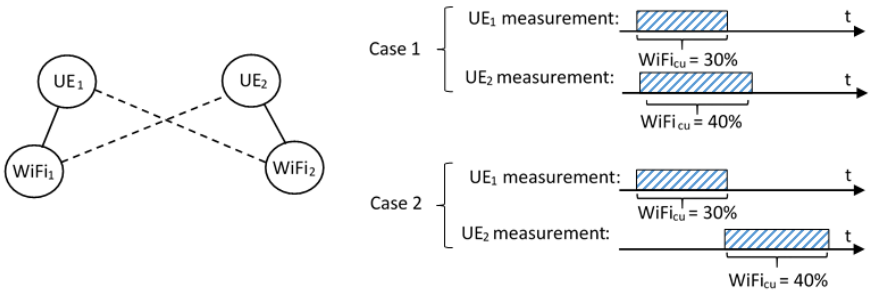

Figure 5.11: Example scenario, where solid line and dotted line represent overhear is possible and impossible

where the elements of the connectivity matrix M are not always 1. For this scenario, we propose *Duet-SCU*.

In *Duet-baseline*, the LTE-U UE reports the WiFi channel utilization to LTE-U small cell. However, in a partially connected network, this information is not enough for the LTE-U small cell to decide the LTE-U ON/OFF period for next cycle. This is because, each LTE-U UE has a different view of the network and hence has different WiFi channel utilization information. Consider the example scenario shown in Fig. 5.11 where two UEs can hear different WiFi nodes (connectivity between UE and WiFi forms matrix M). Let UE_1 and UE_2 estimate the channel utilization individually to be 30% and 40% of LTE-U OFF period, respectively. Cases 1 and 2 represent WiFi transmissions in different time periods. The actual channel utilization for case 1 and 2 is 40% and 70%, respectively, and is different from the estimations made by the UEs. Thus, the channel utilization estimates from a single UE is not enough to compute the overall channel utilization. To have an accurate picture, the timing information of the transmissions is also needed.

Reporting time information of each WiFi packet (start and end time of each WiFi packet transmission) to the LTE-U small cell can be a solution. However, it requires tight time synchronization and generates significant reporting overhead. To alleviate this problem, we introduce slotted channel utilization measurement method. We define each slot as a time block. The WiFi interface of each LTE-U UE measures the channel utilization during each slot with duration D_{slot} according to Algorithm 1. Following that, the $Wifi_{scu}$ for each

Table 5.3: ns-3 Parameters

Parameters	Default Settings
Frame size	1500bytes
Adaptation threshold	90%
Initial LTE-U ON/OFF period	90/90ms
Minimal LTE-U ON/OFF period	10ms
Duty cycle period	180ms
Propagation loss model	Friis propagation loss model
Wi-Fi Tx power	23dbm
Wi-Fi basic transmission rate	6Mbps
Wi-Fi data transmission rate	54Mbps
Wi-Fi CCA Threshold	-62dBm
Wi-Fi CS/CCA Threshold	-82dBm
LTE-U small cell Tx power	23dbm
LTE-U transmission rate	dynamic rate control

slot is set as follows:

$$Wifi_{scu} = \begin{cases} 1 & \text{if } Wifi_{cu} > \text{ half of } D_{slot} \\ 0 & \text{if } Wifi_{cu} <= \text{ half of } D_{slot} \end{cases}$$

$Wifi_{scu}$ is reported to the LTE-U small cell periodically by piggybacking this information with the Channel State Information (CSI) reports[5]. The LTE-U ON/OFF period in *Duet-SCU* are adapted according to the LAPA algorithm as shown in Algorithm 2. Using this algorithm can alleviate tight time synchronization, since reporting time slot utilization requires rougher time synchronization compared with reporting time information of each WiFi packet. Also, reporting time slot utilization lead to less reporting overhead compared with reporting time information of each WiFi packet.

5.5 Evaluation

In this section, we evaluate the *Duet* under static/dynamic traffic loads, partial/fully connected topologies using normal/slotted channel utilization estimation. We use system throughput and channel utilization to evaluate the LTE-U and WiFi network performance. We

[5]CSI reports are periodically sent to the small cell by default

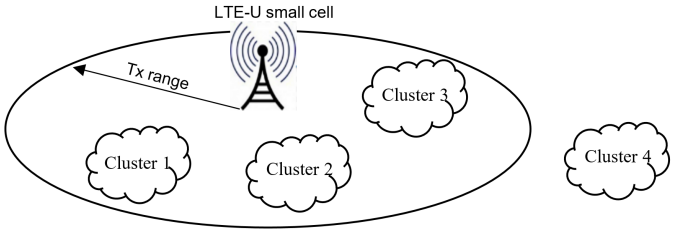

Figure 5.12: Partially connected scenario

evaluate fairness using LTE-U ON/OFF period. If LTE-U ON/OFF period achieves the condition shown in Equation 5.1, then proportional fairness is achieved.

5.5.1 Methodology

We evaluate *Duet* using simulations in ns-3. Various parameters of the WiFi and LTE-U network are shown in Table 5.3. The simulation parameters for WiFi and LTE-U follow the 802.11a[6] [70] and FCC requirements, respectively. To eliminate any random biases, we repeat each experiment 10 times with different random seeds.

The two different topologies considered in the simulations are explained below:

- *Fully connected topology:* The fully connected topology consists of a LTE-U small cell with 8 UEs uniformly distributed around it in a circle of radius 50m. Also, in this circle, 4 WiFi APs, each with a station attached to it, are uniformly distributed. In this scenario, every LTE-U UE can overhear all WiFi transmissions.

- *Partially connected topology:* To generate a partially connected topology, we set up 2 node clusters for LTE-U UEs (Cluster 1 and Cluster 2) with each cluster containing 4 UEs. We also set 2 node clusters for WiFi (Cluster 3 and Cluster 4). Cluster 3 and Cluster 4 contain k ($k \in [0,3]$) and $4-k$ pairs of WiFi AP and client. The default value of k is 3. Nodes in Cluster 1 and Cluster 4 are placed such that they can't overhear each other, and Cluster 4 can't detect LTE-U small cell transmission. All the other clusters can overhear each other. Fig. 5.12 shows the corresponding topology. We also set the D_{slot} to be 100μs, as this value achieves accurate channel

[6]Currently, LTE-U is designed to operate in the 5GHz band

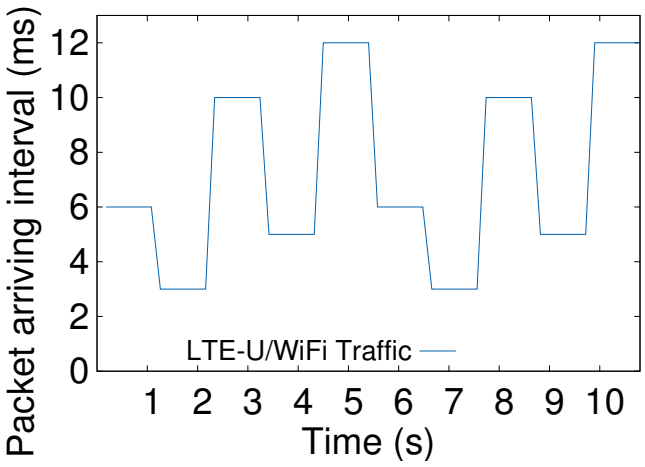

Figure 5.13: Dynamic traffic pattern

utilization without requiring tight time synchronization. We also evaluate the channel utilization accuracy for different D_{slot} values later in this section.

For each of the simulation topology, we send UDP traffic to the LTE-U UEs from a remote host connected to the EPC network of the LTE-U small cell. We also generate UDP traffic between each pair of WiFi AP and client (in both uplink and downlink). The default packet arrival interval ($Interval_p$) for the traffic is 6ms. We evaluate *Duet* by injecting both static load (where the load doesn't change over time) and dynamic load (where the load changes over time). We generate dynamic load conditions by changing the $Interval_p$ at around every second (every 6th duty cycle period) as shown in Fig. 5.13 [7].

5.5.2 Macroscopic Results

Effect of packet arriving interval

Fig. 5.14a and 5.14b illustrate how packet arriving interval $Interval_p$ impacts the LTE-U and WiFi network throughput in fully and partially connected topologies. Since LTE-U network shares time resource with WiFi networks after enabling *Duet*, LTE-U network throughput is nearly not impacted or decreased. In the fully connected topology, the throughput of WiFi network is significantly improved (WiFi throughput increases from

[7] For simplicity, we use deterministic traffic model to observe whether *Duet* will adapt to different load conditions as expected

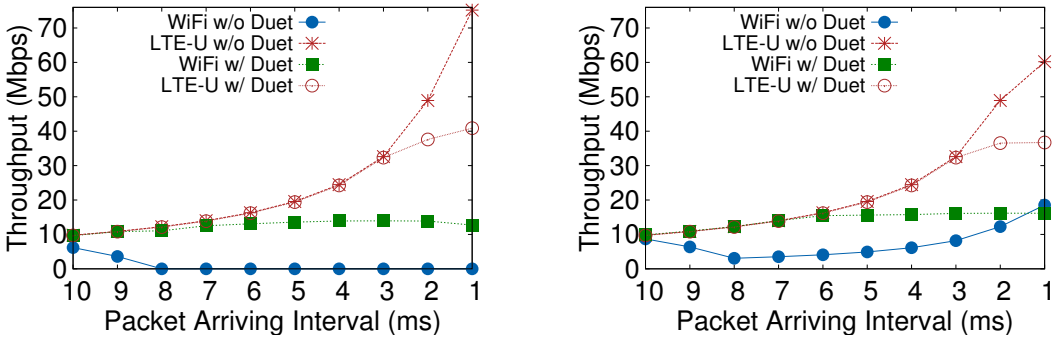

(a) Fully connected topology **(b) Partially connected topology**

Figure 5.14: Impact of $Interval_p$ on network throughput

0 to 13Mbps after enabling *Duet* for packet arriving interval between 1 to 8ms). In the partially connected topology, enabling *Duet* increases the throughput by 112% for WiFi network.

As shown in Fig. 5.14a, enabling *Duet* does not improve the WiFi/LTE-U throughput when packet arriving interval is large. The reason is that as traffic load is low ($Interval_p$ is large), LTE-U and WiFi can almost always find the channel to be idle for transmission without any assistance from *Duet*. As packet arriving interval becomes smaller than 8ms, WiFi throughput is nearly 0 when *Duet* is not enabled. This is because LTE-U small cell always transmits and WiFi always detects the channel to be busy. Enabling *Duet* allows the WiFi nodes to transmit without LTE-U interference during LTE-U OFF period. This increases the WiFi throughput significantly. Also, the LTE-U throughput is not impacted by *Duet* for $Interval_p$ between 3ms and 10ms. This is because the traffic is not saturated. As the size of packet from upper layers is smaller than the Transport Block Size (TBS) in the LTE-U network, the packet will be padded with 0 until it reaches the TBS. When $Interval_p$ is 1ms, the overall network throughput decreases when *Duet* is enabled. This is because LTE-U has higher transmission rate than WiFi (in our simulations), and LTE-U always transmits without letting WiFi transmit when *Duet* is disabled. However, this situation causes starvation in WiFi.

Similar trends discussed above can be observed in Fig. 5.14b. For the partially con-

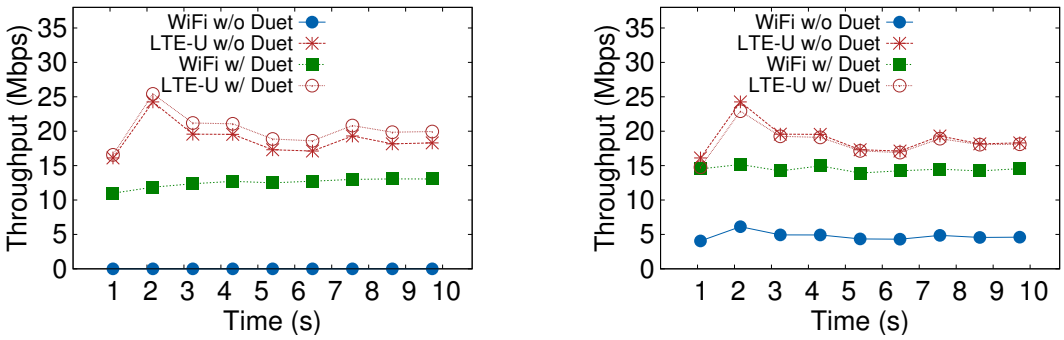

(a) Fully connected topology **(b) Partially connected topology**

Figure 5.15: Impact of load condition on network throughput

nected topology, the WiFi throughput is slightly higher than that of fully connected topology. This is because, there will be 1 pair of WiFi nodes in Cluster 4 who are not affected by LTE-U small cell transmissions. As *Duet* is disabled, it is interesting to note that WiFi throughput decreases initially and increases afterwards. As the packet $Interval_p$ is larger than 8ms, LTE-U will transmit the amount of packets which leads to WiFi nodes in Cluster 3 waiting for an idle channel to transmit. Thus, only partial load of WiFi nodes in Cluster 3 can be transmitted, and it leads to the decrease of WiFi throughput. Since LTE-U does not impact WiFi nodes in Cluster 4, only WiFi nodes in cluster 4 transmit packets as packet arriving interval decreases from 8ms. High traffic load for WiFi nodes in Cluster 4 allows the WiFi throughput to increase.

Effect of dynamic load conditions

For the dynamic load conditions described in Fig. 5.13, Fig. 5.15a and 5.15b illustrate how LTE-U and WiFi throughput varies with time in fully connected and partially connected topologies, respectively. Enabling *Duet* improves the WiFi throughput from 0 to 13Mbps in fully connected topology and by 208% in partially connected topology.

Effect of topology in partially connected scenario

Fig. 5.16a and 5.16b illustrate how the value of k (the WiFi AP and client pair in Cluster 3 described earlier in Section 5.5.1) will impact on LTE-U/WiFi network throughput in static

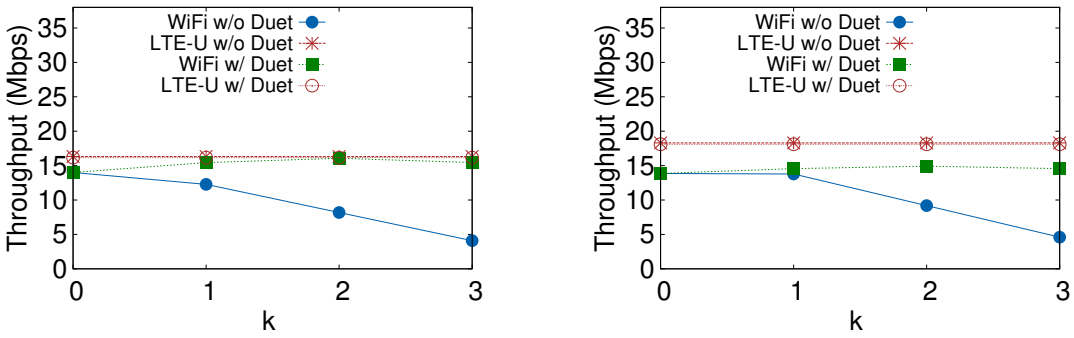

(a) Static load **(b) Dynamic load**

Figure 5.16: Impact of k on network throughput

Table 5.4: D_{slot} effect

D_{slot} (us)	50	100	150	200	250
Channel utilization accuracy	97%	97%	88%	84%	83%

and dynamic load scenario, respectively. Enabling *Duet* improves the network throughput by 110% and 78% for WiFi network in static and dynamic load conditions, respectively. For both load conditions, as k increases, WiFi throughput without *Duet* decreases. This is because more WiFi nodes are put in Cluster 3 (recall that WiFi nodes in Cluster 3 can't transmit when LTE-U transmits).

Channel utilization estimation accuracy

The effect of D_{slot} on channel utilization estimation accuracy is shown in Table II. When D_{slot} decreases, the accuracy increases. This is because the reporting mechanism is error prone for larger values of D_{slot}.

We also evaluated the error of channel utilization estimation under different load conditions and at different time instances. We found the error is at most 3% for both fully connected and partially connected topologies. In the interest of brevity, we omit these results in this paper.

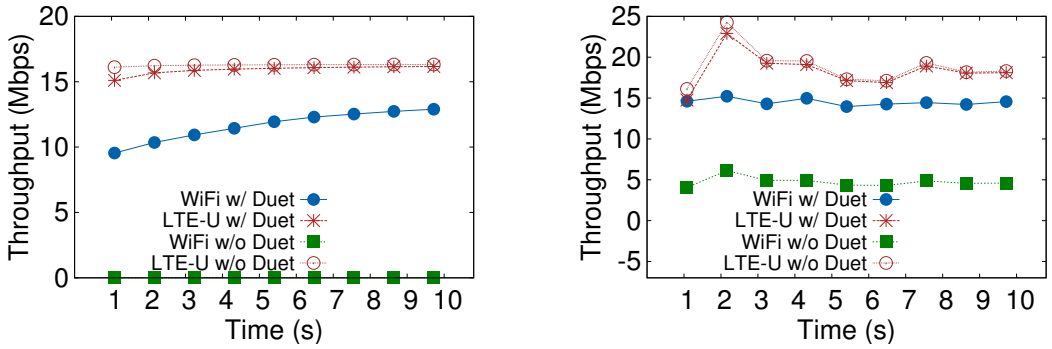

(a) Case 1 **(b) Case 2**

Figure 5.17: Network throughput

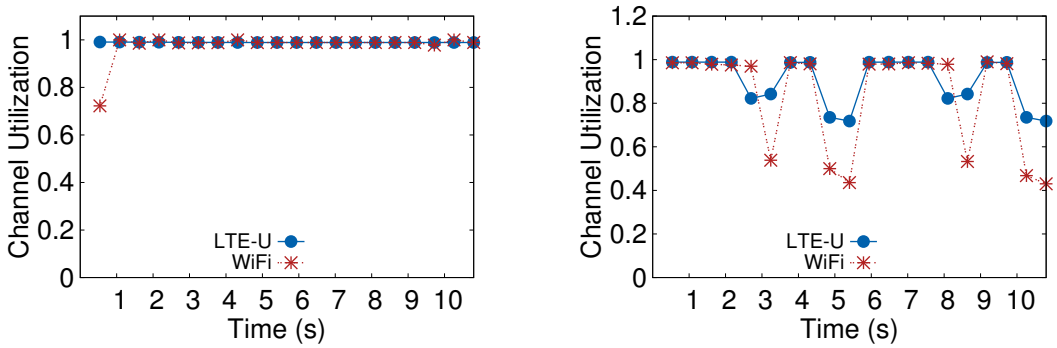

(a) Case 1 **(b) Case 2**

Figure 5.18: Channel Utilization

5.5.3 Microscopic Results

In this section we present two specific cases to show how *Duet* solves the coexistence problem in the time perspective. The goal of these studies is to illustrate that *Duet* not only achieves high network throughput, but also utilizes the channel effectively (channel utilization = 1) and is fair (LTE-U ON period = LTE-U OFF period (applied to the case when LTE-U and WiFi have the same number of links)). For each of these cases, we randomly pick one of the 10 sets of simulations and illustrate how throughput, channel utilization and LTE-U ON/OFF period change with time.

Case 1: Fully connected topology with static load

Fig. 5.17a, 5.18a and 5.19a show the system throughput, channel utilization and LTE-U ON/OFF period versus time, respectively, for both LTE-U and WiFi networks. *Duet* results

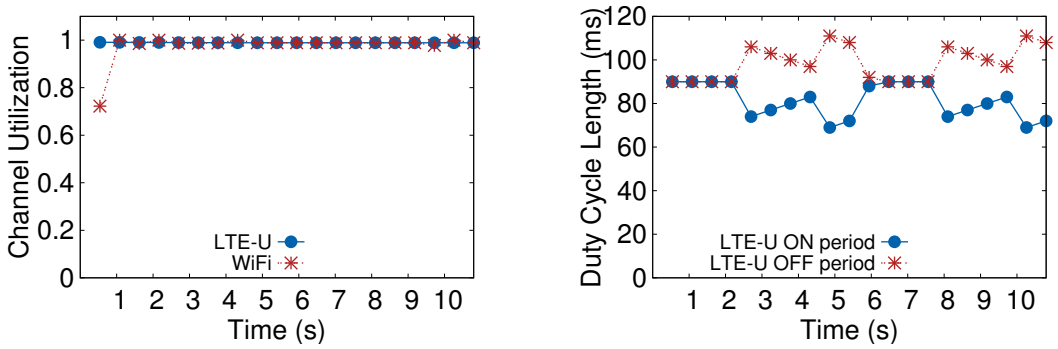

(a) Case 1 **(b) Case 2**

Figure 5.19: LTE-U ON/OFF period

in effective channel utilization, as evidenced by the channel utilization converging to 1 for both WiFi and LTE-U. However, at the beginning, the channel utilization of WiFi is low. This is due to Address Resolution Protocol (ARP) by the WiFi network before the transmission of any UDP packets. We can also observe that the duty cycle of LTE-U and WiFi adapts according to channel utilization. Overall, LTE-U and WiFi networks achieve high channel utilization (channel utilization = 1) and good fairness (LTE-U ON period = LTE-U OFF period) with *Duet* in the fully connected topology with static loads.

Case 2: Dynamic load and partially connected topology

Fig. 5.17b shows the overall network throughput of both LTE-U and WiFi networks at different time instances for the dynamic load described in Fig. 5.13 and with a partially connected topology (k=3). Fig. 5.18b and Fig. 5.19b show the channel utilization and LTE-U ON/OFF period, respectively, for WiFi and LTE-U networks. We can observe that the channel utilization converges to 1 in dynamic load scenario. The channel utilization of LTE-U and WiFi decreases after 2.16s when the traffic load decreases. We can observe that LTE-U utilization decreases faster than WiFi, since WiFi keeps transmitting packets left in the WiFi packet queue (LTE-U has higher transmission rate). Then LTE-U ON period is proportionally decreased and LTE-U OFF period is proportionally increased. After that, LTE-U ON period is linearly increased and LTE-U OFF period is linearly decreased towards fairness. Note that LTE-U channel utilization is higher than WiFi when traffic load

is low. This is because LTE-U will pad 0 to packets with size less than TBS. Overall, LTE-U and WiFi networks achieve high channel utilization and good fairness with *Duet* in the partially connected topology with dynamic loads.

5.6 Summary

In this section we present a solution for the WiFi/LTE-U coexistence problem - *Duet*. Under different traffic load and connectivity scenarios, we show that *Duet* utilizes the channel efficiently and converges to proportional fairness between LTE-U and WiFi networks. However, there are some constraints for *Duet* to work properly: (1) Each LTE-U UE needs to be equipped with a WiFi interface and it is required to be turned ON, which generates extra energy cost; (2) coexistence between LTE-U and WiFi networks is studied with LTE-U downlink only; (3) channel utilization information is only used in the very last duty period to predict current duty cycle length, which may not be accurate; (4) Hidden terminal problem for WiFi nodes is not considered. We intend to relax these constraints as a part of future work.

CHAPTER 6
CHALLENGES AND NEXT STEPS

In the previous chapters of this thesis, we discussed our contributions in three different aspects of improving wireless signal robustness - infrastructure mobility in ultra high frequency (UHF) and super high frequency (SHF), infrastructure mobility in extremely high frequency (EHF), and infrastructure interference mitigation. Explicitly, we 1) propose a WiFi system which can self-positioning itself intelligently to increase network performance; 2) identify the promising potential of applying infrastructure mobility in mmWave networks; and 3) propose centralized coexistence algorithm between LTE-U and WiFi. Given the context of the proposed solutions, there are still several related potential areas that have challenges to solve to further improve network performance. In the rest of this chapter, we discuss three more aspects related to further boosting network performance and outline the next steps and related challenges.

6.1 Infrastructure Mobility with Multiple APs

In this thesis, we presented an SP AP system, *Hermes*, in a single AP network. *Hermes* performs positioning by sequentially solving two related, but independent problems which aim to improve network performance. The first problem is to find the CC, so that path loss phenomenon is optimized from the network perspective. The second problem involves finding an optimal micro position around the CC to optimize the multipath phenomenon. A practical infrastructure mobility solution for multiple APs network needs to be investigated. To be noted, the notions of finding a CC and using brute force search can be directly applied to multiple APs scenario. The benefits of infrastructure mobility may become more significant based on the intelligent collaboration of multiple APs. For multiple APs scenario, the first problem to solve is to identify the optimum pairing set of APs and clients. More specifically, each AP needs to identify which clients should connect to the AP itself in

order to achieve a predefined objective function (such as maximizing the aggregate network performance). As the optimum paring is identified, each AP could optimize each network based on current network information (e.g., identifying the CC and locations with minimum multipath impact).

6.2 Infrastructure Mobility and Interference Mitigation

As infrastructure mobility brings significant network performance improvement by altering the location of wireless infrastructure, it is promising that coexistence of WiFi and unlicensed LTE can also benefit from such infrastructure mobility by minimizing the interference whiling maximizing the performance of its corresponding networks. More specifically, consider the case where unlicensed LTE and WiFi both operate in the 5GHz band, where both unlicensed LTE base station and WiFi AP is able to move. First of all, the WiFi AP and unlicensed LTE base station could optimize its own network performance by identifying optimal location and achieve such an optimum location. If such an optimal location of AP and base station results in large overlapping transmission area, which could lead to severe interference between two networks, an interference mitigation algorithm could be devised. By minimizing the overlapping transmission area of two networks could lead to maximizing the frequency reuse, but it may sabotage the optimum performance considering its own network information. Thus, there is a trade-off between minimizing the overlapping transmission area and maximizing local network performance, which needs to be further studied. In this context, a new optimization problem considering both maximizing the frequency reuse and maximizing local network performance needs to be properly formulated and investigated.

6.3 Infrastructure Mobility and Quality of Service (QoS)

QoS is a critical metric for wireless network, where each WiFi client can have various customized performance requirements. The QoS metric can be designed based on various WiFi performance metrics (e.g., fairness, and throughput). AP mobility is a promising

degree of freedom for optimizing the QoS requirement of each WiFi client. Specifically, AP can move to various physical locations to provide the required channel conditions to each WiFi client.

REFERENCES

[1] *Cisco visual networking index: Forecast and methodology 2017-2022*, https://www.cisco.com/c/en/us/solutions/collateral/service-provider/visual-networking-index-vni/white-paper-c11-741490.html.

[2] *Number of wireless local area network (wlan) connected devices worldwide*, https://www.statista.com/statistics/802706/world-wlan-connected-device.

[3] *Geoba.se world rankings*, http://www.geoba.se/population.php.

[4] *Mushroom networks bandwidth requirements for virtual reality (vr) and augmented reality (ar) - infographic 2017*, https://www.mushroomnetworks.com/infographics/bandwidth-requirements-for-virtual-reality-vr-and-augmented-reality-ar-infographic/.

[5] *Worried about bandwidth for 4k? here comes 8k!* https://www.lightreading.com/video/4k-8k-video/worried-about-bandwidth-for-4k-here-comes-8k!/d/d-id/737330.

[6] H. Hashemi, "The indoor radio propagation channel," *Proceedings of the IEEE*, vol. 81, no. 7, pp. 943–968, 1993.

[7] D. Tse, *Fundamentals of Wireless Communication*. Cambridge University Press, 2005.

[8] M. Gowda and et al., "The case for robotic wireless networks," in *Proc. of 25th International Conference on WWW*, 2016, pp. 1317–1327.

[9] G. Mahanth and et al, "Infrastructure mobility: A what-if analysis," in *Proc. of the 13th Workshop on HotNets*, 2014, pp. 19–20.

[10] S. M. Alamouti, "A simple transmit diversity technique for wireless communications," *1998*, 1998.

[11] Y. Jian, L. Shruti, and S. Raghupathy, "Twirl: On the benefits of adapting orientation of a wifi access point," in *Proc. of 15th International Conference on Mobisys, Poster*, 2017, pp. 1317–1327.

[12] S. Gil, S. Kumar, D. Katabi, and D. Rus, "Adaptive communication in multi-robot systems using directionality of signal strength," *The International Journal of Robotics Research*, vol. 34, no. 7, pp. 946–968, 2015.

[13] F. Adib and et al., "Interference alignment by motion," in *Proc. of the 19th annual international conference on Mobicom*, 2013, pp. 279–290.

[14] M. A. M. Vieira and et al., "Mitigating multi-path fading in a mobile mesh network," *Ad Hoc Networks*, vol. 11, no. 4, pp. 1510–1521, 2013.

[15] A. Klose and A. Drexl, "Facility location models for distribution system design," *European journal of operational research*, vol. 162, no. 1, pp. 4–29, 2005.

[16] C. Boonmee, M. Arimura, and T. Asada, "Facility location optimization model for emergency humanitarian logistics," *International Journal of Disaster Risk Reduction*, vol. 24, pp. 485–498, 2017.

[17] H. Xu, V. Kukshya, and T. S. Rappaport, "Spatial and temporal characteristics of 60-ghz indoor channels," *IEEE JSAC*, vol. 20, no. 3, pp. 620–630, 2002.

[18] S. Sur and et al., "Wifi-assisted 60 ghz wireless networks," in *Proceedings of the 23rd Annual International Conference on Mobicom*, 2017, pp. 28–41.

[19] M. Polese, M. Giordani, M. Mezzavilla, S. Rangan, and M. Zorzi, "Improved handover through dual connectivity in 5g mmwave mobile networks," *IEEE JSAC*, vol. 35, no. 9, pp. 2069–2084, 2017.

[20] M. Polese, R. Jana, and M. Zorzi, "Tcp in 5g mmwave networks: Link level retransmissions and mp-tcp," in *Proc. of the Infocom Workshops*, 2017, pp. 343–348.

[21] Y. Jian, M. Agarwal, Y. Liu, D. M. Blough, and R. Sivakumar, "Poster: Hawkeye-predictive positioning of a ceiling-mounted mobile ap in mmwave wlans for maximizing line-of-sight," in *The 25th Annual International Conference on Mobile Computing and Networking*, 2019, pp. 1–3.

[22] Y. Jian, Y. Liu, S. K. Venkateswaran, D. M. Blough, and R. Sivakumar, "A quantitative exploration of access point mobility for mmwave wifi networks," in *the Annual IEEE International Conference on Communications*, 2020, to appear.

[23] Y. Liu, Y. Jian, D. M. Blough, and R. Sivakumar, "On the potential benefits of mobile access points in mmwave wireless lans," in *International Symposium on Local and Metropolitan Area Networks*, 2020, to appear.

[24] Y. Liu, Y. Jian, R. Sivakumar, and D. M. Blough, "Optimal access point placement for multi-ap mmwave wlans," in *Proceedings of the 22nd International ACM Conference on Modeling, Analysis and Simulation of Wireless and Mobile Systems*, 2019, pp. 35–44.

[25] Y. Jian, S. Lall, and R. Sivakumar, "Toward a self-positioning access point for wifi networks," in *Proceedings of the 16th ACM International Symposium on Mobility Management and Wireless Access*, 2018, pp. 19–28.

[26] S. Sur, I. Pefkianakis, X. Zhang, and K.-H. Kim, "Towards scalable and ubiquitous millimeter-wave wireless networks," in *Proc. of the 24th International Conference on Mobicom*, 2018, pp. 257–271.

[27] Y. Yan, Q. Hu, and D. M. Blough, "Path selection with amplify and forward relays in mmwave backhaul networks," in *IEEE 29th Annual International Symposium on Personal, Indoor and Mobile Radio Communications (PIMRC)*, 2018, pp. 1–6.

[28] Q. Hu and M Blough, "Relay selection and scheduling for millimeter wave backhaul in urban environments," in *14th International Conference on MASS*, 2017, pp. 206–214.

[29] Y. Yan, Q. Hu, and D. M. Blough, "Optimal path construction with decode and forward relays in mmwave backhaul networks," in *Proceedings of the IEEE International Conference on Computing, Networking and Communications*, 2020.

[30] X. Zhou and et al., "Mirror mirror on the ceiling: Flexible wireless links for data centers," *ACM SIGCOMM Computer Communication Review*, vol. 42, no. 4, pp. 443–454, 2012.

[31] O. Abari, D. Bharadia, A. Duffield, and D. Katabi, "Enabling high-quality untethered virtual reality," in *14th {USENIX} Symposium on Networked Systems Design and Implementation ({NSDI} 17)*, 2017, pp. 531–544.

[32] S. Rajagopal, S. Abu-Surra, and M. Malmirchegini, "Channel feasibility for outdoor non-line-of-sight mmwave mobile communication," in *2012 IEEE vehicular technology conference*, 2012, pp. 1–6.

[33] *Internet users in the world*, `www.internetworldstats.com/stats.htm`.

[34] *Telecoms, wireless, broadband and forecasts*, `www.budde.com.au/Research/2010-USA-Telecoms-Wireless-Broadband-and-Forecasts.html?r=51`.

[35] *Lte in unlicensed spectrum*, `http://www.3gpp.org/news-events/3gpp-news/1603-lte_in_unlicensed`.

[36] *U-lte: Unlicensed spectrum utilization of lte*, `www.huawei.com/ilink/en/download/HW_327803`.

[37] *Extending lte advanced to unlicensed spectrum*, `www.qualcomm.com/solutions/wireless-networks/technologies/lte-unlicensed`.

[38] H. Zhang, X. Chu, W. Guo, and S. Wang, "Coexistence of wi-fi and heterogeneous small cell networks sharing unlicensed spectrum," *IEEE Communications Magazine*, vol. 53, no. 3, pp. 158–164, 2015.

[39] Y. Jian, C.-F. Shih, B. Krishnaswamy, and R. Sivakumar, "Coexistence of wi-fi and laa-lte: Experimental evaluation, analysis and insights," in *Proc. of International Conference on ICCW*, 2015, pp. 2325–2331.

[40] Y. Jian, U. P. Moravapalle, C.-F. Shih, and R. Sivakumar, "Duet: An adaptive algorithm for the coexistence of lte-u and wifi in unlicensed spectrum," in *proc. International Conference on ICNC*, IEEE, 2017, pp. 19–25.

[41] C.-F. Shih, Y. Jian, and R. Sivakumar, "Look who's talking: A practical approach for achieving scheduled wifi in a single collision domain," in *Proceedings of the 11th ACM Conference on Emerging Networking Experiments and Technologies*, 2015, pp. 1–13.

[42] C.-F. Shih, B. Krishnaswamy, Y. Jian, and R. Sivakumar, "Scheduled wifi using distributed contention in wlans: Algorithms, experiments, and case-studies," *Wireless Networks*, vol. 24, no. 1, pp. 89–112, 2018.

[43] B. Krishnaswamy and R. Sivakumar, "Amplitude-width encoding for error correction in bacterial communication networks," in *Proceedings of the 5th ACM International Conference on Nanoscale Computing and Communication*, 2018, pp. 1–7.

[44] Y. Jian, B. Krishnaswamy, C. M. Austin, A. O. Bicen, J. E. Perdomo, S. C. Patel, I. F. Akyildiz, C. R. Forest, and R. Sivakumar, "Nanons3: Simulating bacterial molecular communication based nanonetworks in network simulator 3," in *Proceedings of the 3rd ACM International Conference on Nanoscale Computing and Communication*, 2016, pp. 1–7.

[45] Y. Jian, B. Krishnaswamy, C. M. Austin, A. O. Bicen, A. Einolghozati, J. E. Perdomo, S. C. Patel, F. Fekri, I. F. Akyildiz, C. R. Forest, *et al.*, "Nanons3: A network simulator for bacterial nanonetworks based on molecular communication," *Nano communication networks*, vol. 12, pp. 1–11, 2017.

[46] Y. Jian, "Coexistence of wi-fi and laa-lte in unlicensed spectrum," PhD thesis, Georgia Institute of Technology, 2015.

[47] A. Mukherjee and et al., "System architecture and coexistence evaluation of licensed-assisted access lte with ieee 802.11," in *Proc. of International Conference on ICCW*, 2015, pp. 2350–2355.

[48] B. Jia and M. Tao, "A channel sensing based design for lte in unlicensed bands," in *Proc. of International Conference on ICCW*, 2015, pp. 2332–2337.

[49] M. Bennis and et al., "When cellular meets wifi in wireless small cell networks," *IEEE communications magazine*, vol. 51, no. 6, pp. 44–50, 2013.

[50] *Irobot create 2 programmable robot*, `http://www.irobot.com/About-iRobot/STEM/Create-2.aspx`.

[51] *Iperf3*, https://software.es.net/iperf/.

[52] S. Singh, F. Ziliotto, U. Madhow, E Belding, and M. Rodwell, "Blockage and directivity in 60 ghz wireless personal area networks: From cross-layer model to multihop mac design," *JSAC*, vol. 27, no. 8, pp. 1400–1413, 2009.

[53] A. Bose and C. H. Foh, "A practical path loss model for indoor wifi positioning enhancement," in *Proc. of the 6th International Conference on ICSPIC*, 2007, pp. 1–5.

[54] G. Mao, B. D. Anderson, and B. Fidan, "Path loss exponent estimation for wireless sensor network localization," *Computer Networks*, vol. 51, no. 10, pp. 2467–2483, 2007.

[55] F. Zafari, A. Gkelias, and K. Leung, "A survey of indoor localization systems and technologies," *arXiv preprint arXiv:1709.01015*, 2017.

[56] M. Kotaru, K. Joshi, D. Bharadia, and S. Katti, "Spotfi: Decimeter level localization using wifi," *SIGCOMM Computer Communication Review*, vol. 45, no. 4, pp. 269–282, 2015.

[57] J. Xiong and K. Jamieson, "Arraytrack: A fine-grained indoor location system," in *Proc. of the 10th USENIX Symposium on NSDI*, 2013.

[58] P. Cotera, M. Velazquez, D. Cruz, L. Medina, and M. Bandala, "Indoor robot positioning using an enhanced trilateration algorithm," *International Journal of Advanced Robotic Systems*, vol. 13, no. 3, pp. 110–118, 2016.

[59] S. Boyd and L. Vandenberghe, *Convex optimization*. Cambridge university press, 2004.

[60] T. Kamphans and E. Langetepe, "The pledge algorithm reconsidered under errors in sensors and motion," in *International Workshop on Approximation and Online Algorithms*, Springer, 2003, pp. 165–178.

[61] *Ns-3*, `https://www.nsnam.org/`.

[62] J. Lu, D. Steinbach, P. Cabrol, P. Pietraski, and R. V. Pragada, "Propagation characterization of an office building in the 60 ghz band," in *Proc. of 8th European Conference on Antennas and Propagation*, 2014, pp. 809–813.

[63] H. Assasa and J. Widmer, "Implementation and evaluation of a wlan ieee 802.11 ad model in ns-3," in *Proceedings of the Workshop on ns-3*, 2016, pp. 57–64.

[64] P. F. Smulders, "Statistical characterization of 60-ghz indoor radio channels," *IEEE Transactions on Antennas and Propagation*, vol. 57, no. 10, pp. 2820–2829, 2009.

[65] R. K. Jain, D.-M. W. Chiu, and W. R. Hawe, "A quantitative measure of fairness and discrimination," *ACM Transactions on Computer Systems*, pp. 2–7, 1984.

[66] *Progressive automations track linear actuator*, `https://www.progressiveautomations.com/products/track-linear-actuator?variant=18277305811011`.

[67] *Pc mag tp-link talon ad7200 multi-band wi-fi router*, `https://www.pcmag.com/review/347405/tp-link-talon-ad7200-multi-band-wi-fi-router`.

[68] *Number of wireless local area network (wlan) connected devices worldwide*, `https://www.statista.com/statistics/802706/world-wlan-connected-device`.

[69] S. Sur, V. Venkateswaran, X. Zhang, and P. Ramanathan, "60 ghz indoor networking through flexible beams: A link-level profiling," in *ACM SIGMETRICS Performance Evaluation Review*, vol. 43, 2015, pp. 71–84.

[70] *Ieee std 802.11ad-2012*, https://ieeexplore.ieee.org/stamp/stamp.jsp?arnumber=6392842.

[71] C. Wu, Z. Yang, Z. Zhou, K. Qian, Y. Liu, and M. Liu, "Phaseu: Real-time los identification with wifi," in *2015 conference on computer communications*, 2015, pp. 2038–2046.

[72] M. Youssef and A. Agrawala, "The horus wlan location determination system," in *Proceedings of the 3rd international conference on Mobile systems, applications, and services*, 2005, pp. 205–218.

[73] S. Haykin, *Neural networks*. 1994, vol. 2.

[74] Y. LeCun, Y. Bengio, and G. Hinton, "Deep learning," *nature*, vol. 521, no. 7553, p. 436, 2015.

[75] S. Ruder, "An overview of gradient descent optimization algorithms," *arXiv preprint arXiv:1609.04747*, 2016.

[76] R. A. Jacobs, "Increased rates of convergence through learning rate adaptation," *Neural networks*, vol. 1, no. 4, pp. 295–307, 1988.

[77] C. R. Anderson and T. S. Rappaort, "In-building wideband partition loss measurements at 2.5 ghz and 60 ghz," *arXiv preprint arXiv:1701.03415*, 2016.

[78] M. A. et al., *TensorFlow: Large-scale machine learning on heterogeneous systems*, Software available from tensorflow.org, 2015.

[79] *Random permutation tests*, http://danielnee.com/2015/01/random-permutation-tests/.

[80] *Arduino uno rev3*, https://store.arduino.cc/usa/arduino-uno-rev3.

[81] *Megamoto plus motor control shield for arduino*, http://www.robotpower.com/products/MegaMotoPlus_info.html.

[82] *Acer travelmate p648*, https://www.acer.com/ac/en/US/press/2016/175243.

[83] *Qualcomm technologies, lte in unlicensed spectrum: Harmonious coexistence with wi-fi*, https://www.qualcomm.com/media/documents/files/lte-unlicensed-coexistence-whitepaper.pdf.

[84] *National instruments pxi platform", national instruments*, http://www.ni.com/pxi/.

[85] *Warp v3 kit*, http://mangocomm.com/products/ kits/warp-v3-kit.

[86] S. Huaizhou, R. V. Prasad, E. Onur, and I. Niemegeers, "Fairness in wireless networks: Issues, measures and challenges," *IEEE Communications Surveys & Tutorials*, vol. 16, no. 1, pp. 5–24, 2013.

[87] V. Bharghavan, A. Demers, S. Shenker, and L. Zhang, "Macaw: A media access protocol for wireless lan's," *ACM SIGCOMM Computer Communication Review*, vol. 24, no. 4, pp. 212–225, 1994.

[88] G. Bianchi, "Ieee 802.11-saturation throughput analysis," *IEEE communications letters*, vol. 2, no. 12, pp. 318–320, 1998.